

DEVELOPMENT OF THE GC-8000 BRIDGE RAILING AND TRANSITION

Submitted by

Rebecca A. Hitz ¹
Undergraduate Research Assistant

Karla A. Polivka, M.S.M.E., P.E. ¹
Research Associate Engineer

Ronald K. Faller, Ph.D., P.E. ¹
Research Assistant Professor

Michael A. Ritter, P.E. ²
Project Leader

Barry T. Rosson, Ph.D., P.E. ¹
Professor

James C. Holloway, M.S.C.E., E.I.T. ¹
Research Manager

MIDWEST ROADSIDE SAFETY FACILITY ¹

University of Nebraska-Lincoln
527 Nebraska Hall
Lincoln, Nebraska 68588-0529
(402) 472-6864

U.S. DEPARTMENT OF AGRICULTURE ²

Forest Service
Forest Products Laboratory
Engineered Wood Products and Structures
One Gifford Pichot Dr.
Madison, Wisconsin 53705
(608) 231-9229

MwRSF Research Report No. TRP-03-161-06

May 2, 2006

Technical Report Documentation Page

1. Report No.	2.	3. Recipient's Accession No.	
4. Title and Subtitle Development of the GC-8000 Bridge Railing and Transition		5. Report Date May 2, 2006	
		6.	
7. Author(s) Hitz, R.A., Polivka, K.A., Faller, R.K., Ritter, M.A., Rosson, B.T., and Holloway, J.C.		8. Performing Organization Report No. TRP-03-161-06	
9. Performing Organization Name and Address Midwest Roadside Safety Facility (MwRSF) University of Nebraska-Lincoln 527 Nebraska Hall Lincoln, NE 68588-0529		10. Project/Task/Work Unit No.	
		11. Contract © or Grant (G) No. FP-89-1183	
12. Sponsoring Organization Name and Address U.S. Department of Agriculture Forest Service Forest Products Laboratory One Gifford Pinchot Drive Madison, Wisconsin 53705		13. Type of Report and Period Covered Draft Report 1992-2006	
		14. Sponsoring Agency Code	
15. Supplementary Notes Prepared in cooperation with U.S. Department of Transportation, Federal Highway Administration			
16. Abstract (Limit: 200 words) <p>One bridge railing and approach guardrail transition system for use on bridges with longitudinal glue-laminated timber decks was developed and crash tested for use on higher-service-level roadways. The bridge railing and transition system was subjected to full-scale crash tests in accordance with the Test Level 4 (TL-4) safety performance criteria presented in NCHRP Report No. 350, <i>Recommended Procedures for the Safety Performance Evaluation of Highway Features</i> as well as the MSL-2 criteria found in NCHRP Report No. 230, respectively. Four full-scale crash tests were performed - three on the bridge railing and one on the approach guardrail transition. The bridge railing and transition systems were found to be acceptable according to current safety standards.</p>			
17. Document Analysis/Descriptors Highway Safety, Longitudinal Barrier, Bridge Railing, Approach Guardrail Transition, Roadside Appurtenances, Crash Test, Compliance Test, Timber Bridge		18. Availability Statement No restrictions. Document available from: National Technical Information Services, Springfield, Virginia 22161	
19. Security Class (this report) Unclassified	20. Security Class (this page) Unclassified	21. No. of Pages 213	22. Price

DISCLAIMER STATEMENT

The contents of this report reflect the views of the authors who are responsible for the facts and the accuracy of the data presented herein. The contents do not necessarily reflect the official views or policies of the Federal Highway Administration nor the United States Department of Agriculture, Forest Service, Forest Products Laboratory. This report does not constitute a standard, specification, or regulation.

ACKNOWLEDGMENTS

The authors wish to acknowledge several sources that made a contribution to the success of this research project: (1) John Foreman, Alamo Wood Products, Inc., Albert Lea, Minnesota, for all your cooperation and supplying the glulam materials at a very competitive price; (2) MwRSF personnel for constructing the bridge structure and barrier system as well as conducting the crash tests; and (3) the Office of Sponsored Programs and the Center for Infrastructure Research, University of Nebraska-Lincoln, Lincoln, NE for matching support.

A special thanks is also given to the following individuals who made a contribution to the completion of this research project.

Federal Highway Administration

Sheila R. Duwadi, P.E., Turner-Fairbank Highway Research Center

Midwest Roadside Safety Facility

D.L. Sicking, Ph.D., P.E., Professor and MwRSF Director
B.G. Pfeifer, Ph.D., P.E., Former Research Associate Engineer
K.L. Krenk, B.S.M.A., Shop Manager
Undergraduate and Graduate Assistants

Dunlap Photography

James Dunlap, President and Owner

TABLE OF CONTENTS

	Page
TECHNICAL REPORT DOCUMENTATION PAGE	i
DISCLAIMER STATEMENT	ii
ACKNOWLEDGMENTS	iii
TABLE OF CONTENTS	iv
List of Figures	vii
List of Tables	xi
1 INTRODUCTION	1
1.1 Problem Statement	1
1.2 Objective	1
1.3 Scope	2
2 LITERATURE REVIEW	3
2.1 Bridge Railings for Timber Deck Bridges	3
3 TEST REQUIREMENTS AND EVALUATION CRITERIA	5
3.1 Test Requirements	5
3.2 Evaluation Criteria	6
4 TEST SITE PREPARATION	10
4.1 Bridge Deck and Substructure	10
5 TEST CONDITIONS	18
5.1 Test Facility	18
5.2 Vehicle Tow and Guidance System	18
5.3 Test Vehicle	18
5.3.1 Center-of-Mass Determination, Vehicle Targets, and Alignment	19
5.4 Data Acquisition Systems	33
5.4.1 Accelerometers	33
5.4.2 Rate Transducer	33
5.4.3 High-Speed Photography	34
5.4.4 Pressure Tape Switches	35
6 SYSTEM DEVELOPMENT	40
7 SYSTEM DESIGN DETAILS	42
7.1 Wood Bridge Railing	42
7.2 Approach Guardrail Transition	54

8 COMPUTER SIMULATION	68
8.1 Introduction	68
8.2 Design Option	68
8.3 BARRIER VII Results	68
8.3.1 Single-Unit Truck Test - Bridge Railing	68
8.3.2 Pickup Truck Test - Bridge Railing	69
9 CRASH TEST NO. 1 (BRIDGE RAILING)	70
9.1 Test FSCR-1	70
9.2 Test Description	70
9.3 Bridge Rail Damage	71
9.4 Vehicle Damage	72
9.5 Occupant Risk Values	73
9.6 Discussion	73
10 CRASH TEST NO. 2 (APPROACH GUARDRAIL TRANSITION)	100
10.1 Test FSCR-2	100
10.2 Test Description	100
10.3 Bridge Rail and Approach Guardrail Terminal Damage	101
10.4 Vehicle Damage	102
10.5 Occupant Risk Values	103
10.6 Discussion	103
11 CRASH TEST NO. 3 (BRIDGE RAILING)	120
11.1 Test FSCR-3	120
11.2 Test Description	120
11.3 Bridge Rail Damage	121
11.4 Vehicle Damage	121
11.5 Occupant Risk Values	122
11.6 Discussion	122
12 CRASH TEST NO. 4 (BRIDGE RAILING)	135
12.1 Test FSCR-4	135
12.2 Test Description	135
12.3 Bridge Rail Damage	136
12.4 Vehicle Damage	137
12.5 Occupant Risk Values	138
12.6 Discussion	138
13 SUMMARY AND CONCLUSIONS	157
14 RECOMMENDATIONS	162

15 REFERENCES	163
16 APPENDICES	165
APPENDIX A	
BARRIER VII Computer Models	166
APPENDIX B	
Structural Properties of Rail and Post Elements	171
APPENDIX C	
Typical BARRIER VII Input Data Files (CIP)	174
APPENDIX D	
Typical BARRIER VII Input Data Files (SUT, typical)	177
APPENDIX E	
Typical BARRIER VII Input Data Files (PU, typical)	180
APPENDIX F	
Accelerometer Data Analysis - Test FSCR-1	183
APPENDIX G	
Accelerometer Data Analysis - Test FSCR-2	191
APPENDIX H	
Accelerometer Data Analysis - Test FSCR-3	198
APPENDIX I	
Accelerometer Data Analysis - Test FSCR-4	206

List of Figures

	Page
1. Bridge Site Prior to Construction	13
2. Construction of Concrete Bridge Supports.	14
3. Vertical Rebar in Concrete Bridge Supports.	15
4. Top View of the Concrete Bridge Supports with Anchor Placement.	16
5. Longitudinal Glulam Timber Deck.	17
6. Test Vehicle, Test FSCR-1	21
7. Vehicle Dimensions, Test FSCR-1	22
8. Test Vehicle, Test FSCR-2	23
9. Vehicle Dimensions, Test FSCR-2	24
10. Test Vehicle, Test FSCR-3	25
11. Vehicle Dimensions, Test FSCR-3	26
12. Test Vehicle, Test FSCR-4	27
13. Vehicle Dimensions, Test FSCR-4	28
14. Vehicle Target Locations, Test FSCR-1	29
15. Vehicle Target Locations, Test FSCR-2	30
16. Vehicle Target Locations, Test FSCR-3	31
17. Vehicle Target Locations, Test FSCR-4	32
18. Location of High-Speed Cameras, Test FSCR-1	36
19. Location of High-Speed Cameras, Test FSCR-2	37
20. Location of High-Speed Cameras, Test FSCR-3	38
21. Location of High-Speed Cameras, Test FSCR-4	39
22. Bridge Railing System	44
23. Bridge Railing System	45
24. Bridge Railing System - Bridge Posts	46
25. Overall Layout of Bridge Railing System	47
26. General Configuration of Bridge Railing System	48
27. Bridge Railing Design Details	49
28. Post Plate Detail	50
29. Internal Plate Detail	51
30. Rail Connection and Steel Rail Splice Design Details	52
31. Curb Splice Design Detail	53
32. Approach Guardrail Transition - Front View	57
33. Approach Guardrail Transition - Back View	58
34. Connection to Detail Between Approach Guardrail Transition and Bridge Railing - Back-Side View	59
35. Transition Connection - Back-Side Close-Up View	60
36. General Configuration of Transition Connection	61
37. Transition Connection Design Detail	62
38. Transition Post Profiles	63
39. Curb Transition Block Design Detail	64
40. Curb Transition Design Detail	65

41. Boring Detail - Glulam Rail End at Approach Guardrail Transition	66
42. Transition Plate Detail	67
43. Summary of Test Results and Sequential Photographs, Test FSCR-1	75
44. Sequential Photographs, Test FSCR-1	76
45. Documentary Photographs, Test FSCR-1	77
46. Documentary Photographs, Test FSCR-1	78
47. Documentary Photographs, Test FSCR-1	79
48. Documentary Photographs, Test FSCR-1	80
49. Impact Locations, Test FSCR-1	81
50. Final Vehicle Position and Trajectory Marks, Test FSCR-1	82
51. Rail Damage Downstream from Impact, Test FSCR-1	83
52. Rail Damage at Post No. 8, Test FSCR-1	84
53. Rail Damage Between Post Nos. 4 and 5, Test FSCR-1	85
54. Rail Damage at Post Nos. 4 and 5, Test FSCR-1	86
55. Damage to Post Nos. 7 and 8, Test FSCR-1	87
56. Damage to Post Nos. 9 through 11, Test FSCR-1	88
57. Post No. 12 Damage, Test FSCR-1	89
58. Damage to Post Nos. 13 and 14, Test FSCR-1	90
59. Post No. 15 Damage, Test FSCR-1	91
60. Deck Cracking on Upstream Side of Post No. 4, Test FSCR-1	92
61. Deck Cracking at Post No. 4, Test FSCR-1	93
62. Deck Cracking on Downstream Side of Post No. 4, Test FSCR-1	94
63. Vehicle Damage, Test FSCR-1	95
64. Vehicle Damage, Test FSCR-1	96
65. Vehicle Damage, Test FSCR-1	97
66. Vehicle Damage, Test FSCR-1	98
67. Downstream Strong-Post Anchor, Test FSCR-1	99
68. Summary of Test Results and Sequential Photographs, Test FSCR-2	104
69. Sequential Photographs, Test FSCR-2	105
70. Documentary Photographs, Test FSCR-2	106
71. Documentary Photographs, Test FSCR-2	107
72. Documentary Photographs, Test FSCR-2	108
73. Impact Locations, Test FSCR-2	109
74. Final Vehicle Position and Trajectory Marks, Test FSCR-2	110
75. Thrie Beam Damage, Test FSCR-2	111
76. Curb Rail Damage, Test FSCR-2	112
77. Curb Rail Damage, Test FSCR-2	113
78. Deck Cracking, Test FSCR-2	114
79. Permanent Set Deflection of Thrie Beam Rail and Glulam Rail, Test FSCR-2	115
80. Vehicle Damage, Test FSCR-2	116
81. Vehicle Damage, Test FSCR-2	117
82. Vehicle Damage, Test FSCR-2	118
83. Occupant Compartment Deformation, Test FSCR-2	119
84. Summary of Test Results and Sequential Photographs, Test FSCR-3	124

85. Additional Sequential Photographs, Test FSCR-3	125
86. Documentary Photographs, Test FSCR-3	126
87. Documentary Photographs, Test FSCR-3	127
88. Documentary Photographs, Test FSCR-3	128
89. Target Impact Location, Test FSCR-3	129
90. Final Vehicle Position and Trajectory Marks, Test FSCR-3	130
91. Bridge Rail Damage, Test FSCR-3	131
92. Bridge Rail Damage, Test FSCR-3	132
93. Vehicle Damage, Test FSCR-3	133
94. Front-End Vehicle Damage Due to Shear Post Impact, Test FSCR-3	134
95. Summary of Test Results and Sequential Photographs, Test FSCR-4	139
96. Sequential Photographs, Test FSCR-4	140
97. Additional Sequential Photographs, Test FSCR-4	141
98. Impact Locations, Test FSCR-4	142
99. Bridge Rail Damage, Test FSCR-4	143
100. Bridge Rail Damage, Test FSCR-4	144
101. Glulam Rail Deformation at Post No. 8, Test FSCR-4	145
102. Glulam Rail Fracture at Post No. 8, Test FSCR-4	146
103. Damage at Post No. 8, Test FSCR-4	147
104. Internal Deck-Side end of High-Strength Bar Located at Post No. 8 (Note residual nut threads left on the end of the bar), Test FSCR-4	148
105. Plate washer deformation at Post No. 8, Test FSCR-4	149
106. Curb Rail Damage Between Post Nos. 8 through 10, Test FSCR-4	150
107. Deck Cracking Between Post Nos. 6 and 7, 8 and 9, Test FSCR-4	151
108. Deck Cracking at Post Nos. 7 and 8, Test FSCR-4	152
109. Final Position, Test FSCR-4	153
110. Vehicle Damage, Test FSCR-4	154
111. Vehicle Damage, Test FSCR-4	155
112. Occupant Compartment Deformation, Test FSCR-4	156
A-1. Model of the AASHTO PL-2 Curb Rail Bridge Rail System (FSCR-1,3,4).	167
A-2. Model of the Approach Guardrail Transition for the AASHTO PL-2 Curb System (FSCR-2).	168
A-3. Idealized Finite Element, 2 Dimensional Vehicle Model for the 8,000-kg (17,637-lb) Single-Unit Truck	169
A-4. Idealized Finite Element, 2 Dimensional Vehicle Model for the 2,000-kg (4,409-lb) Pickup Truck	170
F-1. Graph of Longitudinal Deceleration, Test FSCR-1	184
F-2. Graph of Longitudinal Occupant Impact Velocity, Test FSCR-1	185
F-3. Graph of Longitudinal Occupant Displacement, Test FSCR-1	186
F-4. Graph of Lateral Deceleration, Test FSCR-1	187
F-5. Graph of Lateral Occupant Impact Velocity, Test FSCR-1	188
F-6. Graph of Lateral Occupant Displacement, Test FSCR-1	189
F-7. Graph of Roll, Pitch and Yaw Angular Displacements, Test FSCR-1	190
G-1. Graph of Longitudinal Deceleration, Test FSCR-2	192

G-2. Graph of Longitudinal Occupant Impact Velocity, Test FSCR-2	193
G-3. Graph of Longitudinal Occupant Displacement, Test FSCR-2	194
G-4. Graph of Lateral Deceleration, Test FSCR-2	195
G-5. Graph of Lateral Occupant Impact Velocity, Test FSCR-2	196
G-6. Graph of Lateral Occupant Displacement, Test FSCR-2	197
H-1. Graph of Longitudinal Deceleration, Test FSCR-3	199
H-2. Graph of Longitudinal Occupant Impact Velocity, Test FSCR-3	200
H-3. Graph of Longitudinal Occupant Displacement, Test FSCR-3	201
H-4. Graph of Lateral Deceleration, Test FSCR-3	202
H-5. Graph of Lateral Occupant Impact Velocity, Test FSCR-3	203
H-6. Graph of Lateral Occupant Displacement, Test FSCR-3	204
H-7. Graph of Roll, Pitch and Yaw Angular Displacements, Test FSCR-3	205
I-1. Graph of Longitudinal Deceleration, Test FSCR-4	207
I-2. Graph of Longitudinal Occupant Impact Velocity, Test FSCR-4	208
I-3. Graph of Longitudinal Occupant Displacement, Test FSCR-4	209
I-4. Graph of Lateral Deceleration, Test FSCR-4	210
I-5. Graph of Lateral Occupant Impact Velocity, Test FSCR-4	211
I-6. Graph of Lateral Occupant Displacement, Test FSCR-4	212
I-7. Graph of Roll and Pitch Angular Displacements, Test FSCR-4	213

List of Tables

Page

1. NCHRP Report No. 350 Test Levels, Crash Test Conditions, and Evaluation Criteria for Longitudinal Barriers	7
2. NCHRP Report No. 230 Crash Test Conditions and Evaluation Criteria for Longitudinal Barrier Transitions	7
3. Relevant NCHRP Report No. 350 Evaluation Criteria	8
4. Relevant NCHRP Report No. 230 Evaluation Criteria	9
5. NCHRP Report No. 350 TL-4 Evaluation Results - Wood System (Bridge Railing)	160
6. NCHRP Report No. 230 Evaluation Results - Wood System (Transition)	161

1 INTRODUCTION

1.1 Problem Statement

The majority of crashworthy bridge railing systems have been developed using materials such as concrete, steel, and aluminum. In addition, most of these railing systems have been constructed on reinforced concrete decks. However, a majority of the existing bridge railings have not been adapted for use on timber decks. The demand for crashworthy railing systems on timber decks has become increasingly important with the increased use of timber bridges on local roads and secondary highways.

Only recently have researchers begun to develop crashworthy railing systems for timber bridge decks. Further, all of these railing systems were designed for low to medium service level bridges. In order for timber to be a viable material in the new construction of higher service level bridges, additional bridge railing systems must be developed and crash tested for longitudinal, glue-laminated, timber bridges.

In recognition of the need to develop bridge railing systems for this higher-service level, the United States Department of Agriculture (USDA), Forest Service, Forest Products Laboratory (FPL), in cooperation with the Midwest Roadside Safety Facility (MwRSF) and the Federal Highway Administration (FHWA), undertook the task of developing a higher-service-level bridge railing and approach guardrail transition.

1.2 Objective

The objective of this research project was to further develop an aesthetic and economical bridge railing system for longitudinal, glue-laminated, timber bridges found on higher service level roadways. Consequently, the railing system would need to satisfy the Test Level 4 (TL-4) safety

performance criteria set forth in National Cooperative Highway Research Program (NCHRP) Report No. 350, *Recommended Procedures for the Safety Performance Evaluation of Highway Features* (1).

1.3 Scope

The research objective was accomplished with the successful completion of several tasks. First, a literature review was performed on previously developed low-to-medium-performance level bridge railing systems, as well as bridge railings developed for timber deck bridges. This review was deemed necessary because it was envisioned that the new bridge railing design would likely use technologies and design details from existing crashworthy railing systems. Second, bridge railing concepts were prepared so that an analysis and design phase could be performed on all structural members and connections. Third, computer simulation modeling was conducted using BARRIER VII to aid in the analysis and design of the bridge railing and approach guardrail transition systems. Fourth, a total of four full-scale vehicle crash tests were performed by using an 8000-kg single unit truck, a 2,041-kg sedan, and two $\frac{3}{4}$ -ton pickup trucks impacting the bridge rail and transition. Finally, the test results were analyzed, evaluated, and documented. Conclusions and recommendations were then made that pertain to the safety performance of each bridge railing and transition system.

2 LITERATURE REVIEW

2.1 Bridge Railings for Timber Deck Bridges

In 1988, Southwest Research Institute (SwRI) performed an evaluation of a longitudinal glulam timber and sawn lumber curb railing system attached to a longitudinal spike-laminated timber deck (2). The system evaluated at SwRI was constructed and tested with sawn lumber posts measuring nominal 203-mm wide x 305-mm deep (8-in. x 12-in.). The system had also been constructed with a non-standard size glulam rail of 152-mm x 273-mm (6-in. x 10¾ in.). The curb rail had dimensions of 152-mm x 305-mm (6-in. x 12-in.) and was attached to the deck with four 190-mm (7½-in.) diameter ASTM A325 bolts. Two crash tests were conducted according to the American Association of State Highway and Transportation Officials' (AASHTO's) *Guide Specifications for Bridge Railings* (3). The first crash test was a Performance Level 1 (PL-1) test using a 2,383-kg (5,254-lb) pickup impacting at a speed of 76.4 km/h (47.5 mph) and at an angle of 20 degrees. The second crash test was a PL-2 test using an 825-kg (1,818-lb) minicompact sedan traveling at a speed of 95.3 km/h (59.2 mph) and at an angle of 20 degrees. Although the system met AASHTO PL-1 requirements, delamination of several of the deck timbers and minor pull-out of several spikes was observed. Since this system was not widely used and was the only available crash tested railing for timber bridges, the demand continued for crashworthy bridge railings that would not damage the timber decks and would be adaptable for use on other timber decks.

In the early 1990s, researchers at the Midwest Roadside Safety Facility (MwRSF), in conjunction with the United States Department of Agriculture (USDA), Forest Service, Forest Product Laboratory (FPL), developed and tested three PL-1 bridge railings for use on longitudinal timber bridge decks - two glulam timber railings systems and one steel railing system (4-5). This

research effort provided a variety of aesthetically pleasing and economical bridge railings for timber bridge decks on low-to-medium service-level highways.

3 TEST REQUIREMENTS AND EVALUATION CRITERIA

3.1 Test Requirements

Longitudinal barriers, such as bridge railings, must satisfy the requirements provided in NCHRP Report No. 350 to be accepted for use on National Highway System (NHS) construction projects or as replacements for existing systems not meeting current safety standards. According to TL-4 of NCHRP Report No. 350, the barrier system must be subjected to three full-scale vehicle crash tests. The three crash tests are as follows:

1. Test Designation 4-10 consists of an 820-kg (1,808-lb) small car impacting at a nominal speed and angle of 100.0 km/h (62.1 mph) and 20 degrees, respectively.
2. Test Designation 4-11 consists of a 2,000-kg (4,409-lb) pickup truck impacting at a nominal speed and angle of 100.0 km/h (62.1 mph) and 25 degrees, respectively.
3. Test Designation 4-12 consists of an 8,000-kg (17,637-lb) single-unit truck impacting at a nominal speed and angle of 80.0 km/h (49.7 mph) and 15 degrees, respectively.

It should be noted that the GC-8000 bridge railing system and approach guardrail transition was designed prior to the publication of the NCHRP Report No. 350 safety performance guidelines. As such, the bridge railing system was developed according to the criteria provided in the 1989 AASHTO *Guide Specification for Bridge Railings*.

However, the AASHTO PL1 “curb system” which was successfully evaluated according to AASHTO *Guide Specifications for Bridge Railings* was used as the basis for the design of the NCHRP Report 350 TL-4 glulam railing. Further, the glulam rail previously tested at SwRI (2) was crash tested using an 825-kg (1,818-lb) minicompact sedan at 95.3 km/h (59.2 mph) and 20 degrees and a 2,383-kg (5,254-lb) pickup at 76.4 km/h (47.5 mph) and 20 degrees. Because the basic geometry of the PL1 curb system and the newly developed bridge rail were essentially the same as

the system tested at SwRI, repeating the minicompact sedan was deemed unnecessary. The test conditions for TL-4 longitudinal barriers are summarized in Table 1.

At the time the approach guardrail transition was designed and tested, it was intended to meet the requirements provided in NCHRP Report No. 230 (6). According to the Multiple Service Level 2 (MSL-2) of NCHRP Report No. 230, the transition system must be subjected to one full-scale vehicle crash test. The crash test is as follows:

1. Test Designation 30 consists of a 2,041-kg (4,500-lb) large sedan impacting the transition at 4.57 m (15 ft) upstream from the second system at a nominal speed and angle of 96.6 km/h (60 mph) and 25 degrees, respectively.

The test conditions for MSL-2 transitions are summarized in Table 2. The crash test was performed on the approach guardrail transition according to the NCHRP Report No. 230 criteria because at the time the transition was developed and tested, the GC-8000 was not intended to meet the NCHRP Report No. 350 TL-4 criteria.

3.2 Evaluation Criteria

Evaluation criteria for full-scale crash testing are based on three appraisal areas: (1) structural adequacy; (2) occupant risk; and (3) vehicle trajectory after collision. Criteria for structural adequacy are intended to evaluate the ability of the railing to contain, redirect, or allow controlled vehicle penetration in a predictable manner. Occupant risk evaluates the degree of hazard to occupants of the impacting vehicle. Vehicle trajectory after collision is a measure of the potential for the post-impact trajectory of the vehicle to cause subsequent multi-vehicle accidents. It is also an indicator of the potential safety hazard for the occupants of the other vehicles or the occupants of the impacting vehicle when subjected to secondary collisions with other fixed objects.

The evaluation criteria for NCHRP Report No. 350 and NCHRP Report No. 230 are defined in Tables 3 and 4, respectively.

Table 1. NCHRP Report No. 350 Test Levels, Crash Test Conditions, and Evaluation Criteria for Longitudinal Barriers (1).

Test Article	Test Designation	Test Article	Impact Conditions			Evaluation Criteria ¹
			Speed		Angle (degrees)	
			(km/h)	(mph)		
Longitudinal Barrier	4-10	820C	100	62.1	20	A,D,F,H,I,K,M
	4-11	2000P	100	62.1	25	A,D,F,K,L,M
	4-12	8000S	80	49.7	15	A,D,G,K,M

¹ Evaluation criteria explained in Table 3.

Table 2. NCHRP Report No. 230 Crash Test Conditions and Evaluation Criteria for Longitudinal Barrier Transitions (6).

Test Article	Test Designation	Test Vehicle	Impact Conditions			Evaluation Criteria ²
			Speed		Angle (degrees)	
			(km/h)	(mph)		
Transition	30	4500S	96.6	60	25	A,D,E,H,I

² Evaluation criteria is explained in Table 4.

Table 3. Relevant NCHRP Report No. 350 Evaluation Criteria (1)

Structural Adequacy	A. Test article should contain and redirect the vehicle; the vehicle should not penetrate, underide, or override the installation although controlled lateral deflection of the test article is acceptable.
Occupant Risk	D. Detached elements, fragments or other debris from the test article should not penetrate or show potential for penetrating the occupant compartment, or present an undue hazard to other traffic, pedestrians, or personnel in a work zone. Deformations of, or intrusions into, the occupant compartment that could cause serious injuries should not be permitted.
	F. The vehicle should remain upright during and after collision although moderate roll, pitching and yawing are acceptable.
	G. It is preferable, although not essential, that the vehicle remain upright during and after collision.
	H. Longitudinal and lateral occupant impact velocities should fall below the preferred value of 9 m/s (29.5 ft/s), or at least below the maximum allowable value of 12 m/s (39.4 ft/s).
	I. Longitudinal and lateral occupant ridedown accelerations should fall below the preferred value of 15 g's, or at least below the maximum allowable value of 20 g's.
Vehicle Trajectory	K. After collision it is preferable that the vehicle's trajectory not intrude into adjacent traffic lanes.
	L. The occupant impact velocity in the longitudinal direction should not exceed 12 m/s (39.4 ft/s) and the occupant ridedown acceleration in the longitudinal direction should not exceed 20 g's.
	M. The exit angle from the test article preferably should be less than 60 percent of test impact angle, measured at time of vehicle loss of contact with test device.

Table 4. Relevant NCHRP Report No. 230 Evaluation Criteria (6)

Structural Adequacy	A. Test article shall smoothly redirect the vehicle; the vehicle shall not penetrate or go over the installation although controlled lateral deflection of the test article is acceptable.
	D. Detached elements, fragments or other debris from the test article shall not penetrate or show potential for penetrating the passenger compartment or present undue hazard to other traffic.
Occupant Risk	E. The vehicle shall remain upright during and after collision although moderate roll, pitching and yawing are acceptable. Integrity of the passenger compartment must be maintained with essentially no deformation or intrusion.
Vehicle Trajectory	H. After collision, the vehicle trajectory and final stopping position shall intrude a minimum distance, if at all, into adjacent traffic lanes.
	I. In test where the vehicle is judged to be redirected into or stopped while in adjacent lanes, vehicle speed change during test article collision should be less than 24.1 km/h (15 mph) and the exit angle from the test article should be less than 60 percent of test impact angle, both measured at time of vehicle loss of contact with test device.

4 TEST SITE PREPARATION

4.1 Bridge Deck and Substructure

A full-size simulated timber bridge system was constructed at the MwRSF outdoor test site. In order to simulate an actual timber bridge installation, the longitudinal glulam timber bridge deck was mounted on six reinforced concrete bridge supports (retaining wall spread footings). The construction site is provided in Figure 1. The construction phase of the supports is shown in Figures 2 and 3. The inner three concrete bridge supports had a center-to-center spacing of 5.72 m (18 ft-9 in.) while the outer two spacing were 5.56 m (18 ft-3 in.). The concrete bridge supports were constructed perpendicular to the longitudinal glulam timber bridge deck, providing a simple span between the concrete bridge supports.

The top of the two exterior concrete bridge supports were 305-mm wide x 2,743-mm long (1-ft x 9-ft). Six bolt anchors were placed in the top surface of the support for the future mounting of the timber deck, as shown in Figure 4. The edge distance of the first anchor from the traffic side of the support was 203-mm (8-in.) with a 406-mm (1-ft 4-in.) center-to-center spacing for the remaining five anchors in the row. The anchors were placed on the centerline of the outer two concrete bridge supports.

The top of the four interior concrete bridge supports were 610-mm wide x 2,743-mm long (2-ft x 9-ft). Twelve bolt anchors were placed in the top surface of the support for the mounting of the timber deck. The edge distance of the anchors from the traffic side of the support was 203-mm (8-in.) for the first anchor with a 406-mm (1-ft 4-in.) center-to-center spacing for the remaining five anchors in the row. The two rows of anchors were placed in the center of the four supports at 152-mm (6-in.) off center.

The longitudinal glulam timber deck consisted of ten rectangular panels. The panels measured 1,216-mm wide x 5,702-mm long x 273-mm thick (3-ft 11⁷/₈-in. x 18-ft 8¹/₂-in. x 10³/₄-in.). The timber deck was constructed so that two panels formed the width of the deck and the five panels formed the length of the deck. The longitudinal glulam timber deck was fabricated with West Coast Douglas Fir and treated with pentachlorophenol in heavy oil to a minimum net retention of 9.61 kg/m³ (0.6 lb/ft³) as specified in AWWA Standard C14 (7). The timber deck is shown in Figure 5.

The timber deck panels were placed on a neoprene bearing pad located between the concrete bridge supports and the timber deck panels, as shown in Figure 5. The thickness of the neoprene bearing pad varied between 1.59 mm (1/16 in.) and 12.7 mm (½ in.). The pad was used to level the timber deck panels. The timber deck panels were mounted on the concrete bridge supports with 25-mm (1-in.) diameter ASTM A307 bolts. The head of each bolt was recessed into the top of the timber deck panels.

Structural steel angles, measuring 127 mm x 127 mm x 7.94 mm (5 in. x 5 in. x ⁵/₁₆ in.), were bolted between the backside vertical face of the timber deck and the top surface of the concrete bridge supports in order to provide additional lateral support. One section of angle was placed on each of the six concrete bridge supports. The length of the angle was 305-mm (1-ft) and 610-mm (2-ft) for the exterior and interior supports, respectively. The angles were bolted to the top of the concrete bridge supports with two 19-mm (³/₄-in.) diameter ASTM A325 bolts with self-drilling anchors recessed in the supports.

At each longitudinal midspan location of the timber deck panels, stiffener beams were bolted transversely across the bottom side of the timber deck panels per AASHTO bridge design requirements. The stiffener beams measured 130-mm wide x 152-mm thick x 2,438-mm long (5¹/₈-

in. x 6-in. x 8-ft). Six ASTM A307 19-mm ($\frac{3}{4}$ -in.) diameter x 483-mm (19-in.) long bolts were used to attach the beams.



Figure 1. Bridge Site Prior to Construction



Figure 2. Construction of Concrete Bridge Supports.

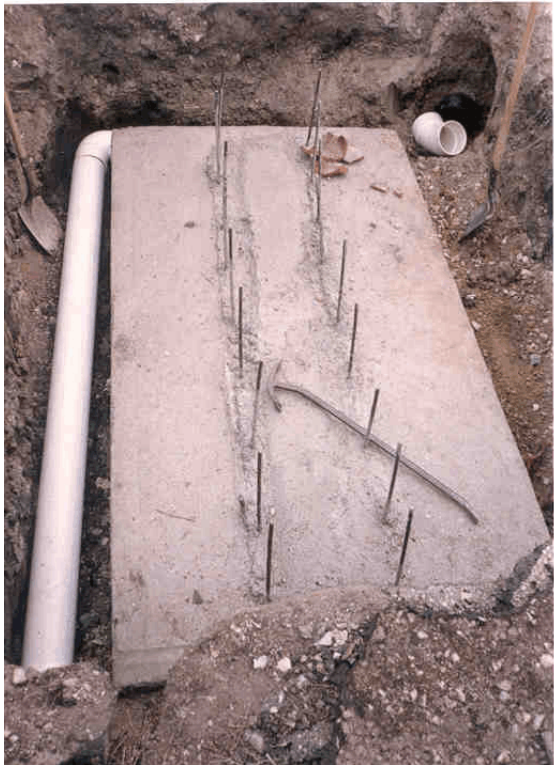


Figure 3. Vertical Rebar in Concrete Bridge Supports.



Figure 4. Top View of the Concrete Bridge Supports with Anchor Placement.



Figure 5. Longitudinal Glulam Timber Deck.

5 TEST CONDITIONS

5.1 Test Facility

The testing facility is located at the Lincoln Air-Park on the northwest (NW) side of the Lincoln Municipal Airport and is approximately 8.0 km (5 mi) NW of the University of Nebraska-Lincoln.

5.2 Vehicle Tow and Guidance System

A reverse cable tow system with a 1:2 mechanical advantage was used to propel the test vehicle. The distance traveled and the speed of the tow vehicle were one-half that of the test vehicle. The test vehicle was released from the tow cable before impact with the barrier. A fifth wheel, built by Nucleus Corporation, was located on the tow vehicle and used in conjunction with a digital speedometer increase the accuracy of the test vehicle impact speed.

A vehicle guidance system developed by Hinch (8) was used to steer the test vehicle. A guide-flag, attached to the left-front wheel and the guide cable, was sheared off before impact. The 9.5-mm (0.37-in.) diameter guide cable was tensioned to approximately 13.3-kN (2990-lbf), and supported laterally and vertically every 30.48 m (100 ft) by hinged stanchions. The hinged stanchions stood upright while holding up the guide cable, but as the vehicle was towed down the line, the guide-flag struck and knocked each stanchion to the ground. For the single-unit truck test, the vehicle guidance system was approximately 610-m (2,001-ft) long. For the sedan and pickup truck tests, the vehicle guidance system was approximately 305-m (1,000-ft) long.

5.3 Test Vehicle

Four full-scale vehicle crash tests were performed during the development of the steel bridge railing and approach guardrail transition system. Test nos. FSCR-1, FSCR-3, and FSCR-4 were

performed on the bridge railing, while test no. FSCR-2 was conducted on the approach guardrail transition.

For test no. FSCR-1, a 1986 GMC 7000 series single-unit truck was used as the test vehicle. The test inertial and gross static weights were 8,165 kg (18,000 lbs). The test vehicle is shown in Figure 6, and vehicle dimensions are shown in Figure 7.

For test no. FSCR-2, a 1987 Ford LTD Crown Victoria was used as the test vehicle. The test inertial and gross static weights were 2,044 kg (4,506 lbs). The test vehicle is shown in Figure 8, and vehicle dimensions are shown in Figure 9.

For test no. FSCR-3, a 1986 Ford F-250 $\frac{3}{4}$ -ton pickup truck was used as the test vehicle. The test inertial and gross static weights were 2,045 kg (4,509 lbs). The test vehicle is shown in Figure 10, and vehicle dimensions are shown in Figure 11.

For test no. FSCR-4, a 1984 Chevrolet Custom Deluxe 20 $\frac{3}{4}$ -ton pickup truck was used as the test vehicle. The test inertial and gross static weights were 2,087 kg (4,600 lbs). The test vehicle is shown in Figure 12, and vehicle dimensions are shown in Figure 13.

5.3.1 Center-of-Mass Determination, Vehicle Targets, and Alignment

The Suspension Method (9) was used to determine the vertical component of the center of gravity for the pickup truck test vehicles. This method is based on the principle that the center of gravity of any freely suspended body is in the vertical plane through the point of suspension. The vehicle was suspended successively in three positions, and the respective planes containing the center of gravity were established. The intersection of these planes pinpointed the location of the center of gravity. The Elevated Axle Method (10) was used to determine the vertical component of the center of gravity for the single-unit trucks. This method converts measured wheel weights at

different elevations to the location of the vertical component of the center of gravity. The longitudinal component of the center of gravity was determined using the measured axle weights. The locations of the final centers of gravity are shown in Figures 6 through 13. Vehicle ballast, consisting of steel plates and/or sand bags, was used to obtain the desired test weight.

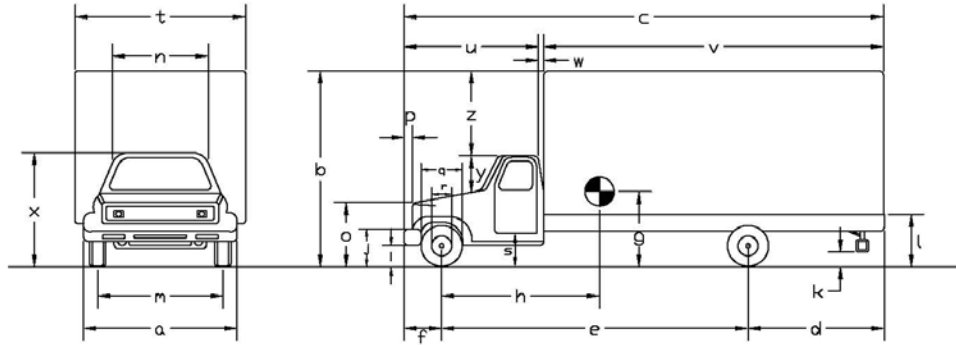
Square, black and white-checkered targets were placed on the vehicle to aid in the analysis of the high-speed film, as shown in Figures 6, 8, 10, 12, and 14 through 17. Round, checkered targets were placed on the center of gravity on the driver's side, the passenger's side, and on the roof of the vehicle. The remaining targets were located at convenient reference locations for viewing from the high-speed cameras for film analysis.

The front wheels of the test vehicles were aligned for camber, caster, and toe-in values of zero so that the vehicles would track properly along the guide cable. Two 5B flash bulbs were mounted on both the hood and roof of the vehicles to pinpoint the time of impact with the barrier on the high-speed film. The flash bulbs were fired by a pressure tape switch mounted on the front face of the bumper. A remote controlled brake system was installed in the test vehicles so the vehicles could be brought safely to a stop after the test.



Figure 6. Test Vehicle, Test FSCR-1

Date: 4/2/03 Test Number: FSCR-1 Model: 7000 Series
 Tire Sz FR: -- Odometer: -- Make: GMC
 Tire Sz RR: -- V.I.N. #: -- Year: 1986



Vehicle Geometry - mm (inches)

a> fr. bump. width	<u>2261 (89)</u>	j> fr. bump. top	<u>--</u>	s> bot. door height	<u>--</u>
b> overall height	<u>3353 (132)</u>	k> rr. bump. bot.	<u>--</u>	t> overall width	<u>2436 (95.9)</u>
c> overall length	<u>10056 (395.9)</u>	l> rr. frame top	<u>1232 (48.5)</u>	u> cab length	<u>2426 (95.5)</u>
d> rear overhang	<u>3251 (128)</u>	m> fr. track width	<u>1937 (76.25)</u>	v> trlr/box length	<u>7516 (295.9)</u>
e> wheel base	<u>6068 (238.9)</u>	n> roof width	<u>1473 (58)</u>	w> gap width	<u>114 (4.5)</u>
f> front overhang	<u>737 (29)</u>	o> hood height	<u>1664 (65.5)</u>	x> overall fr. height	<u>2210 (87)</u>
g> C.G. height	<u>1245 (49)</u>	p> bump. extension	<u>--</u>	y> roof-hood dist.	<u>546 (21.5)</u>
h> C.G. hor. dist.	<u>3165 (124.6)</u>	q> fr. tire width	<u>--</u>	z> roof height dif.	<u>1143 (45)</u>
i> fr. bump. bot.	<u>521 (20.5)</u>	r> fr. wheel width	<u>--</u>		

Weights - kg (lbs)

	Curb	Test Inertial	Gross Static
W _{front axle}	<u>2094 (4616)</u>	<u>3906 (8611)</u>	<u>3906 (8611)</u>
W _{rear axle}	<u>2981 (6572)</u>	<u>4259 (9389)</u>	<u>4259 (9389)</u>
W _{TOTAL}	<u>5075 (11188)</u>	<u>8165 (18000)</u>	<u>8165 (18000)</u>

Ballast 2976 (6560)

wheel center height front --
 wheel center height rear --
 wheel well clearance (FR) --
 wheel well clearance (RR) --
 Engine Type --
 Engine Size --
 Transmission Type:
 Automatic or Manual
 FWD or RWD or 4WD

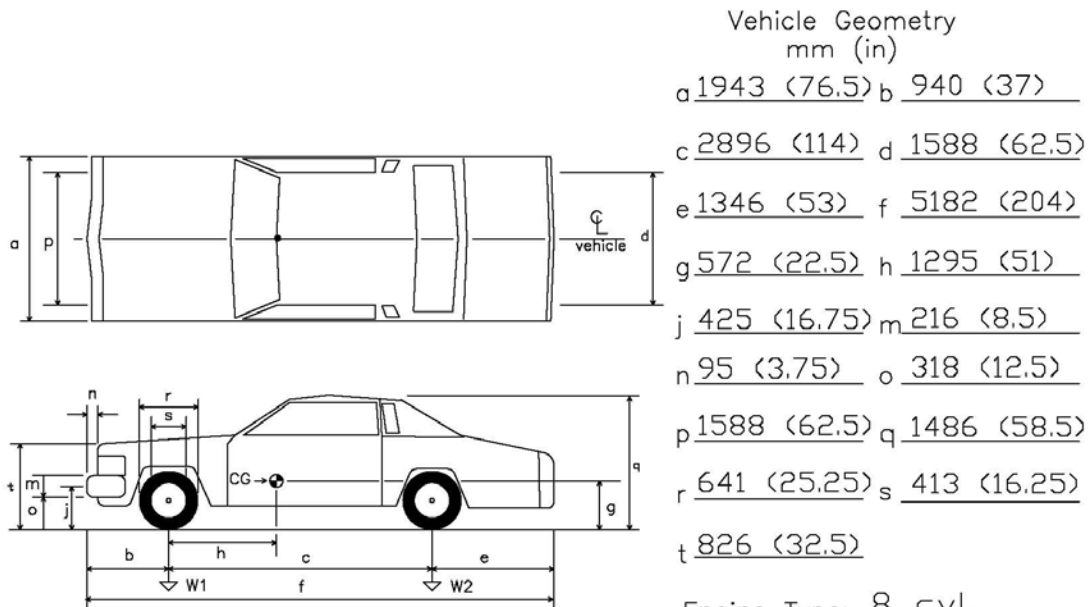
Note any damage prior to test: _____

Figure 7. Vehicle Dimensions, Test FSCR-1



Figure 8. Test Vehicle, Test FSCR-2

Date: 11/10/93 Test No.: FSCR-2 Year: 1987
 Make: Ford Vehicle I.D.#: 2FABP72G8HX170763
 Tire Size: P215-75R15 front Model: Crown Victoria
P225-75r15 rear Odometer: 138,876 miles



Engine Type: 8 cyl.

Engine Size: 351 ci

Transmission Type:
automatic

Weight			
kg (lb)	Curb	Test Inertial	Gross Static
W1	<u>1052 (2320)</u>	<u>1129 (2490)</u>	<u>1129 (2490)</u>
W2	<u>721 (1590)</u>	<u>914 (2016)</u>	<u>914 (2016)</u>
Wtotal	<u>1774 (3910)</u>	<u>2044 (4506)</u>	<u>2044 (4506)</u>

Damage prior to test: none

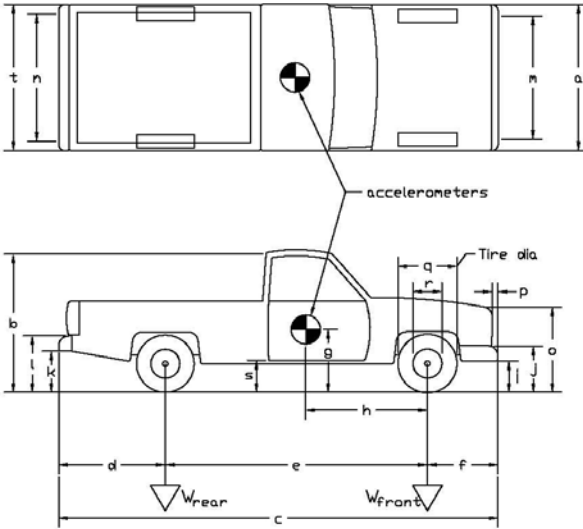
Figure 9. Vehicle Dimensions, Test FSCR-2



Figure 10. Test Vehicle, Test FSCR-3

Date: 11/18/93 Test Number: FSCR-3 Model: F250
 Make: Ford Vehicle I.D.#: 2FTHF25YOGCB47711
 Tire Size: P235/85R16 Year: 1986 Odometer: 78048

*(All Measurements Refer to Impacting Side)

		Vehicle Geometry - mm (in.)																					
		a <u>1905 (75)</u>	b <u>1905 (75)</u>																				
		c <u>5436 (214)</u>	d <u>1295 (51)</u>																				
		e <u>3391 (133.5)</u>	f <u>737 (29)</u>																				
		g <u>749 (29.5)</u>	h <u>1549 (61)</u>																				
		i <u>508 (20)</u>	j <u>724 (28.5)</u>																				
		k <u>--</u>	l <u>--</u>																				
		m <u>1664 (65.5)</u>	n <u>--</u>																				
		o <u>1219 (48)</u>	p <u>127 (5)</u>																				
		q <u>787 (31)</u>	r <u>432 (17)</u>																				
		s <u>--</u>	t <u>--</u>																				
		Wheel Center Height Front <u>--</u>																					
		Wheel Center Height Rear <u>--</u>																					
		Wheel Well Clearance (FR) <u>--</u>																					
		Wheel Well Clearance (RR) <u>--</u>																					
<table border="0"> <tr> <td>Weights</td> <td></td> <td></td> <td></td> </tr> <tr> <td>kg (lbs)</td> <td>Curb</td> <td>Test Inertial</td> <td>Gross Static</td> </tr> <tr> <td>W_{front}</td> <td><u>1025 (2260)</u></td> <td><u>1104 (2434)</u></td> <td><u>1104 (2434)</u></td> </tr> <tr> <td>W_{rear}</td> <td><u>889 (1960)</u></td> <td><u>941 (2075)</u></td> <td><u>941 (2075)</u></td> </tr> <tr> <td>W_{total}</td> <td><u>1914 (4220)</u></td> <td><u>2045 (4509)</u></td> <td><u>2045 (4509)</u></td> </tr> </table>		Weights				kg (lbs)	Curb	Test Inertial	Gross Static	W_{front}	<u>1025 (2260)</u>	<u>1104 (2434)</u>	<u>1104 (2434)</u>	W_{rear}	<u>889 (1960)</u>	<u>941 (2075)</u>	<u>941 (2075)</u>	W_{total}	<u>1914 (4220)</u>	<u>2045 (4509)</u>	<u>2045 (4509)</u>	Engine Type <u>Gasoline</u> Engine Size <u>4.9 L</u> Transmission Type: <input checked="" type="checkbox"/> Automatic or Manual FWD or <input checked="" type="checkbox"/> RWD or 4WD	
Weights																							
kg (lbs)	Curb	Test Inertial	Gross Static																				
W_{front}	<u>1025 (2260)</u>	<u>1104 (2434)</u>	<u>1104 (2434)</u>																				
W_{rear}	<u>889 (1960)</u>	<u>941 (2075)</u>	<u>941 (2075)</u>																				
W_{total}	<u>1914 (4220)</u>	<u>2045 (4509)</u>	<u>2045 (4509)</u>																				

Note any damage prior to test: None

Figure 11. Vehicle Dimensions, Test FSCR-3

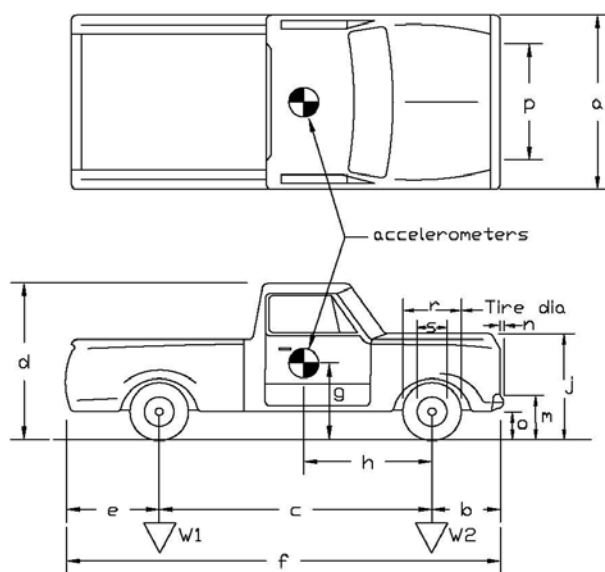


Figure 12. Test Vehicle, Test FSCR-4

Date: 11/23/93 Test No.: FSCR-4 Vehicle I.D.# 1GCGC24JDEJ162667

Make: Chevrolet Model: Custom Deluxe 20 Year: 1984

Tire Size: LT 235/85R16



Vehicle Geometry - inches

a 1981 (78) b 876 (34.5)
c 3327 (131) d 1842 (72.5)
e 1321 (52) f 5524 (217.5)
g 762 (30) h 1394 (54.9)
i _____ j 1156 (45.5)
k _____ l _____
m 656 (27) n 102 (4)
o 457 (18) p 1676 (66)
r 787 (31) s 445 (17.5)

Engine Type: Gasoline

Engine Size: 350 c.i.

4 - wheel weight: lf _____ rf _____ lr _____ rr _____

Transmission Type:

Automatic or Manual

Weight - pounds	Curb	Test Inertial	Gross Static
W1	<u>826</u> (1820)	<u>875</u> (1930)	<u>875</u> (1930)
W2	<u>1148</u> (2530)	<u>1211</u> (2670)	<u>1211</u> (2670)
Wtotal	<u>1973</u> (4350)	<u>2087</u> (4600)	<u>2087</u> (4600)

FWD or RWD or 4WD

Note any damage prior to test: Test vehicle repaired and
reused after previous testing.

Figure 13. Vehicle Dimensions, Test FSCR-4

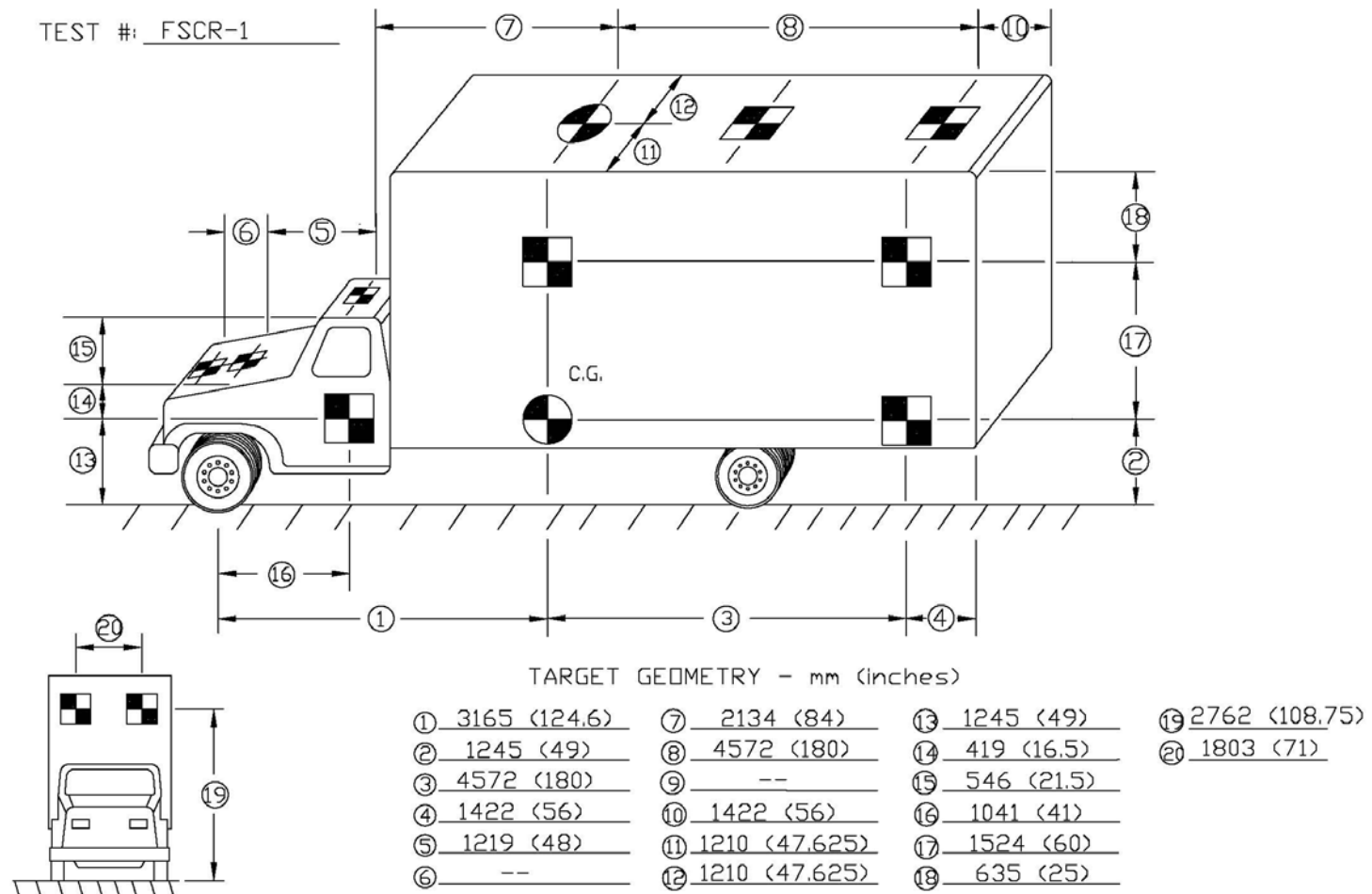


Figure 14. Vehicle Target Locations, Test FSCR-1

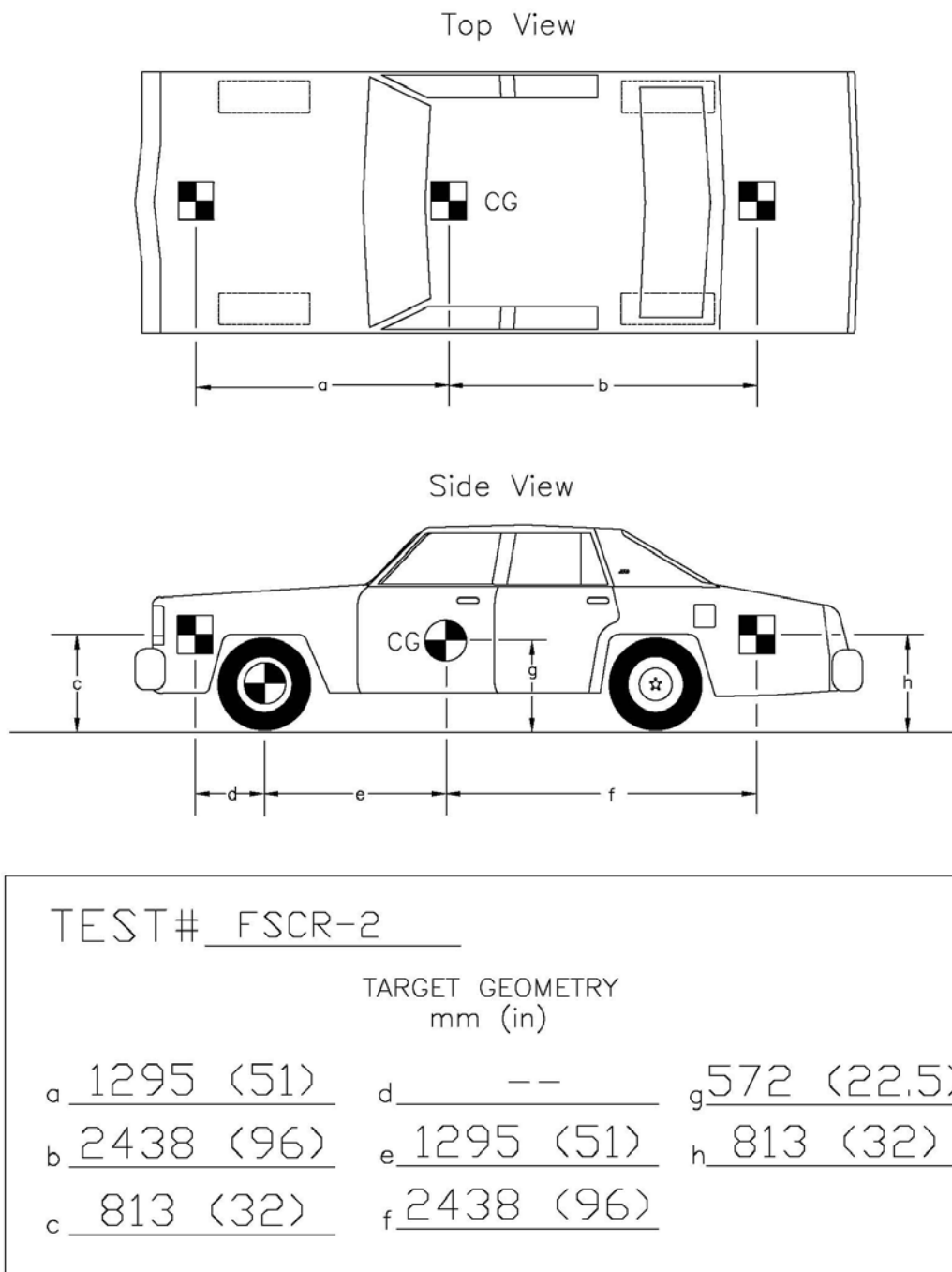
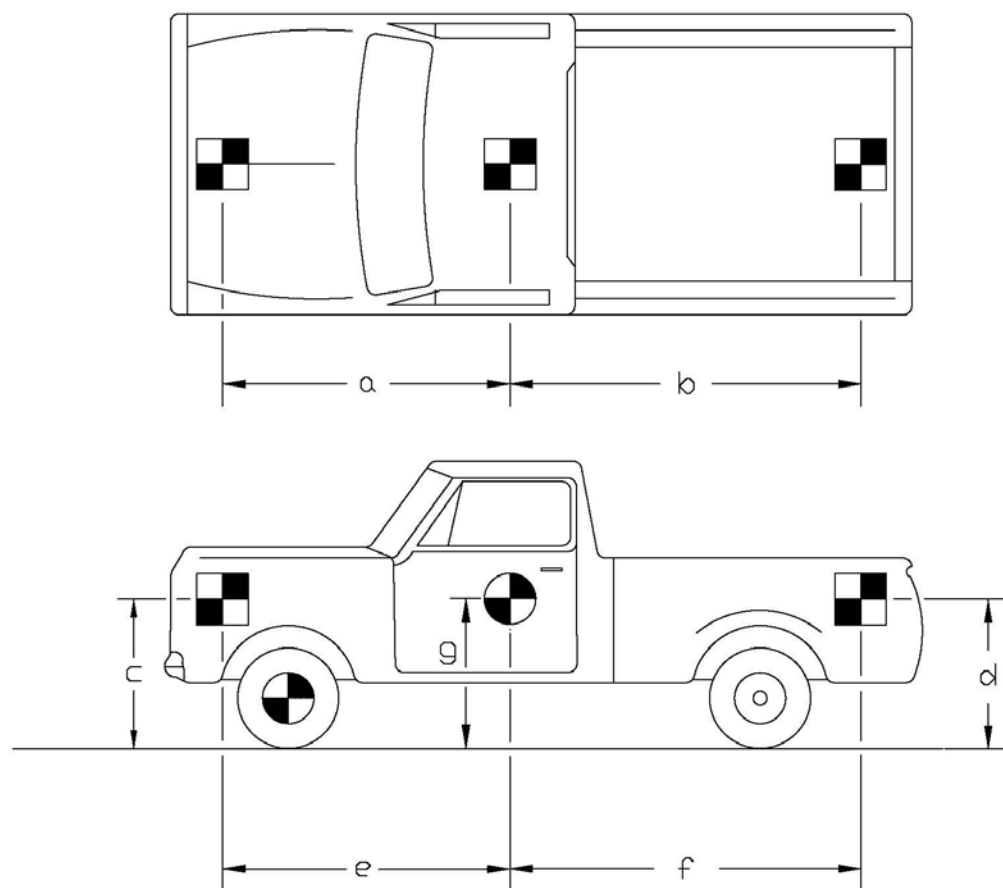
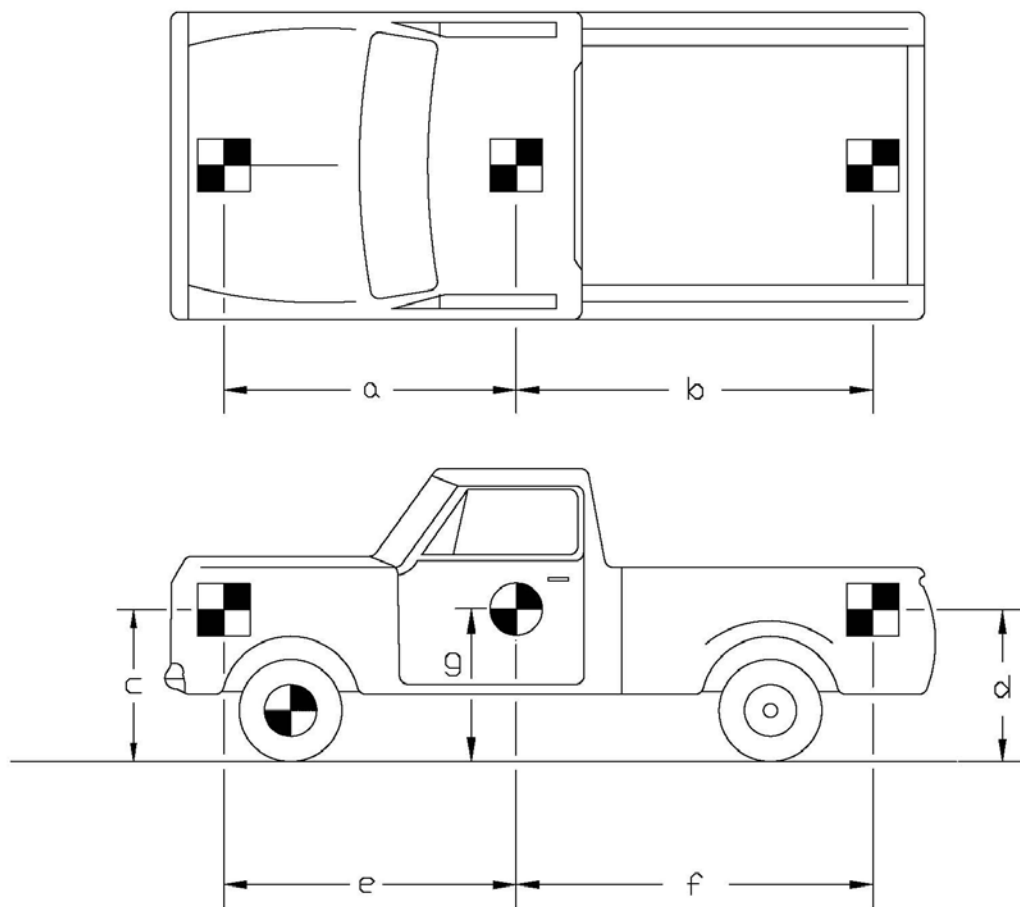


Figure 15. Vehicle Target Locations, Test FSCR-2



TEST# <u>FSCR-3</u>			
TARGET GEOMETRY			
mm (in)			
a <u>1524 (60)</u>	b <u>2743 (108)</u>	c <u>1156 (45.5)</u>	d <u>1156 (45.5)</u>
e <u>1524 (60)</u>	f <u>2743 (108)</u>	g <u>--</u>	

Figure 16. Vehicle Target Locations, Test FSCR-3



TEST# FSCR-4

TARGET GEOMETRY
mm (in)

a 1397 (55) b 2438 (96) c 1143 (45) d 1143 (45)

e 1397 (55) f 2438 (96) g 762 (30)

Figure 17. Vehicle Target Locations, Test FSCR-4

5.4 Data Acquisition Systems

5.4.1 Accelerometers

For no. test FSCR-1, one triaxial piezoresistive accelerometer system with a range of ± 200 G's (Endevco Model 7264) was used to measure the acceleration in the longitudinal, lateral, and vertical directions. The accelerometers were rigidly attached to an aluminum block mounted near the vehicle's center of gravity. Accelerometer signals were received and conditioned by an onboard Series 300 Multiplexed FM Data System built by Metraplex Corporation. The multiplexed signal was then transmitted to a Honeywell 101 Analog Tape Recorder. Computer software, "EGAA" and "DADiSP", were used to digitize, analyze, and plot the accelerometer data.

For test nos. FSCR-2, FSCR-3, and FSCR-4, a triaxial piezoresistive accelerometer system with a range of ± 200 G's was used to measure the acceleration in the longitudinal, lateral, and vertical directions at a sample rate of 3,200 Hz. The environmental shock and vibration sensor/recorder system, Model EDR-3, was developed by Instrumented Sensor Technology (IST) of Okemos, Michigan. The EDR-3 was configured with 256 Kb of RAM memory and a 1,120 Hz lowpass filter. Computer software, "DynaMax 1 (DM-1)" and "DADiSP", were used to digitize, analyze, and plot the accelerometer data.

5.4.2 Rate Transducer

For test nos. FSCR-1, FSCR-2, FSCR-3 and FSCR-4, a Humphrey 3-axis rate transducer with a range of 250 deg/sec in each of the three directions (pitch, roll, and yaw) was used to measure the angular velocity of the test vehicles. The rate transducer was rigidly attached to the vehicles near the center of gravity of the test vehicle. Rate transducer signals, excited by a 28 volt DC power source, were received and conditioned by an onboard Series 300 Multiplexed FM Data System built

by Metraplex Corporation. The multiplexed signal was then transmitted to a Honeywell 101 Analog Tape Recorder. Computer software, “EGAA” and “DADiSP”, were used to digitize, analyze, and plot the accelerometer data.

5.4.3 High-Speed Photography

For test nos. FSCR-1, FSCR-2, and FSCR-3, four high-speed 16-mm cameras, with operating speeds of approximately 500 frames/sec, were used to film the crash tests. A Redlake Locam, with a wide-angle 12.5-mm lens, was placed above the test installation to provide an overhead field of view perpendicular to the ground. A Locam, with a 76-mm lens, and a Photec IV camera, with an 80-mm lens, were placed downstream from the impact point and had a field of view parallel to the barrier. Another Photec IV camera, with a 55-mm lens, was placed on the traffic side of the barrier and had a field of view perpendicular to the barrier. A schematic of all four camera locations for test nos. FSCR-1, FSCR-2, and FSCR-3 are shown in Figures 18, 19, and 20 respectively.

For test no. FSCR-4, five high-speed 16-mm cameras, with operating speeds of approximately 500 frames/sec, were used to film the crash test. A Redlake Locam, with a wide-angle 12.5-mm lens, was placed above the test installation to provide an overhead field of view perpendicular to the ground. A Locam, with a 76-mm lens, and a Photec IV camera, with an 80-mm lens, were placed downstream from the impact point and had a field of view parallel to the barrier. Another Photec IV camera, with a 55-mm lens, was placed on the traffic side of the barrier and had a field of view perpendicular to the barrier. Another Locam, with a 25 mm lens, was placed downstream and behind the barrier. A schematic of all five camera locations for test FSCR-4 is shown in Figure 21.

For test nos. FSCR-1, FSCR-2, FSCR-3, and FSCR-4, four white reference lines were

painted on the bridge deck wearing surface on the traffic side of the bridge rail. The lines were incremented on approximately 2.4-m (8-ft) centers and provided a visible reference system for use in the analysis of the overhead high-speed film. The film was analyzed using the Vanguard Motion Analyzer. Actual camera speed and camera divergence factors were considered in the analysis of the high-speed film.

5.4.4 Pressure Tape Switches

For test nos. FSCR-1, FSCR-2, and FSCR-3, seven pressure-activated tape switches, spaced at 1.52-m (5-ft) intervals, were used to determine the speed of the vehicle before impact. For test no. FSCR-4, five pressure-activated tape switches, spaced at 1.52-m (5-ft) intervals, were used to determine the speed of the vehicle before impact. Each tape switch fired a strobe light which sent an electronic timing signal to the data acquisition system as the left-front tire of the test vehicle passed over it. Test vehicle speeds were determined from electronic timing mark data recorded on "EGAA" software. Strobe lights and high-speed film analysis are used only as a backup in the event that vehicle speeds cannot be determined from the electronic data.

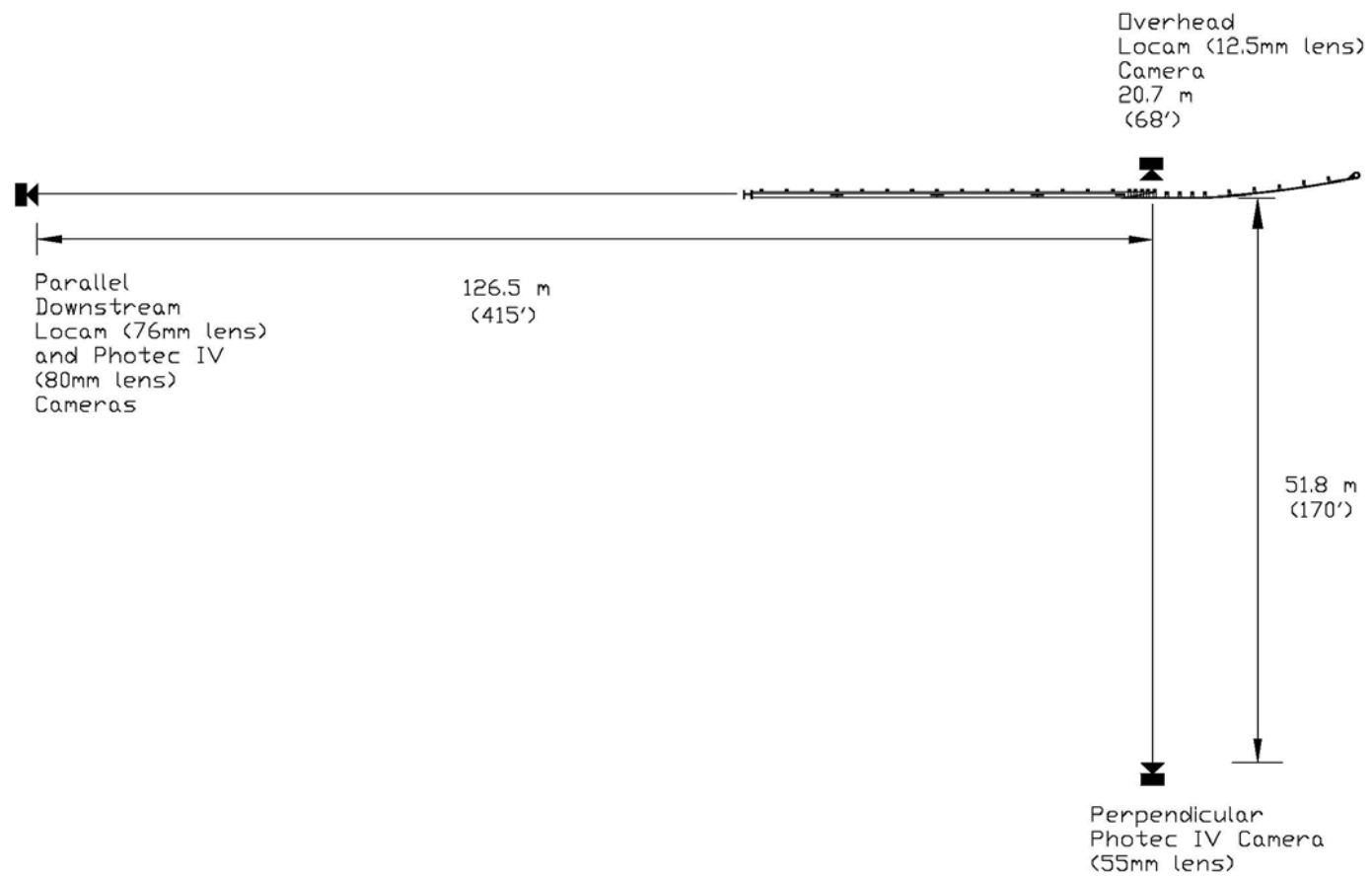


Figure 18. Location of High-Speed Cameras, Test FSCR-1

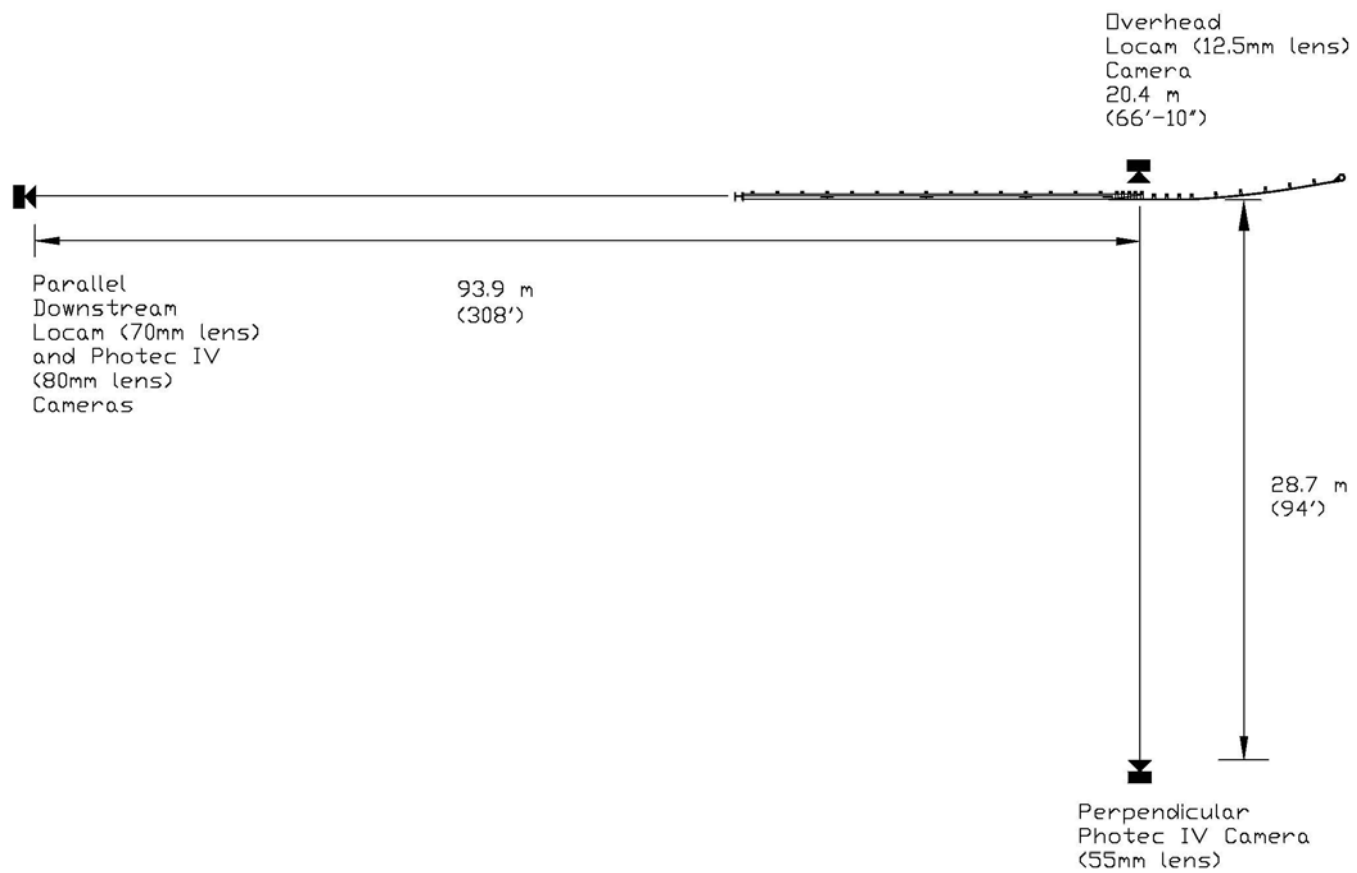


Figure 19. Location of High-Speed Cameras, Test FSCR-2

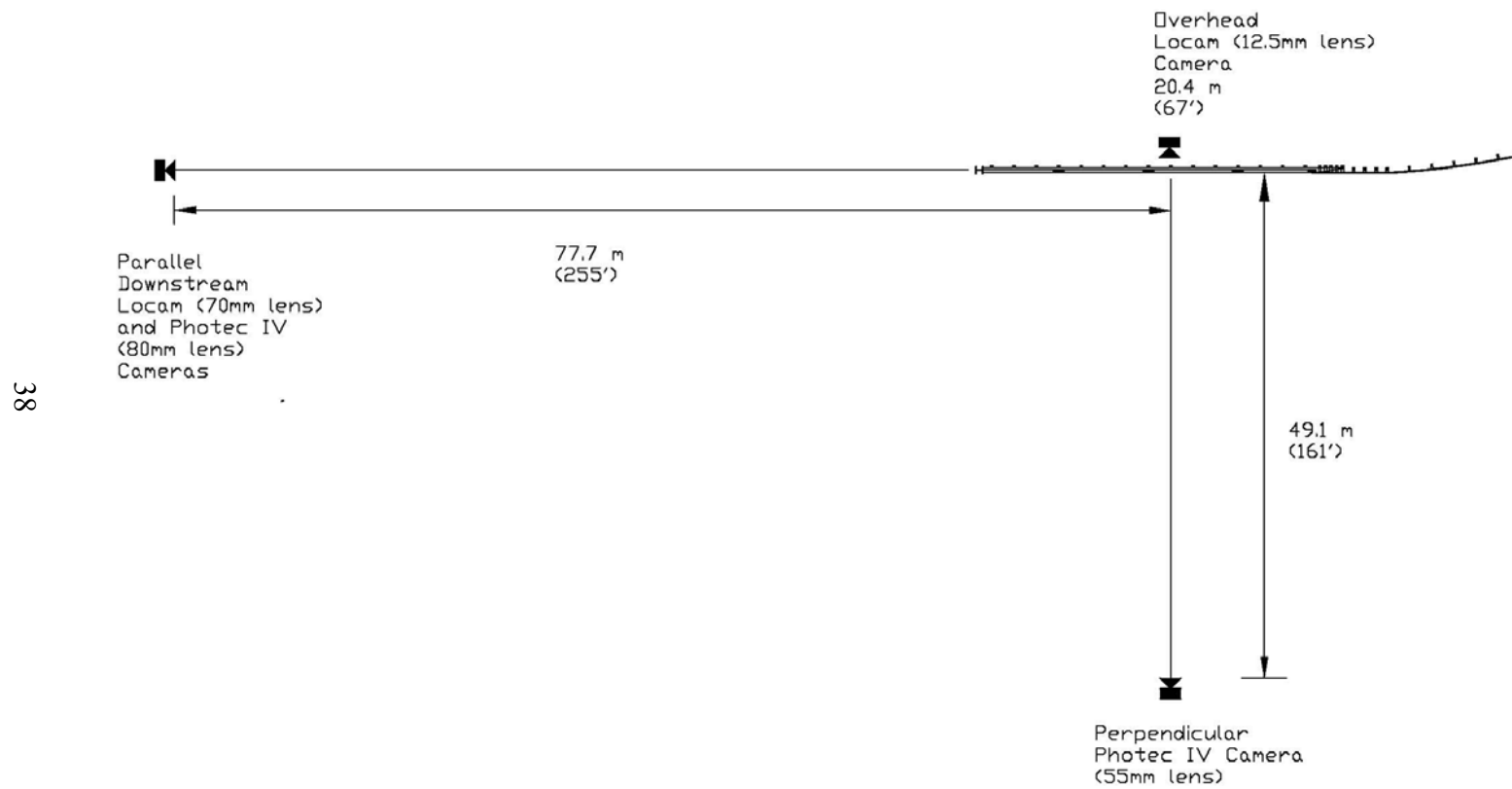


Figure 20. Location of High-Speed Cameras, Test FSCR-3

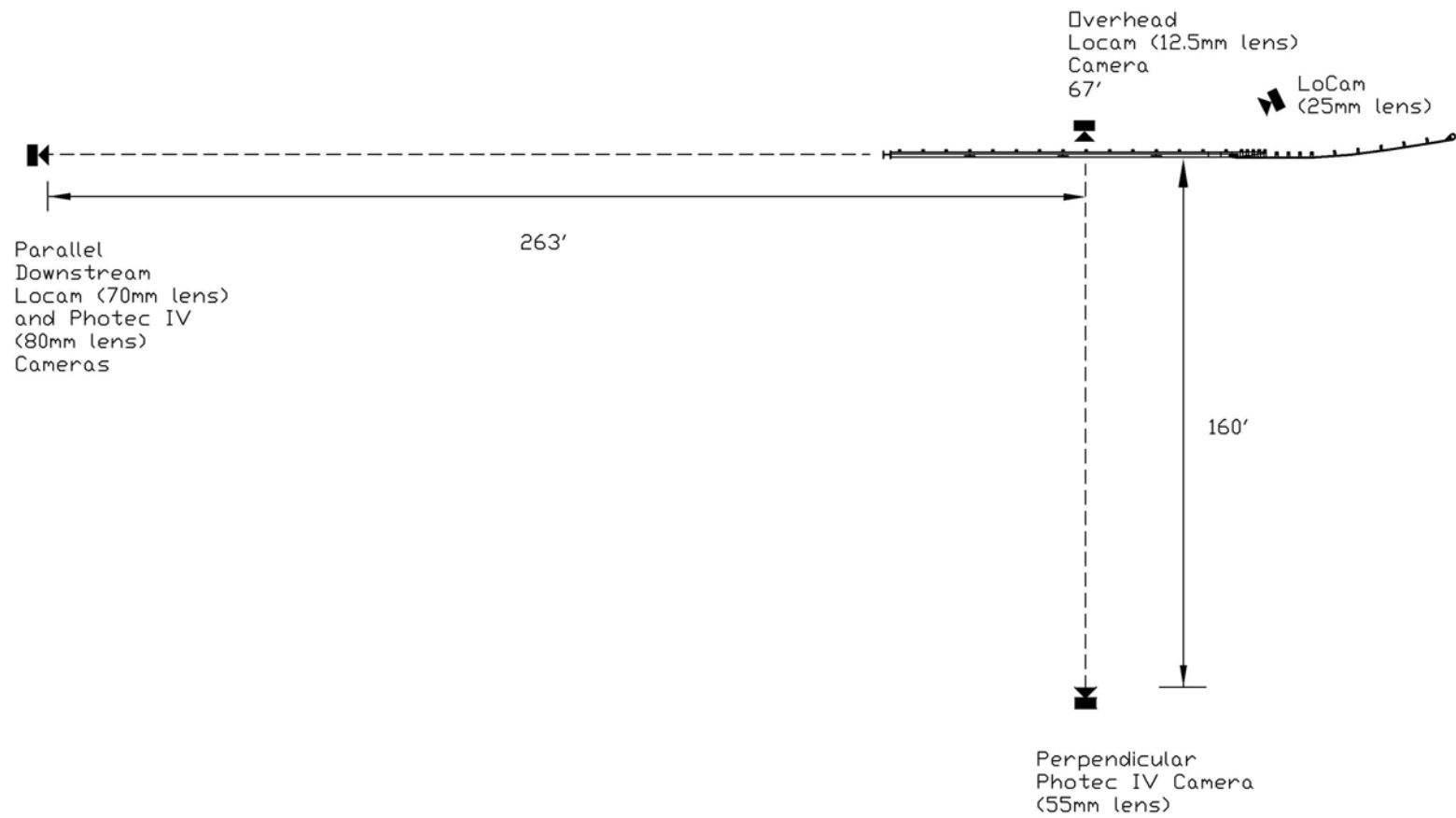


Figure 21. Location of High-Speed Cameras, Test FSCR-4

6 SYSTEM DEVELOPMENT

Following the successful development and full-scale vehicle crash testing of the AASHTO PL-1 "Curb System" (4-5), it was determined that the PL-1 bridge railing had adequate structural capacity and could be modified to meet a higher performance level. Therefore, the AASHTO PL-1 "Curb System" served as the basis for the design of the NCHRP Report 350 TL-4 glulam railing. The glulam rail previously tested at SwRI (2) was crash tested using an 825-kg (1,818-lb) minicompact at 95.3 km/hr (59.2 mph) and 20 degrees, and a 2,383-kg (5,254-lb) pickup at 76.4 km/hr (47.5 mph) and 20 degrees. Because the basic geometry of the PL-1 curb system and the newly developed GC-8000 were essentially the same as the system tested at SwRI, repeating the minicompact sedan was deemed unnecessary. However, to meet the TL-4 criteria, the 2000-kg (4,409-lb) unballasted pickup truck test at 100km/h (62.1 mph) and 25 degrees and the 8,000-kg (17,637-lb) single-unit truck test at 80 km/h (49.7 mph) and 15 degrees would have to be conducted.

Development of the GC-8000 consisted of resizing the structural components previously used with the AASHTO PL-1 "Curb System" to withstand the higher impact forces generated from the TL-4 crash test conditions. The components changed included the timber glulam rail, lumber posts, spacer and scupper blocks, and structural steel hardware. The PL-1 "Curb System" was constructed with sawn lumber Douglas fir posts measuring 203-mm (8-in.) wide and 203-mm (8-in.) deep. The glulam rail was 171-mm (6¾-in.) wide and 267-mm (10½-in.) deep. However, computer simulation modeling indicated that the GC-8000 bridge rail posts needed to be 203-mm (8-in.) wide and 254-mm (10-in.) deep, and the glulam rail needed to be 171-mm (6¾-in.) wide and 343-mm (13½-in.) deep. The scupper blocks, used to support the sawn lumber curb rail and transfer the impact forces into the timber deck, were increased in length from 0.91 to 1.22 m (3 to 4 ft) and in

depth from 140 to 191 mm ($5\frac{1}{2}$ to $7\frac{1}{2}$ in.). The increase in length of the scupper blocks was required to accommodate the six 19-mm ($\frac{3}{4}$ -in.) diameter ASTM A307 bolts needed to carry the increased impact forces into the deck. The increase in depth of the scupper blocks was used to accommodate a 51-mm (2-in.) asphalt wearing surface placed on the timber deck.

7 SYSTEM DESIGN DETAILS

7.1 Wood Bridge Railing

The GC-8000 bridge railing system consisted of five major components: (1) sawed lumber scupper blocks; (2) sawed lumber curb rail; (3) sawed lumber posts; (4) longitudinal glulam timber rail; and (5) timber spacer blocks. Photographs of the bridge railing system are shown in Figures 22 through 24. The overall layout of the bridge railing system is shown in Figure 25. Design details of the bridge railing system are shown in Figures 26 through 31.

One timber scupper block was bolted to the timber deck at each post location with six 19-mm ($\frac{3}{4}$ -in.) diameter by 660-mm (26-in.) long, ASTM A307 galvanized dome head bolts. The scupper blocks were fabricated with S4S No. 1 Grade Douglas Fir measuring 190-mm thick x 292-mm wide x 1.22-m long ($7\frac{1}{2}$ -in. x $11\frac{1}{2}$ -in. x 4-ft). The scupper blocks were attached to the curb rail and timber deck surface with 102-mm (4-in.) diameter shear plate connectors. The curb rail was fabricated with S4S No. 1 Grade Douglas Fir measuring 140-mm deep and 292-mm wide ($5\frac{1}{2}$ -in. x $11\frac{1}{2}$ -in.), with the top of the curb rail positioned 280-mm (11-in.) above the asphalt wearing surface. One 32-mm ($1\frac{1}{4}$ -in.) diameter x 635-mm (25-in.) long ASTM A307 dome head bolt was used to attach each of the fifteen bridge posts to the curb rail. Two 1.37-m (4-ft 6-in.) long, high-strength bars were placed 559-mm (22-in.) apart and positioned transversely through the outer timber deck panel at each post. Fifteen No. 1 Grade rough-sawn lumber Douglas Fir posts, measuring approximately 203-mm wide x 254-mm deep x 1.16-m long (8-in. x 10-in. x 3-ft. $9\frac{3}{4}$ -in.), were used to support the upper glulam railing at a spacing of 1.90 m (6 ft 3 in.) on centers. The posts were treated to meet AWP Standard C14 with 192.22 kg/m^3 (12 lbs/ft³) creosote (7).

The longitudinal glulam rail was fabricated from Combination No. 2 West Coast Douglas

Fir and treated in the same manner as the timber deck. The glulam rail measured 171-mm wide x 343-mm deep ($6\frac{3}{4}$ -in. x $13\frac{1}{2}$ -in.). The top mounting height of the glulam rail was 838 mm (2 ft-9 in.) above the asphalt wearing surface. The glulam rail was offset from the posts with timber spacer blocks measuring 121-mm thick x 203-mm wide x 343-mm deep ($4\frac{3}{4}$ -in. x 8-in. x $13\frac{1}{2}$ -in.). Two 16-mm ($\frac{5}{8}$ -in.) diameter x 610-mm (24 in.) long, ASTM A307 galvanized dome head bolts were used to attach the glulam rail to the timber posts.

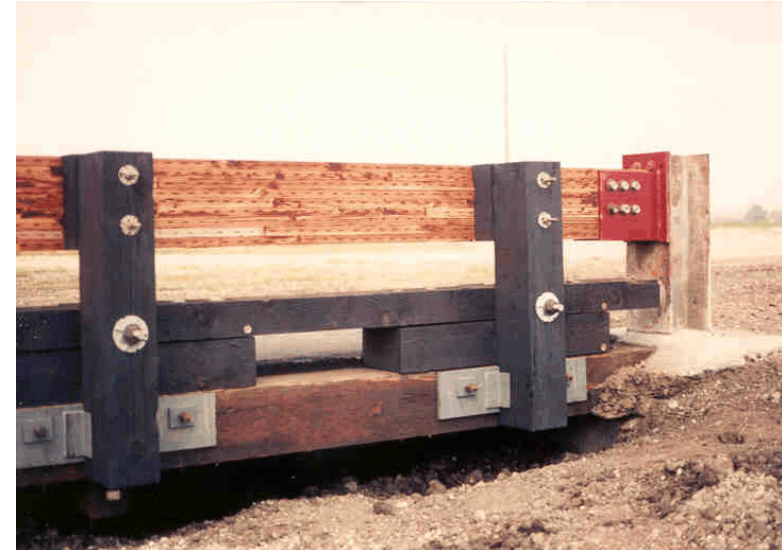


Figure 22. Bridge Railing System



Figure 23. Bridge Railing System

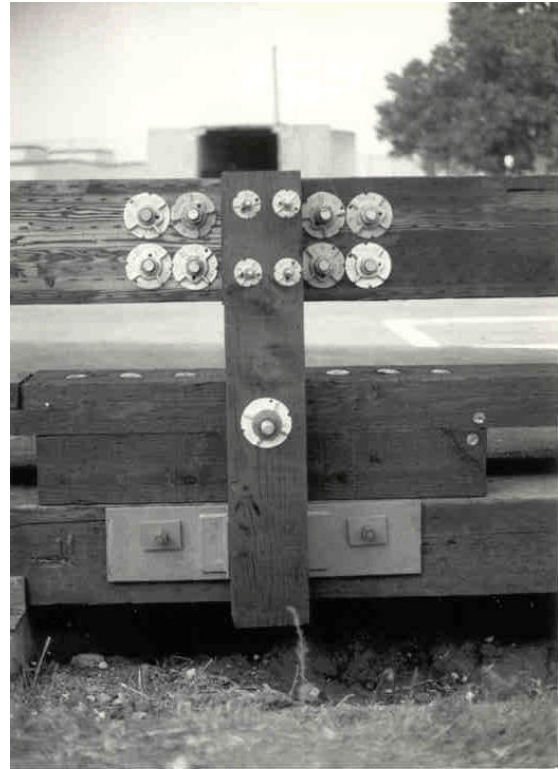


Figure 24. Bridge Railing System - Bridge Posts

Figure 25. Overall Layout of Bridge Railing System

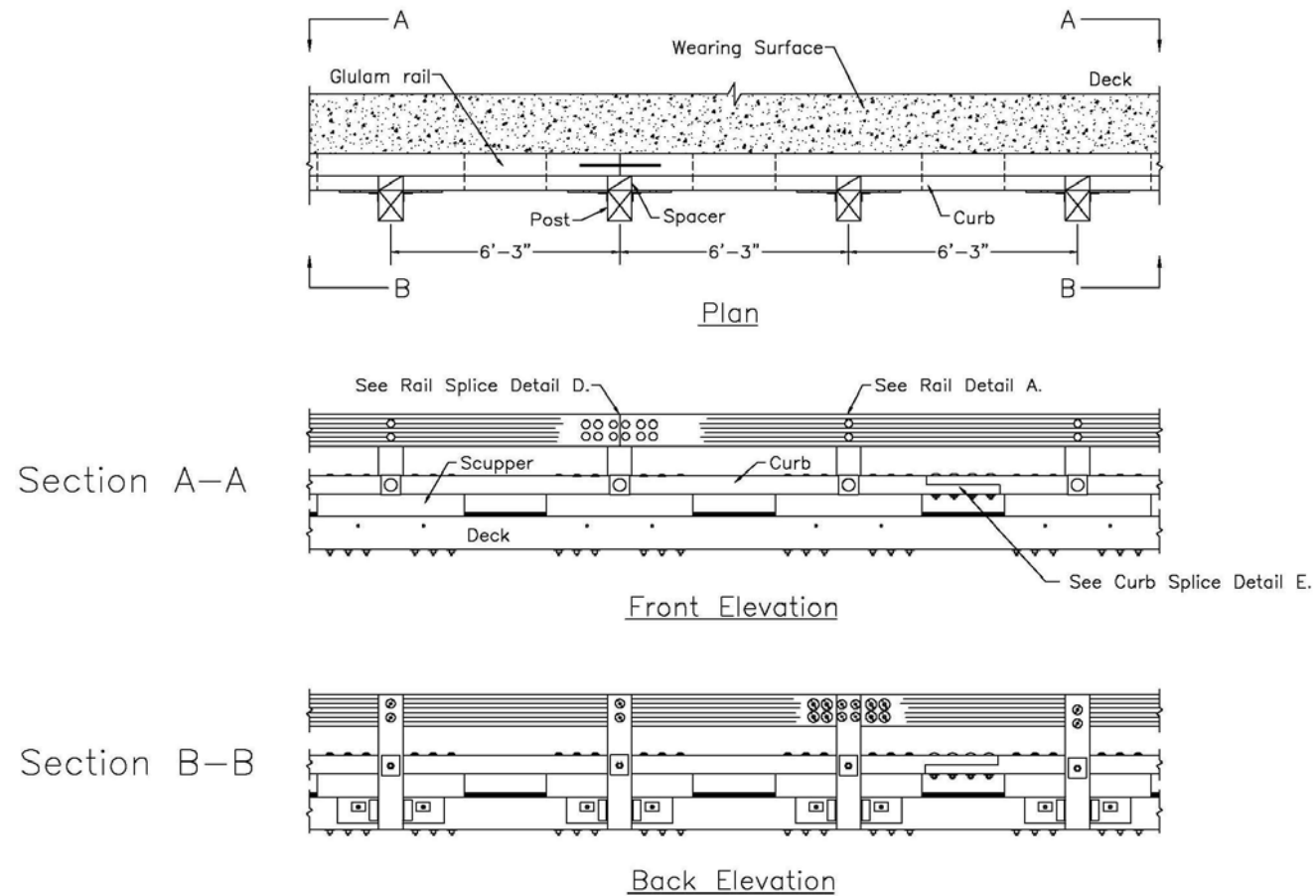


Figure 26. General Configuration of Bridge Railing System

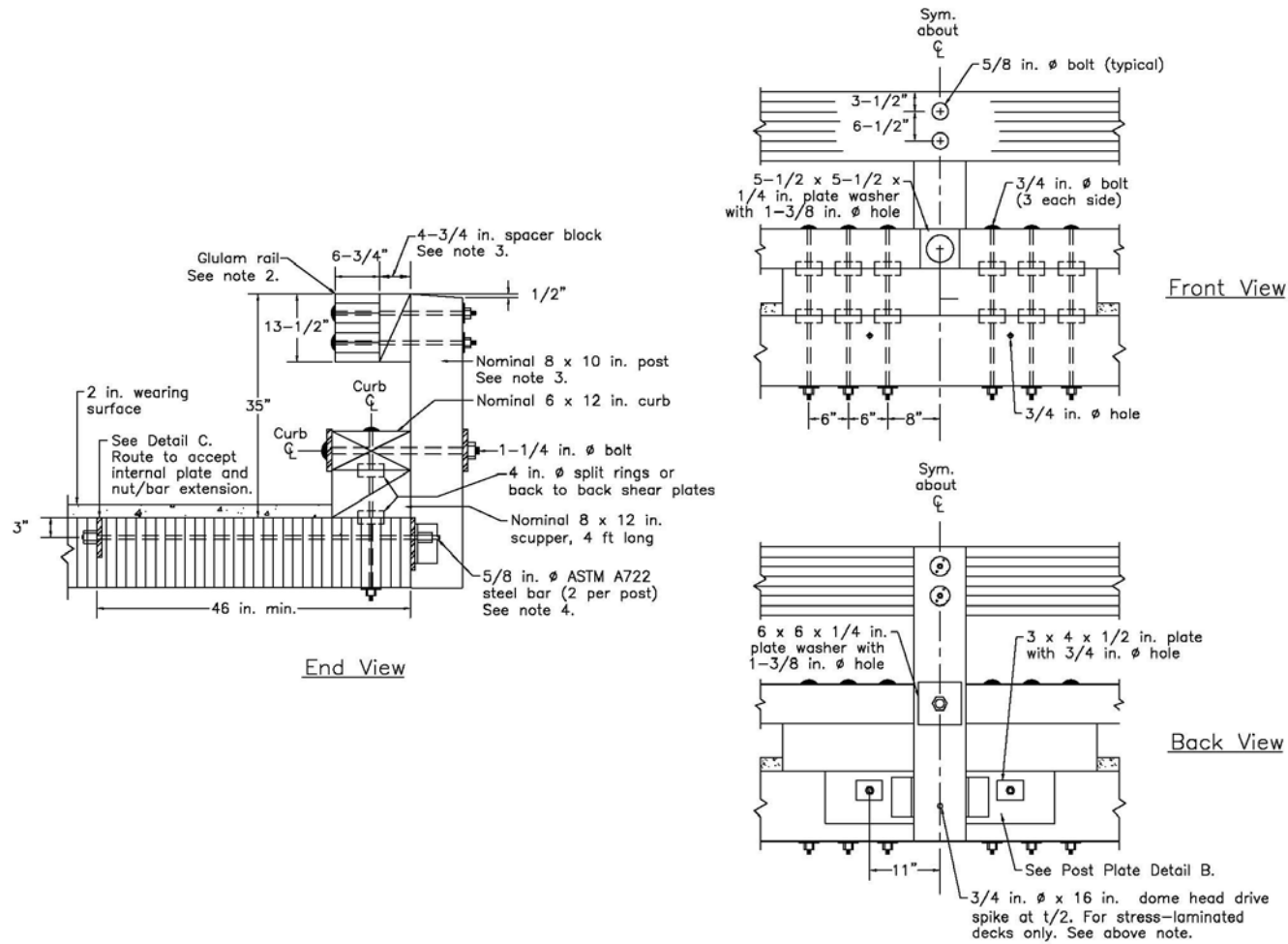


Figure 27. Bridge Railing Design Details

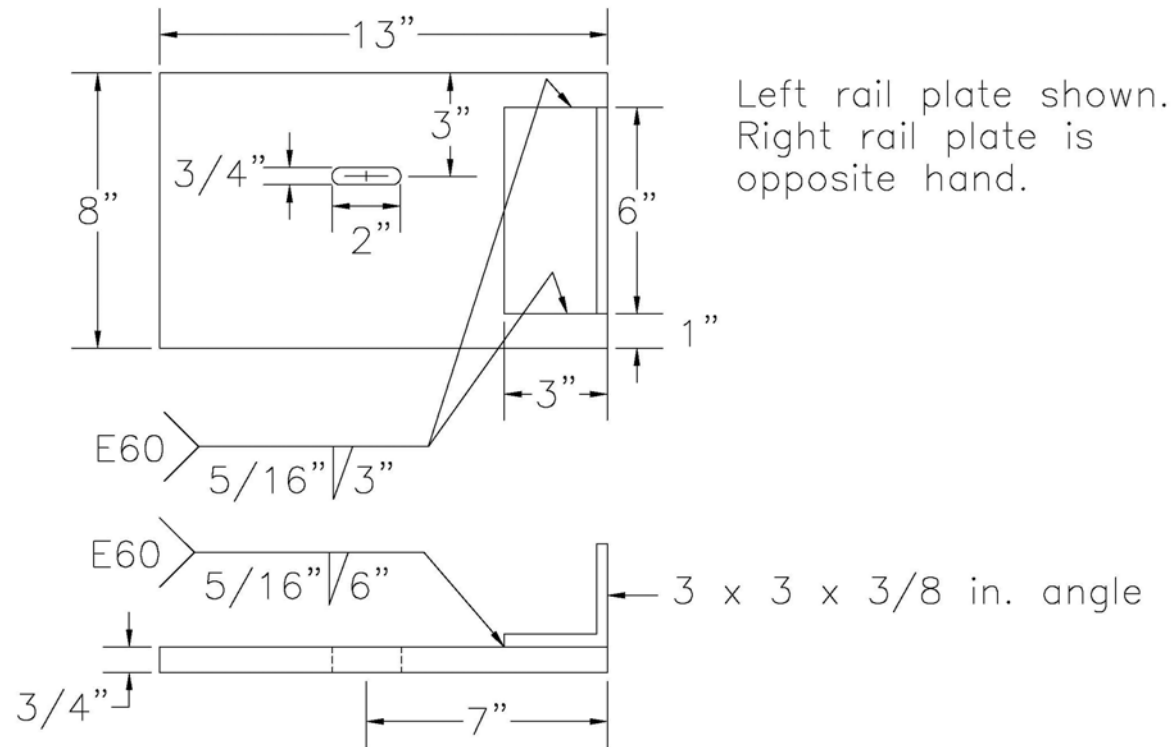


Figure 28. Post Plate Detail

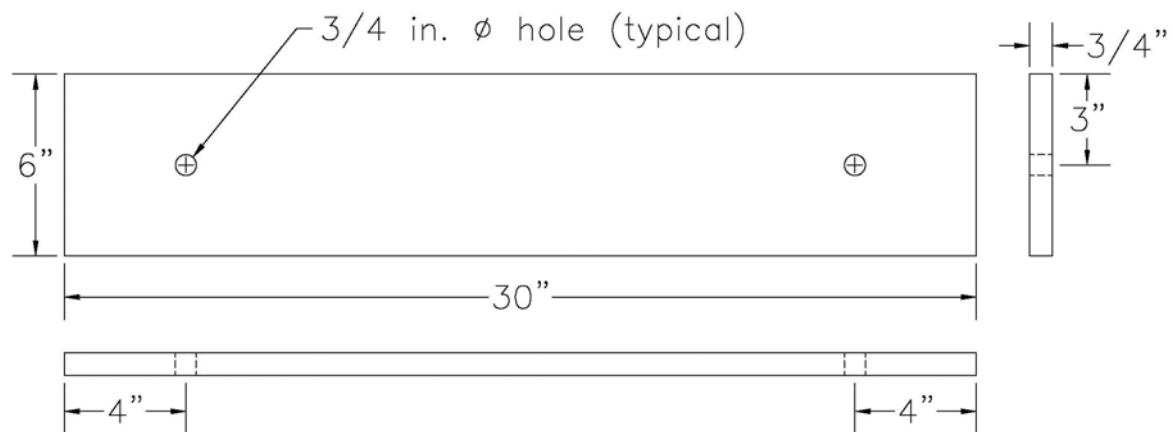


Figure 29. Internal Plate Detail

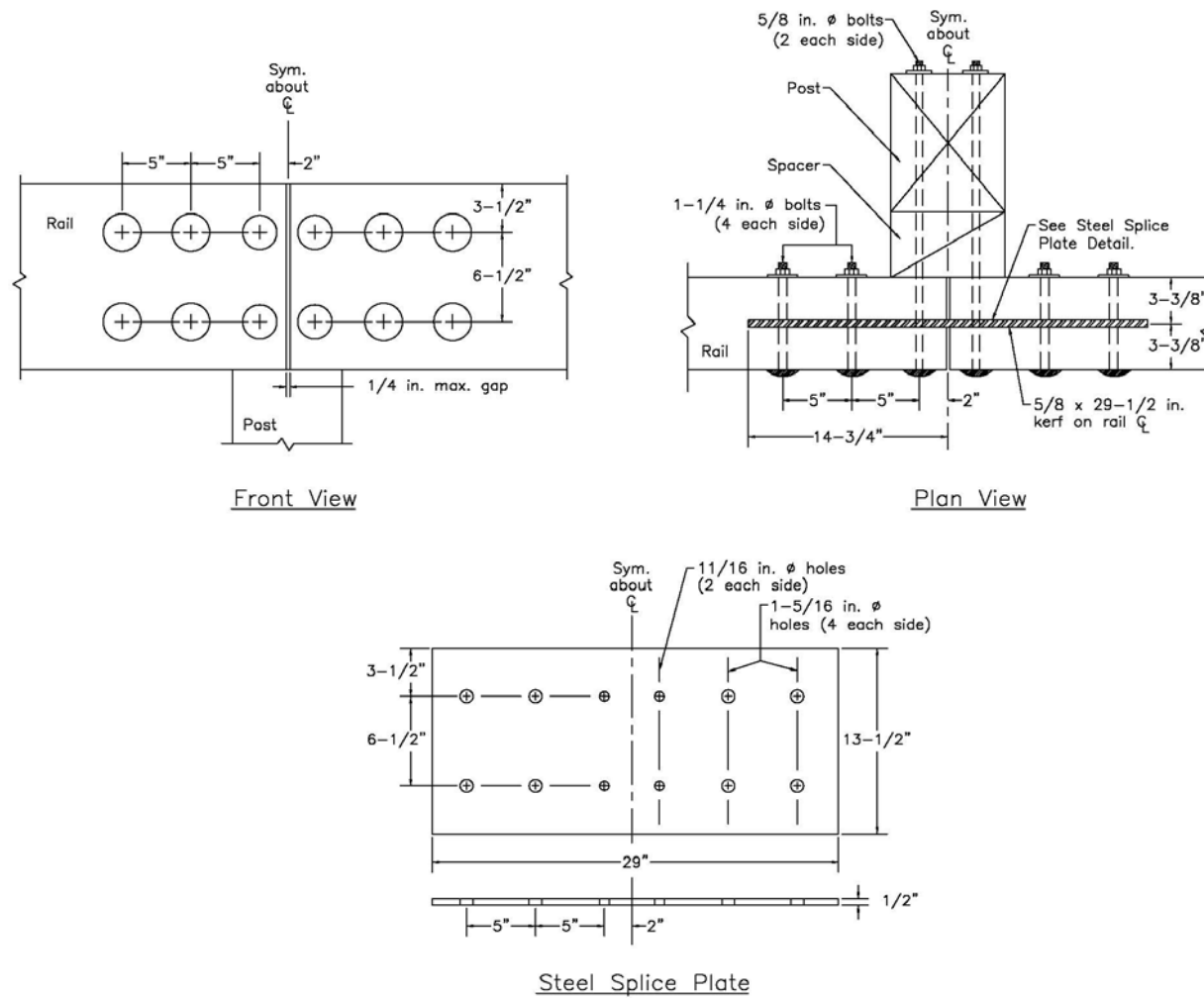


Figure 30. Rail Connection and Steel Rail Splice Design Details

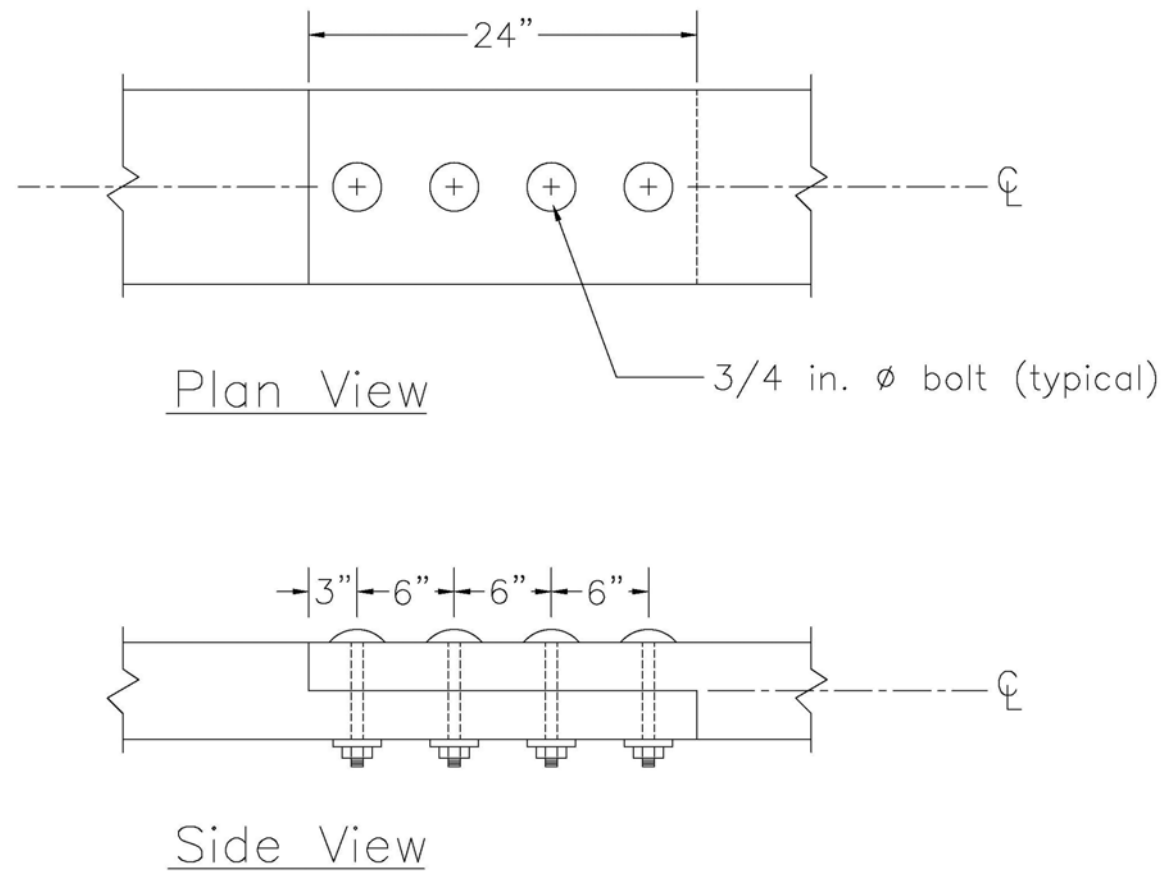


Figure 31.Curb Splice Design Detail

7.2 Approach Guardrail Transition

An approach guardrail system was attached to the upstream end of the bridge railing system and was used to connect the standard guardrail to the bridge rail. The approach guardrail transition systems consisted of 8 major components: (1) a thrie beam terminal connector; (2) a thrie beam rail section; (3) a W-beam to thrie beam transition section; (4) standard W-beam guardrail; (5) timber guardrail posts; (6) a curb transition rail; (7) a transition block; and (8) a simulated end anchorage system. Photographs of the approach guardrail transition system are shown in Figures 32 through 35. The overall layout of the approach guardrail transition system is shown in Figure 36. Design details of the approach guardrail transition system are provided in Figures 37 through 42.

The approach guardrail transition system was configured with a steel thrie beam rail. The thrie beam rail was 3,810-mm (12-ft 6-in.) long and fabricated from 3.42-mm (10-gauge) thick steel. A 2.66-mm (12-gauge) thick W-beam to thrie beam transition section, measuring 1,905-mm (6-ft 3-in.) long, was used to connect the thrie beam guardrail to 11,430-mm (37-ft 6-in.) of standard 2.66-mm (12-gauge) W-beam guardrail. The thrie beam and W-beam rails had a top mounting height of 787 mm (31 in.) and 702 mm (27 in.), respectively, as measured from the roadway surface to the top of the rails. Lap splice connections between the steel rail sections were configured to reduce vehicle snagging at the splice during the crash tests.

A 2.66-mm (12-gauge) thick thrie beam terminal connector was used to attach the thrie beam rail to the glulam rail of the bridge railing system. Subsequently, the thrie beam terminal connector bolted to a 12.7-mm (0.5-in.) thick steel rail transition plate that mounted within the centerline cut of the glulam upper rail.

A sawn lumber curb transition block was developed and bolted to the bottom of the upper glulam rail. The sawn lumber curb transition block was required in order to increase the vertical depth of the upper rail and provide a surface for rigidly attaching the lower one-third of the thrie beam terminal connector to the upper rail. The downstream end of block was beveled away from the traffic-side face in order to eliminate any potential for vehicle snag resulting from a “reverse hit” impact. The transition block was sawn lumber, fabricated from graded No. 1 Southern Pine in accordance with the requirements of AASHTO M168 and was pressure treated with wood preservative in accordance with AASHTO M133.

The system was constructed with fifteen guardrail posts, as shown in Figures 25 and 32 through 35. Post nos. 1A through 15A were fabricated from SYP, Grade No. 1 and treated with chromated copper arsenate (CCA). Post nos. 1A and 2A consisted of 203-mm wide x 203-mm deep x 1,981-mm long (8-in. x 8-in. x 78-in.) timber guardrail posts. Post nos. 3A through 14A consisted of 203-mm wide x 203-mm deep x 1,829-mm long (8-in x 8-in x 72-in.) timber guardrail posts. Post no. 15A consisted of a 140-mm wide x 191-mm deep (5½-in. x 7½-in.) BCT timber post and was placed in a steel foundation tube. Post no. 15A and the foundation tube were part of an anchorage system used to develop the required tensile capacity of the guardrail.

For post nos. 1A through 14A, treated timber blockouts were used to space the thrie beam and W-beam guardrails away from the traffic-side face of each guardrail post. The blockouts were fabricated from SYP, Grade No. 1 material and treated with CCA. For post nos. 1A through 5A, a wood blockout, measuring 203-mm wide x 292-mm deep x 572-mm long (8-in. x 11½-in. x 22½-in.), was used with the thrie beam guardrail. For post nos. 6A and 7A, a wood blockout, measuring 203-mm wide x 203-mm deep x 572-mm long (8-in. x 8-in. x 22½-in.), was also used with the thrie

beam guardrail. At post no. 8A, a wood blockout, measuring 203-mm wide x 203-mm deep x 457-mm long (8-in. x 8-in. x 18-in.), was used at the midspan of the W-beam to thrie beam transition section. At post nos. 9A through 14A, a wood blockout, measuring 203-mm wide x 203-mm deep x 356-mm long (8-in. x 8-in. x 14-in.), was used with the W-beam guardrail.

The soil embedment depths for posts 1A and 2A, 3A through 8A, and 9A through 15A were 1,168 mm (46 in.), 1,016 mm (40 in.), and 1,118 mm (44 in.), as shown in Figure 38. The timber posts were placed in a compacted coarse, crushed limestone material that met Grading B of AASHTO M147-65 (1990) as found in NCHRP Report No. 350 (1).



Figure 32. Approach Guardrail Transition - Front View



Figure 33. Approach Guardrail Transition - Back View



Figure 34. Connection to Detail Between Approach Guardrail Transition and Bridge Railing - Back-Side View



Figure 35. Transition Connection - Back-Side Close-Up View

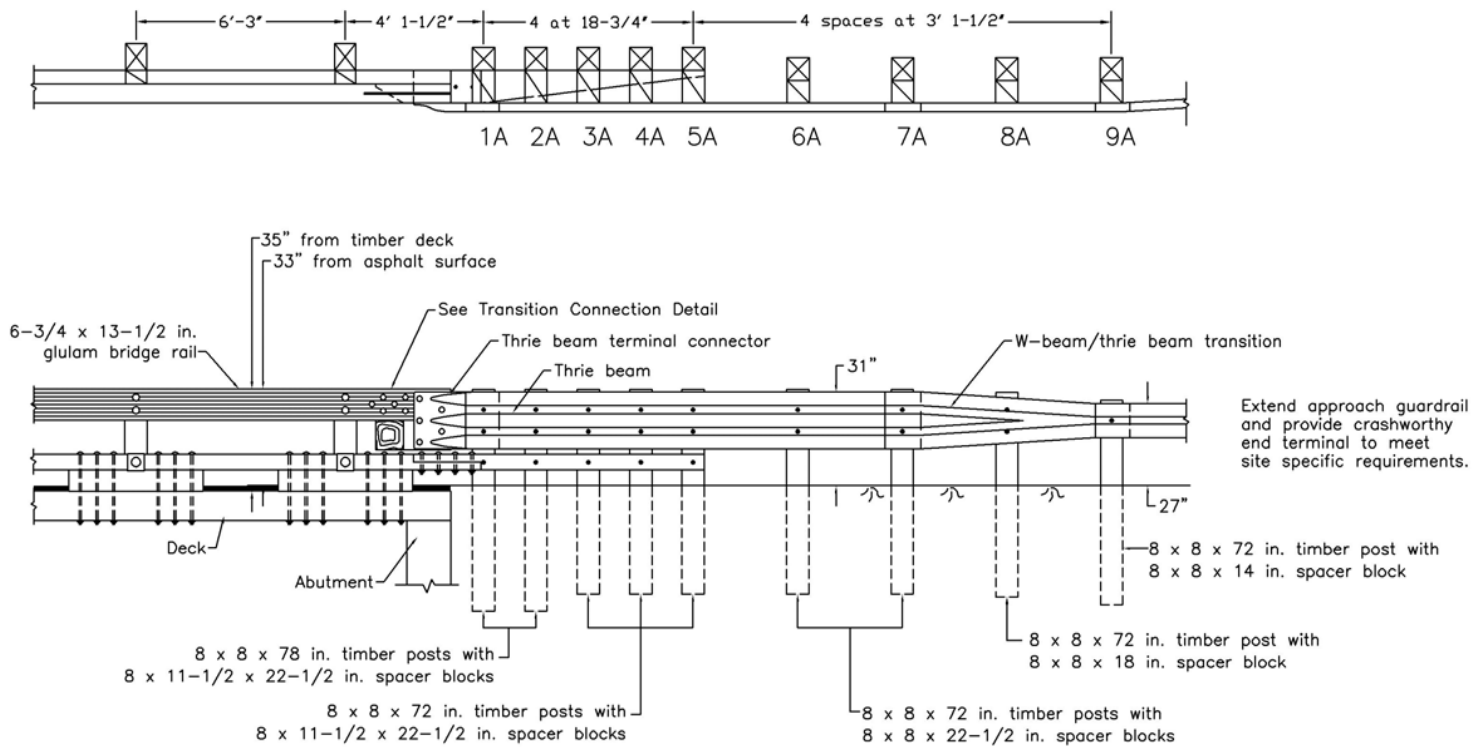


Figure 36. General Configuration of Transition Connection

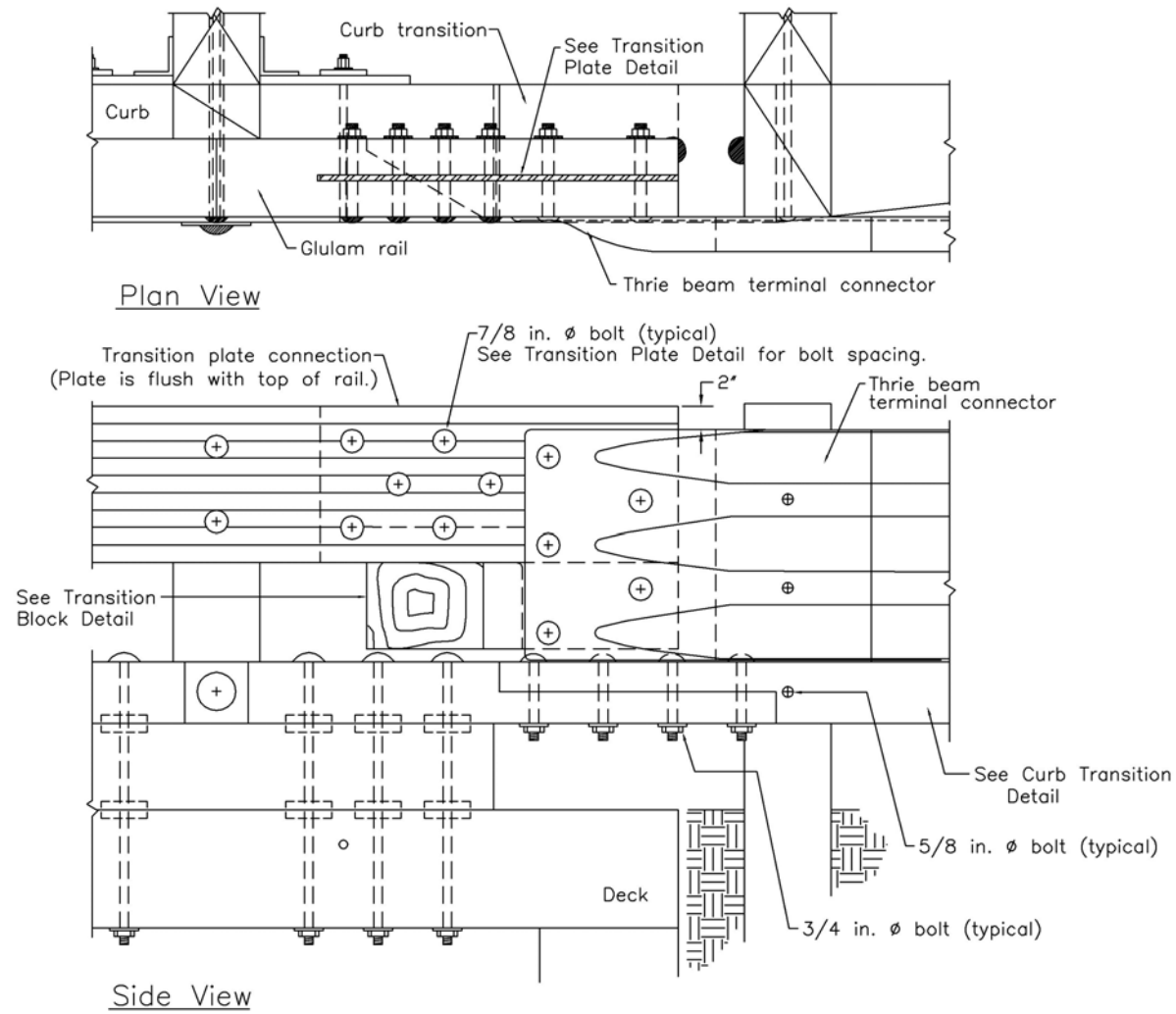


Figure 37. Transition Connection Design Detail

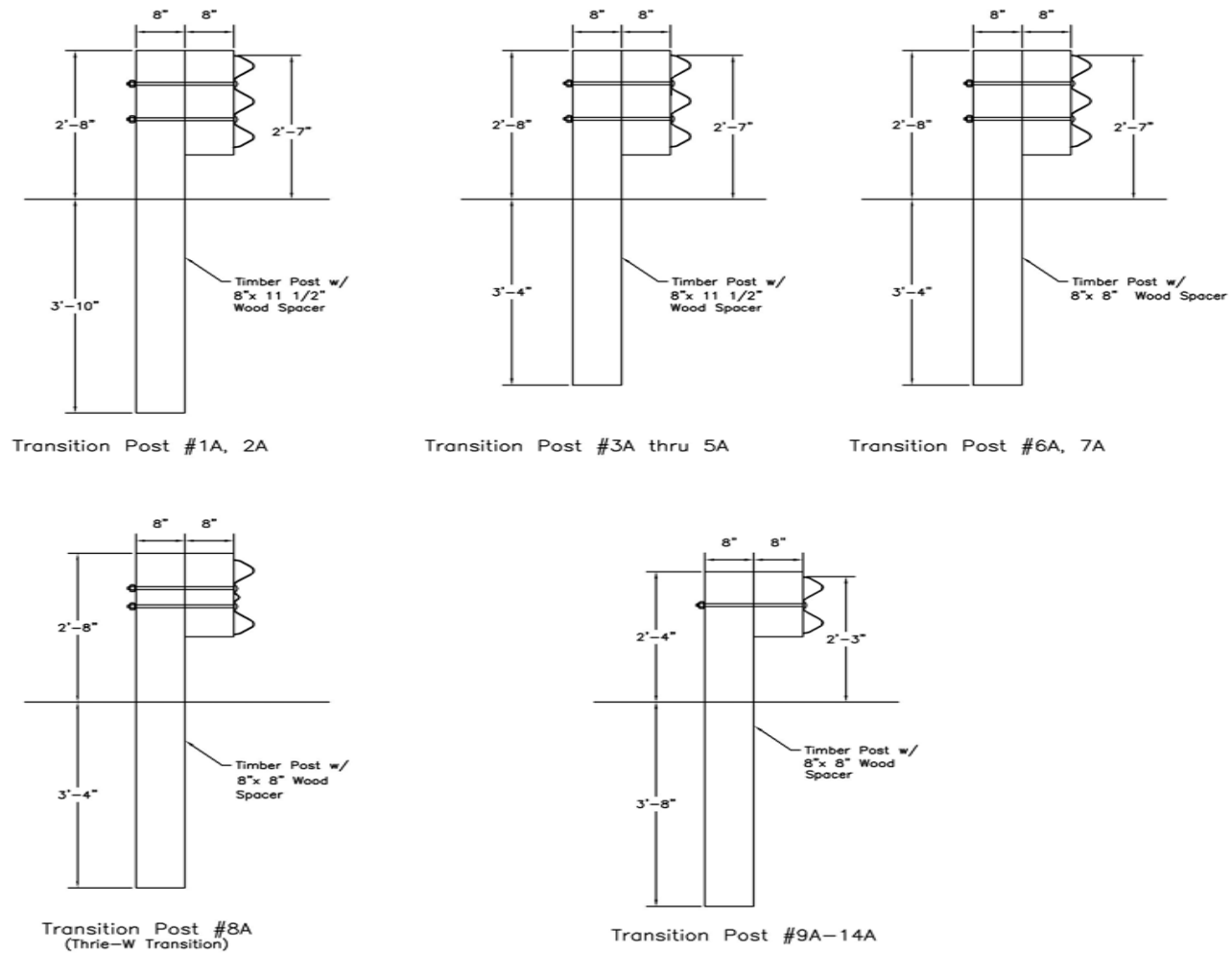
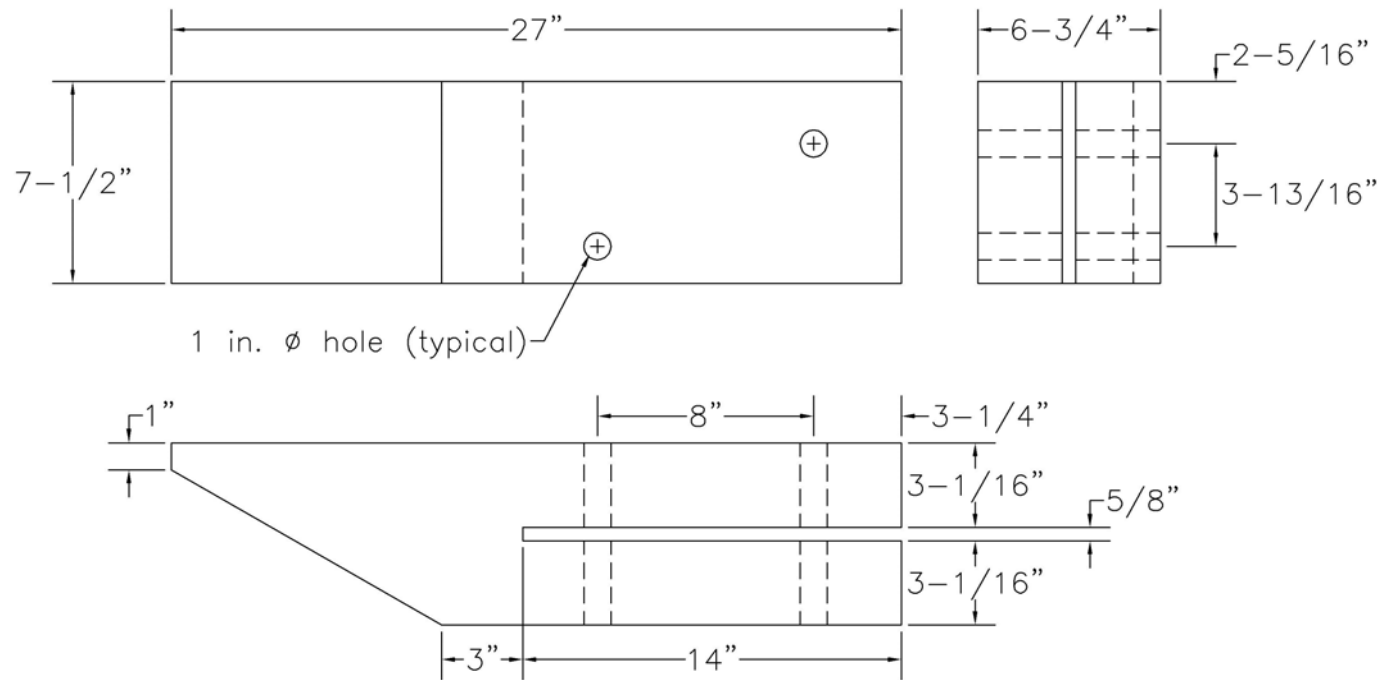


Figure 38. Transition Post Profiles



Depth of transition block is based on rail depth of $13\frac{1}{2}$ in. and dressed curb and scupper ($5\frac{1}{2}$ and $7\frac{1}{2}$ in. in height, respectively). If dimensions of any components increase, depth of transition block must be verified and reduced as necessary.

Figure 39. Curb Transition Block Design Detail

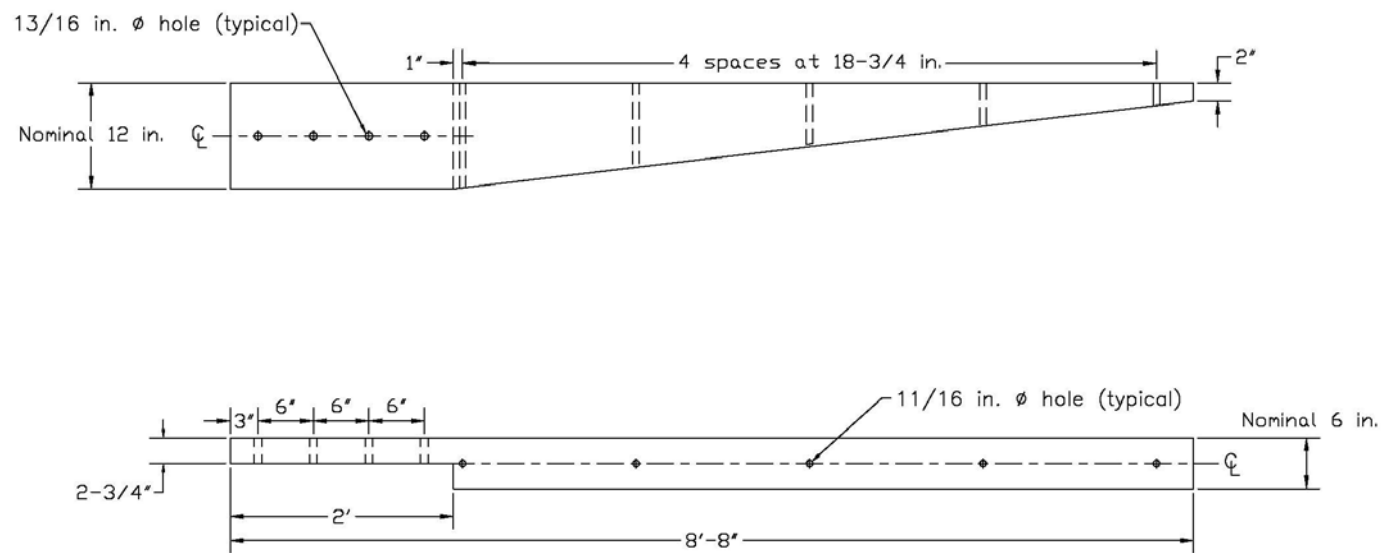


Figure 40. Curb Transition Design Detail

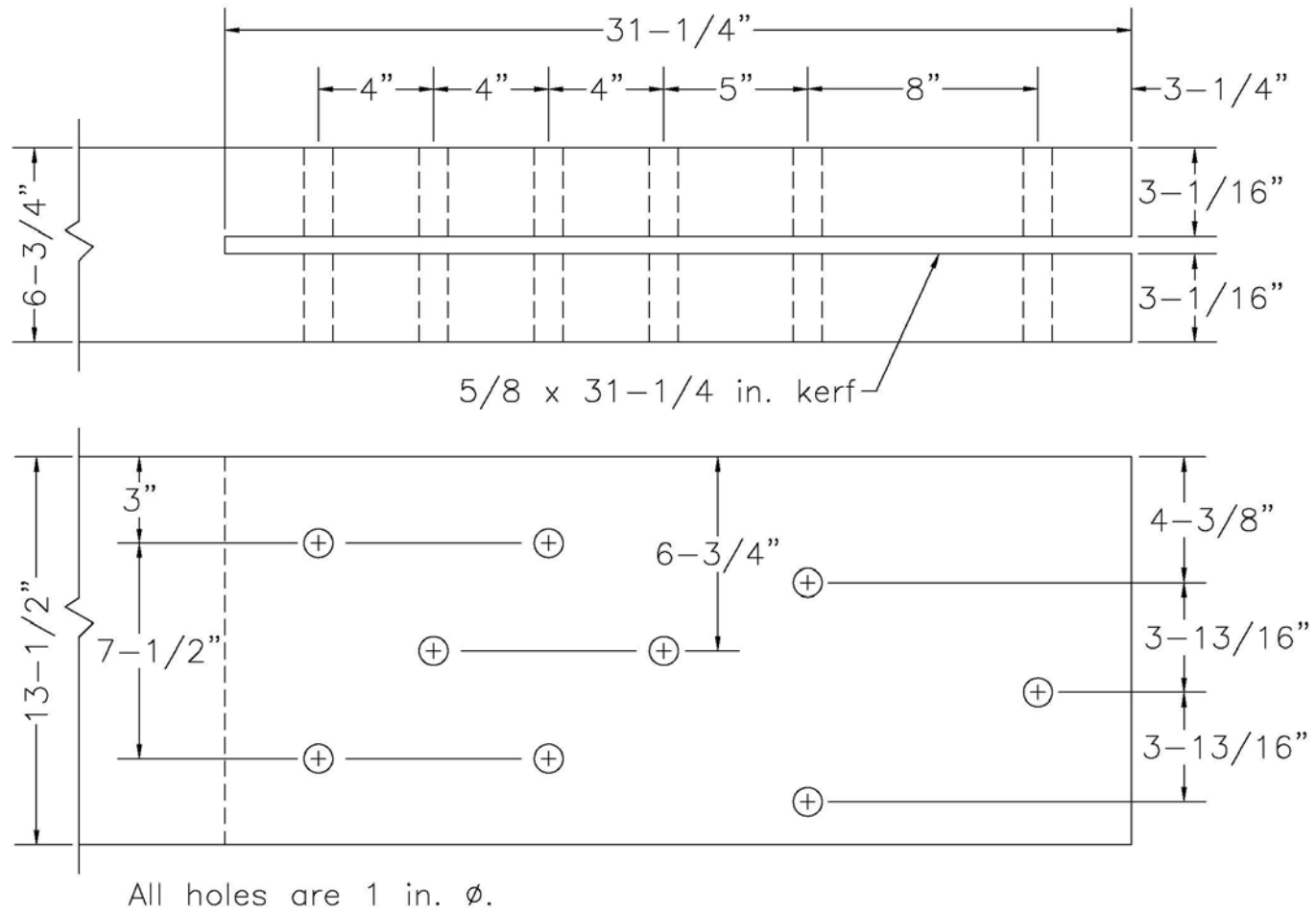


Figure 41. Boring Detail - Glulam Rail End at Approach Guardrail Transition

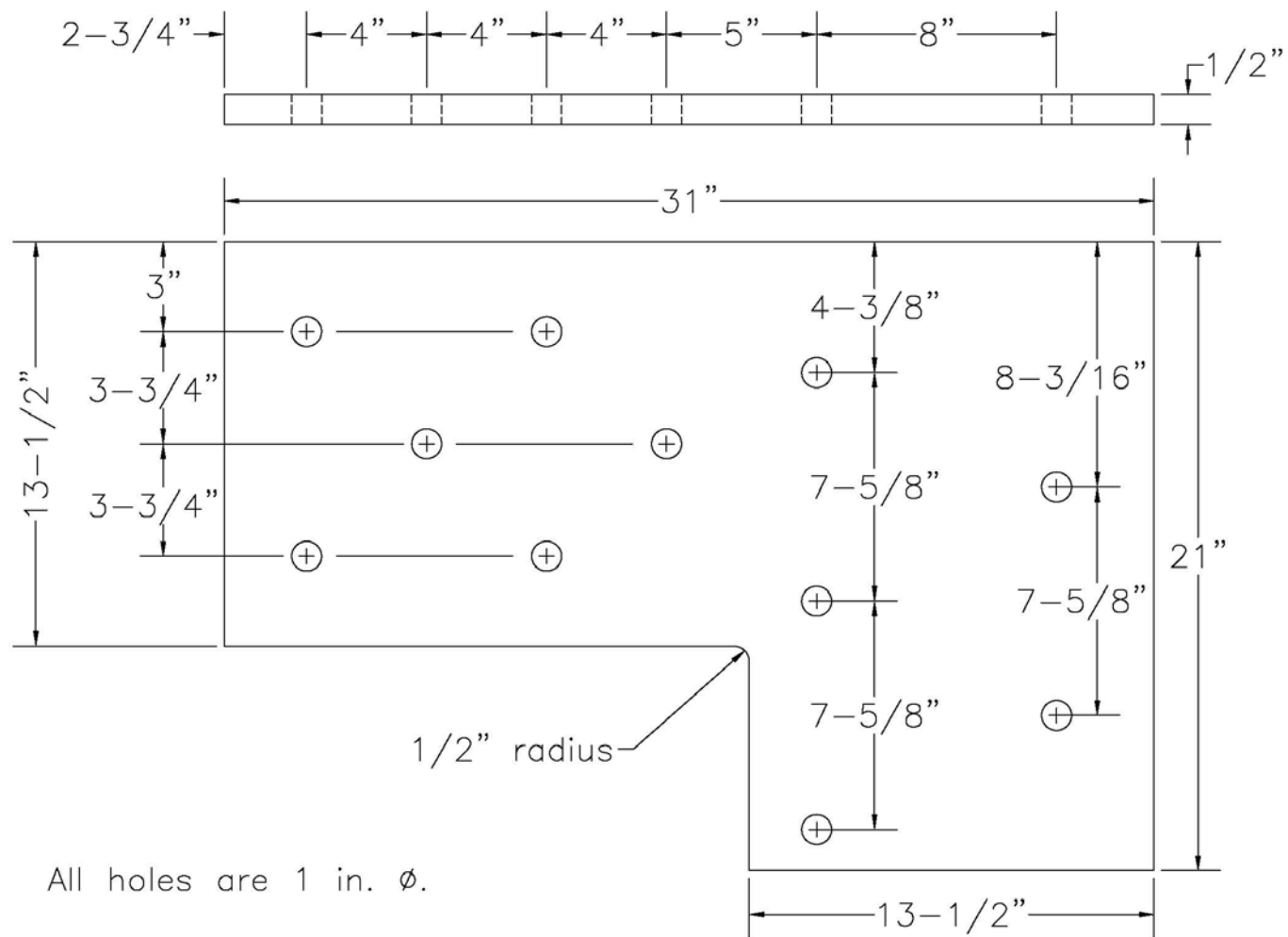


Figure 42. Transition Plate Detail

8 COMPUTER SIMULATION

8.1 Introduction

Following the preliminary design of the GC-8000, computer simulation modeling with BARRIER VII was performed to analyze the dynamic performance of the bridge railing and approach guardrail transition prior to full-scale crash testing (11). Computer simulations were conducted with (1) an 8,165-kg (18,000-lb) single-unit truck impacting the rail at a speed of 80.5 km/hr (50 mph) and at an angle of 15 degrees, and (2) a 1,996-kg (4,400-lb) pickup truck impacting the rail at a speed of 100 km/hr (62.1 mph) and at an impact angle of 25 degrees.

8.2 Design Option

The GC-8000 bridge railing design was constructed with a 343-mm wide x 171-mm deep (13½-in. x 6¾-in.) glue-laminated timber beam rail supported by fifteen 203-mm wide x 254-mm deep (8-in x 10-in.) timber posts and an approach guardrail transition located on the upstream end. Post nos. 1 through 15 were 1,162-mm (3-ft 9¾-in.) long and were spaced on 1,905-mm (6-ft 3-in.) centers. The BARRIER VII finite element model of the glulam bridge railing is shown in Appendix A. The structural properties used for the rail and post elements are shown in Appendix B. Typical computer simulation input data files for each system and vehicle are shown in Appendices C, D, and E. Computer simulation was also used to determine the critical impact point (CIP) for the wood bridge railing.

8.3 BARRIER VII Results

8.3.1 Single-Unit Truck Test - Bridge Railing

The simulation results indicated that the GC-8000 bridge railing satisfactorily redirected the 8,000-kg (17,637-lb) single-unit truck. In addition, all structural hardware remained functional

during the impact (i.e., failure was not predicted for any posts or rails elements). The maximum dynamic and permanent set deflections of the glulam rail were 152 mm (6.0 in.) and 41 mm (1.6 in.), respectively. The maximum 0.010-sec average lateral and longitudinal decelerations were 3.3 and 2.1 g's, respectively. The peak 0.050-sec average impact force perpendicular to the bridge railing was approximately 285 kN (64 kips). The truck became parallel to the bridge railing at 0.323 sec. At 0.625 sec, the truck exited the bridge railing at an angle of 12.3 degrees.

8.3.2 Pickup Truck Test - Bridge Railing

The simulation results indicated that the GC-8000 bridge railing satisfactorily redirected the 2,000-kg (4,409-lb) pickup truck. In addition, all structural hardware remained functional during the impact (i.e., failure was not predicted for any posts or rails elements). The maximum dynamic and permanent set deflections of the glulam rail were 178 mm (7.0 in.) and 74 mm (2.9 in.), respectively. The maximum 0.010-sec average lateral and longitudinal decelerations were 13.2 and 10.9 g's, respectively. The peak 0.050-sec average impact force perpendicular to the bridge railing was approximately 276 kN (62 kips). The truck became parallel to the bridge railing at 0.180 sec. At 0.260 sec, the truck exited the bridge railing at an angle of 9.4 degrees.

9 CRASH TEST NO. 1 (BRIDGE RAILING)

9.1 Test FSCR-1

The 8,165-kg (18,000-lb) single unit truck impacted the bridge railing at a speed of 82.4 km/h (51.2 mph) and at an angle of 16.8 degrees. A summary of the test results and the sequential photographs are shown in Figure 43. Additional sequential photographs are shown in Figure 44. Documentary photographs of the crash test are shown in Figures 45 through 48.

9.2 Test Description

Initial impact occurred between bridge post nos. 3 and 4, approximately 457 mm (1 ft - 6 in.) upstream from post no. 4, as shown in Figure 49. After the initial impact with the bridge rail, the right-front corner of the bumper and quarter panel crushed inward. At 0.103 sec, the maximum dynamic lateral deflections were measured at post no. 5. In addition, the front end of the truck cab began to lift and roll clockwise (CW) toward the rail. At 0.124 sec, the right-front corner of the truck box and the right-front tire were near post nos. 4 and 5, respectively. At this same time, the longitudinal centerline of the truck cab and box remained parallel. At 0.145 sec, the truck box began rotating CW toward the rail while the truck cab began rotating counter clockwise (CCW) away from the rail. At 0.160 sec, the right-front corner of the truck box extended over the rail and the right-front tire was crushed inward under the engine. At 0.207 sec, the right-front tire was near post no. 6. At 0.300 sec, the right-front tire was near post no. 7, and the left-front tire lost contact with the ground. At 0.340 sec, the truck cab began rotating CW toward the rail. At 0.382 sec, the right-front tire was near post no. 8. At 0.400 sec, the left-rear tire lost contact with the ground. At 0.413 sec, the truck cab was approximately parallel to the bridge rail with a velocity of 69.8 km/h (43.4 mph). The truck box achieved a maximum CW roll angle of approximately 31 degrees toward the rail at 0.649 sec.

At this same time, the right-rear tire also lost contact with the ground. At 0.739 sec, the truck cab achieved a maximum CW roll angle of approximately 23 degrees toward the rail. At 1.500 sec, the truck box rolled CCW away from the rail. At 1.739 sec, the left-front tire contacted the ground. At this same time, the vehicle exited the bridge railing at a speed of approximately 66.5 km/h (41.3 mph) and an angle of 0 degrees. The vehicle's trajectory and final position are shown in Figure 50. The vehicle came to rest approximately 30.40-m (99-ft 9-in.) downstream from the impact point.

9.3 Bridge Rail Damage

The moderate bridge railing damage is shown in Figures 51 through 59. Significant gouging and scrapes occurred to the glulam rail from the midspan between post nos. 3 and 4 to post no. 5. The curb rail received major gouges between post nos. 4 and 5. Minor scrapes were found on the glulam rail between post nos. 5 and 7. Major gouging and scrapes occurred to the top of the glulam rail from post nos. 7 through 12. Significant gouging and scrapes occurred to the glulam rail from the midspan between post nos. 12 and 13 to the midspan between post nos. 13 and 14, as shown in Figure 51. Minor scrapes were evident on the curb rail near post no. 13, as shown in Figure 51. The lower portion of the downstream end of glulam rail no. 1, located at post no. 4, was fractured on the lower part of the rail. Timber material was removed from the lower portion of the upstream end of glulam rail no. 2, also located at post no. 4. Three steel plate washers, located on the face of the curb rail at post nos. 4 through 6, were deformed due to wheel hub contact. At post nos. 4 and 5, the dome heads of several bolts on the rail face were deformed and/or severed due to vehicle gouging on the glulam rail, as shown in Figure 54.

Post nos. 7 and 8 were damaged near the top of each post due to contact between the truck box and timber posts. Vehicle contact on post no. 8 was measured approximately 229 mm (9 in.)

below the top of the post. Post nos. 9 through 11 were fractured away from the bridge rail due to the truck box extending over the rail and impacting the posts. Damage to the top of post no. 12 was the result of vehicle contact. Post no. 13 was fractured on the downstream side. Minor gouging and scrapes were evident on post no. 14. The top of post no. 15 was gouged from the truck box. The spacer blocks at post nos. 7 and 8 were scraped and fractured, respectively. The spacers at post nos. 9 through 11 were fractured and removed. The spacers at post nos. 12, 14, and 15 were also fractured.

The glulam timber bridge deck received some surface cracks near post no. 4, as shown in Figures 60 through 62. The crack width ranged between 1.6 mm ($\frac{1}{16}$ in.) and 3.2 mm ($\frac{1}{8}$ in.). The maximum lateral permanent set deflections for midspan rail and post locations were approximately 30 mm (1.2 in.) and 28 mm (1.1 in.), respectively, as measured in the field. The maximum lateral dynamic deflections for midspan rail and post locations were 145 mm (5.7 in.) and 165 mm (6.5 in.), respectively, as determined from high-speed analysis. The effective coefficient of friction was determined to be approximately 0.38.

9.4 Vehicle Damage

Exterior vehicle damage was moderate as shown in Figures 63 through 67. Vehicle damage occurred to several body locations, such as door and quarter panels, engine hood, front bumper, right-side wheels and rims, front axle, engine hood, truck box and support frame, side-mounted foot steps, and fuel tank. The right corner of the front bumper and the right-side door and quarter panels were crushed inward. The front axle, with attached tires and steel rims, became detached from the truck and came to rest under the left-side of the truck cab. The right-front and right-rear (outer dual) tires were deflated. The right-front steel rim, bolts, and nuts were worn and deformed. The right-side

step and fuel tank were also removed. The truck box was shifted to the right of the longitudinal centerline of the truck cab and support frame. U-bolts, used to attach the box to the frame, were also deformed due to the box shift. The right-front lower corner of the box was deformed inward. Black creosote oil was found on the right-front lower corner of the box due to contact with the top and sides of the timber posts and spacer blocks located behind the glulam rail. The right-side vertical wall of the truck box collapsed outward due to the sandbag and steel plate ballast shifting. The floor support beam and corner frame on the lower right-side of the box was bent, deformed, and torn. It should be noted that some of the right-side vehicle damage occurred after the truck traveled parallel to the rail and impacted the downstream strong-post anchor, as shown in Figure 66.

9.5 Occupant Risk Values

The longitudinal and lateral normalized occupant impact velocities were determined to be 2.71 m/s (8.89 ft/s) and 2.10 m/s (6.89 ft/s), respectively. The maximum 0.010-sec average occupant ridedown decelerations in the longitudinal and lateral directions were 1.0 g's and 1.8 g's, respectively. It is noted that the occupant impact velocities and occupant ridedown decelerations were within the suggested limits provided in AASHTO. The results of the occupant risk, determined from accelerometer data, are summarized in Figure 43. Results are shown graphically in Appendix F.

9.6 Discussion

The analysis of the test results for test FSCR-1 showed that the bridge rail adequately contained and redirected the test vehicle with controlled lateral displacements of the bridge rail. There were no detached elements or fragments which showed potential for penetrating the occupant compartment nor presented undue hazard to other traffic. Deformations of, or intrusions into, the

occupant compartment that could have caused serious injury did not occur. The test vehicle did not penetrate nor ride over the bridge rail and remained upright during and after the collision. Vehicle roll, pitch, and yaw angular displacements were noted, but they were deemed acceptable because they did not adversely influence occupant risk safety criteria nor cause rollover. After collision, the vehicle's trajectory did not intrude into adjacent traffic lanes. In addition, the vehicle's exit angle was less than 60 percent of the impact angle. The effective coefficient of friction, $\mu=0.38$, was marginal ($\mu>0.35$). Therefore, test no. FSCR-1 conducted on the bridge railing was deemed to be acceptable according to the AASHTO PL-2 and NCHRP 350 TL-4 safety performance criteria.

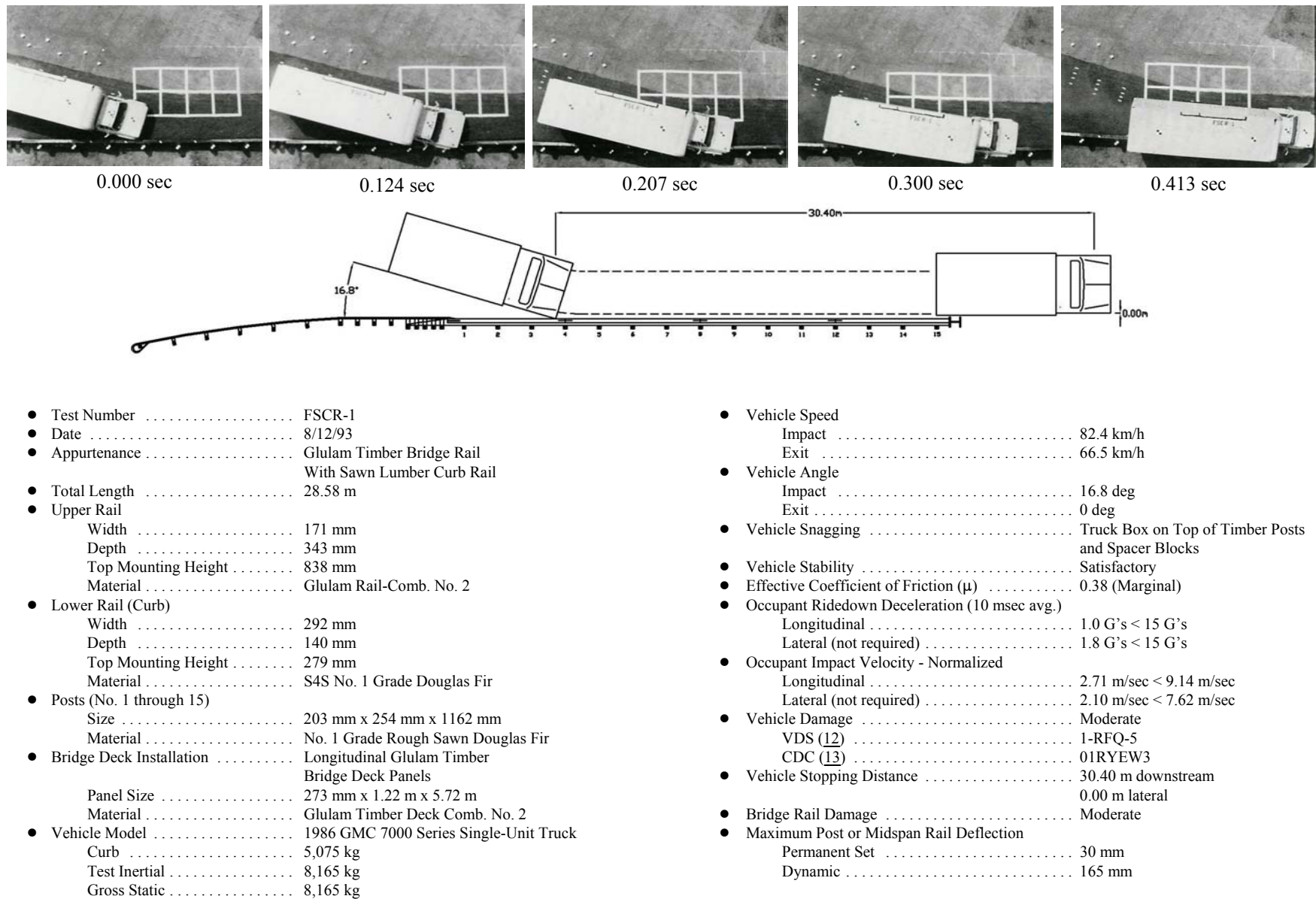


Figure 43. Summary of Test Results and Sequential Photographs, Test FSCR-1



0.000 sec



0.300 sec



0.103 sec



0.413 sec



0.160 sec



0.649 sec



0.207 sec



0.739 sec

Figure 44. Sequential Photographs, Test FSCR-1



Figure 45. Documentary Photographs, Test FSCR-1



Figure 46. Documentary Photographs, Test FSCR-1



Figure 47. Documentary Photographs, Test FSCR-1



Figure 48. Documentary Photographs, Test FSCR-1



Figure 49. Impact Locations, Test FSCR-1



Figure 50. Final Vehicle Position and Trajectory Marks, Test FSCR-1



Figure 51. Rail Damage Downstream from Impact, Test FSCR-1

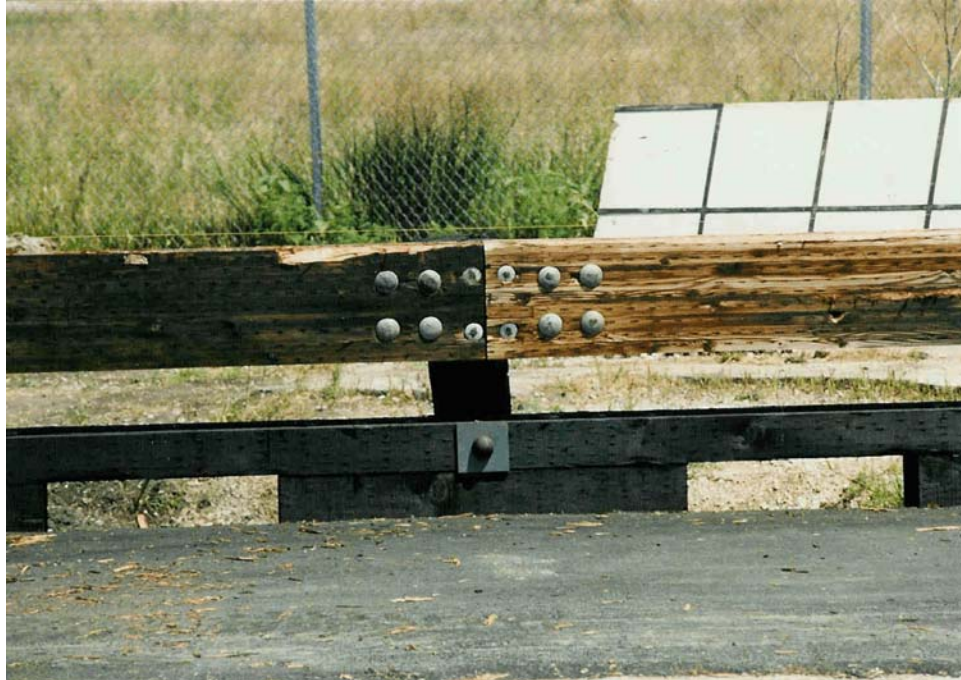


Figure 52. Rail Damage at Post No. 8, Test FSCR-1



Figure 53. Rail Damage Between Post Nos. 4 and 5, Test FSCR-1



Figure 54. Rail Damage at Post Nos. 4 and 5, Test FSCR-1

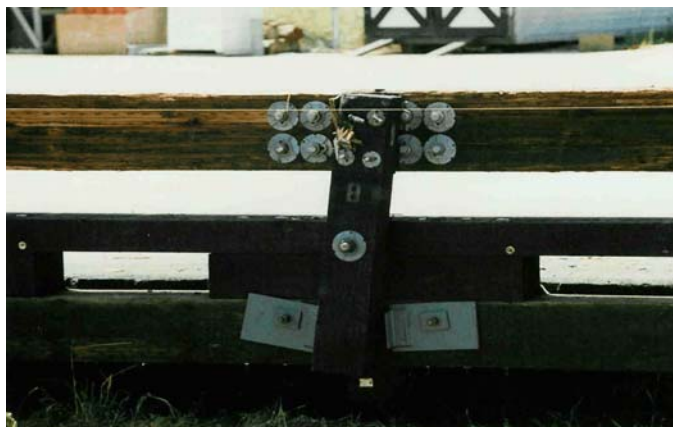


Figure 55. Damage to Post Nos. 7 and 8, Test FSCR-1

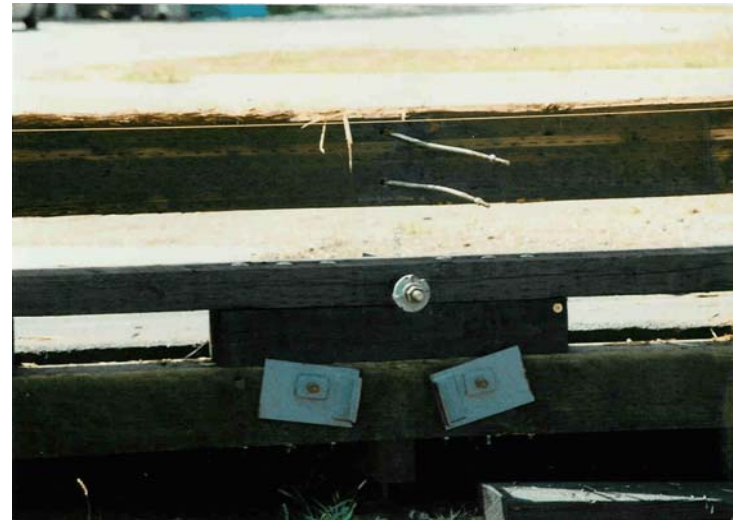
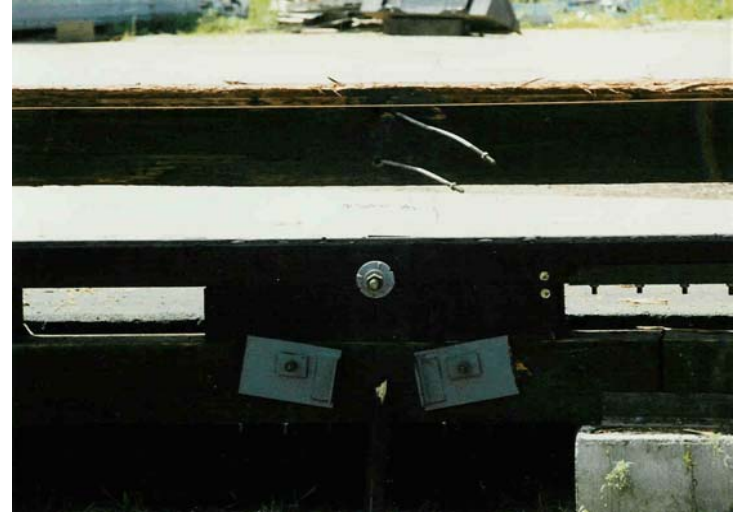


Figure 56. Damage to Post Nos. 9 through 11, Test FSCR-1

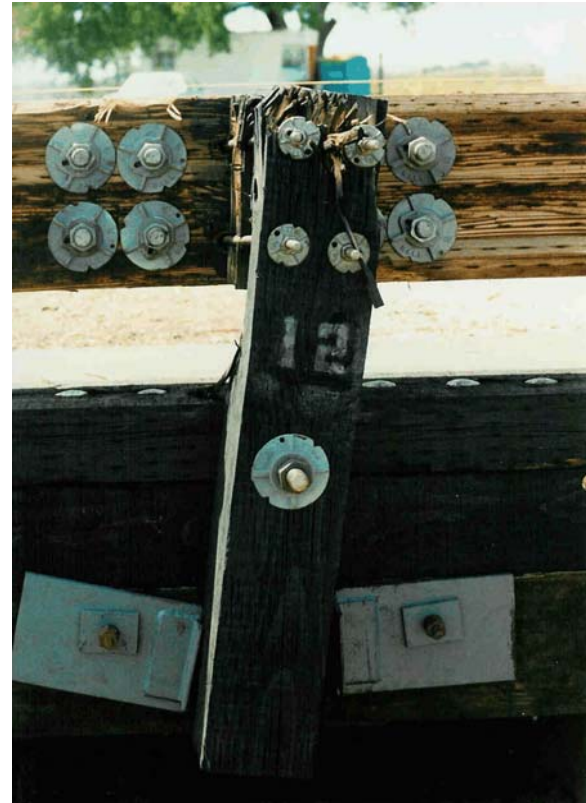
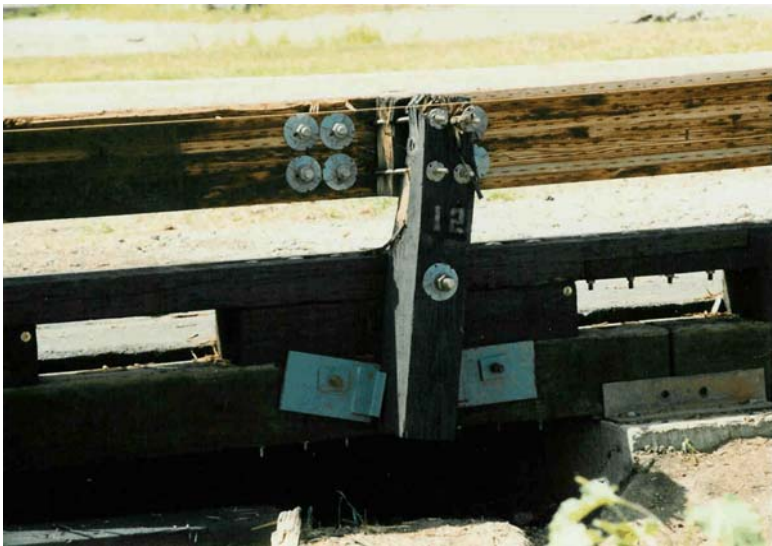


Figure 57. Post No. 12 Damage, Test FSCR-1

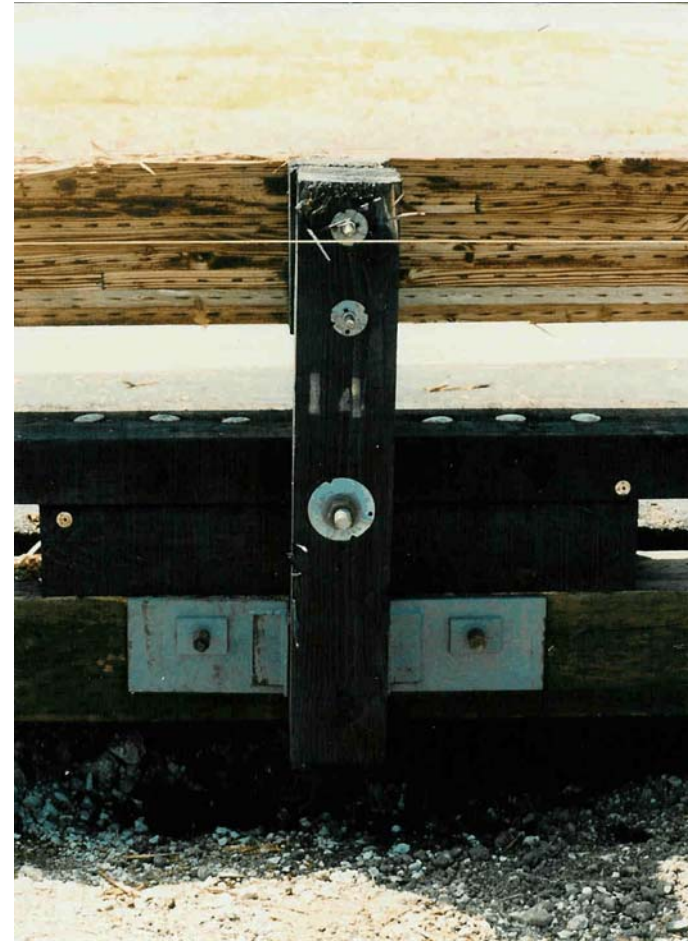


Figure 58. Damage to Post Nos. 13 and 14, Test FSCR-1



Figure 59. Post No. 15 Damage, Test FSCR-1

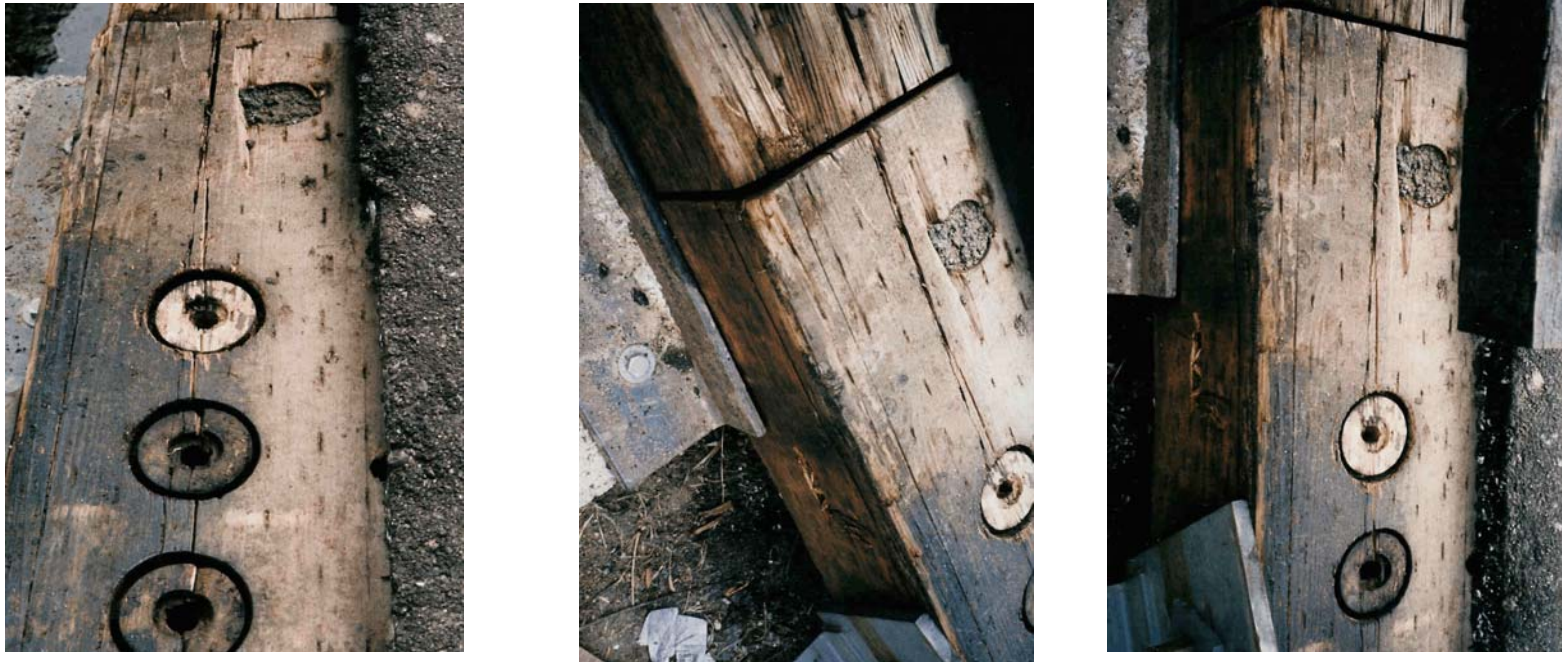


Figure 60. Deck Cracking on Upstream Side of Post No. 4, Test FSCR-1



Figure 61. Deck Cracking at Post No. 4, Test FSCR-1

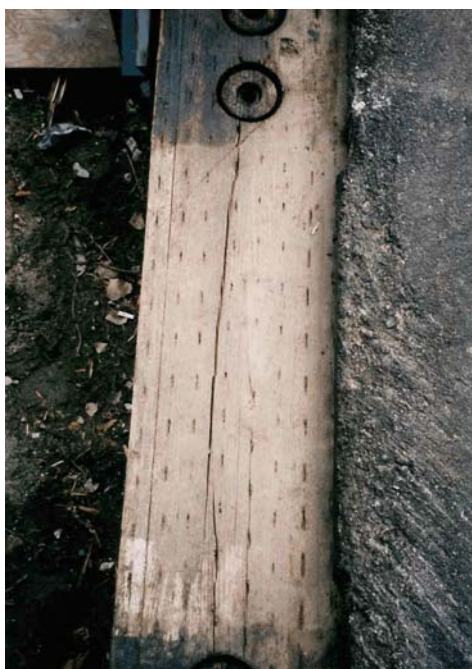


Figure 62. Deck Cracking on Downstream Side of Post No. 4, Test FSCR-1



Figure 63. Vehicle Damage, Test FSCR-1



Figure 64. Vehicle Damage, Test FSCR-1



Figure 65. Vehicle Damage, Test FSCR-1



Figure 66. Vehicle Damage, Test FSCR-1



Figure 67. Downstream Strong-Post Anchor, Test FSCR-1

10 CRASH TEST NO. 2 (APPROACH GUARDRAIL TRANSITION)

10.1 Test FSCR-2

The 2,041-kg (4,506-lb) sedan impacted the approach guardrail transition at a speed of 100.4 km/h (62.4 mph) and at an angle of 24.8 degrees. A summary of the test results and the sequential photographs are shown in Figure 68. Additional sequential photographs are shown in Figure 69. Documentary photographs of the crash test are shown in Figures 70 through 72.

10.2 Test Description

Impact occurred between guardrail post nos. 4A and 5A, approximately 2,924 mm (9 ft - 7 $\frac{1}{8}$ in.) upstream from bridge post no. 1, as shown in Figure 73. After initial impact with the transition, the right-front corner of the bumper and quarter panel crushed inward. At 0.039 sec, the right-front tire was near post no. 2A. Also at this same time, there was evidence of uplift of the vehicle's right-front corner, as well as the left-front corner of the engine hood opening. At 0.053 sec, the maximum dynamic lateral midspan deflection was measured between post nos. 1A and 2A. At 0.069 sec, the maximum dynamic lateral post deflection was measured at post no. 1A. At 0.079 sec, the vehicle's right-front corner was near the end of the transition or the beginning of the glulam bridge rail. At 0.157 sec, the vehicle was approximately parallel to the transition with a velocity of 78.9 km/h (49.0 mph). At 0.275 sec, the right-rear corner of the vehicle was near the end of the transition. At 0.295 sec, the vehicle exited the railing at a speed of approximately 71.8 km/h (44.6 mph) and at an angle of 3.7 degrees. The vehicle's trajectory and final position are shown in Figures 68 and 74. The vehicle came to rest approximately 57.9 m (190 ft) downstream from the impact point.

10.3 Bridge Rail and Approach Guardrail Terminal Damage

The moderate bridge railing damage is shown in Figures 75 through 79. Marks and scrapes were found on the thrie beam rail from post no. 1A to the end of the thrie terminal connector. Approximately one 1,905-mm (6-ft 3-in.) section of thrie beam was damaged. Most of the thrie deformation occurred on the lower corrugation, as shown in Figure 75. Vehicle contact with the curb rail was first evident at the location where the curb rail was blocked out 292 mm (11 ½ in.) away from the front face of the guardrail posts. The curb rail was fractured from post no. 1A to the downstream end of the splice connecting the transition curb rail to the bridge curb rail. The upstream end of the bridge curb rail was also fractured at the splice between the bridge and transition curb rails. Scrapes and gouging from vehicle contact were found on the upstream end of the glulam and curb bridge rails. Gouges were also found on the timber transition block located between the glulam and curb rails. No damage occurred to the guardrail posts or spacer blocks. However, the posts were rotated in the compacted aggregate soil mix. No damage occurred to the bridge posts or spacer blocks. Minor permanent set deflection was observed at bridge post no. 1. The steel plate washer, located on the front face of the curb rail at post no. 1, was deformed due to contact with the vehicle sheet metal on the right-side lower doors. A longitudinal centerline crack was found in the timber scupper block located at bridge post no. 1.

The glulam timber bridge deck received some surface cracking upstream from post no. 1. The crack width ranged between 1.59 and 3.18 mm ($\frac{1}{16}$ and $\frac{1}{8}$ in.). The maximum lateral permanent set deflections for midspan rail and post locations of the transition were approximately 74 mm (2.9 in.) and 81 mm (3.2 in.), respectively, as measured in the field. The maximum dynamic lateral deflections for midspan rail and post locations of the transition were 241 mm (9.5 in.) and 246 mm

(9.7 in.), respectively, as determined from high-speed film analysis. The maximum lateral permanent set deflections for midspan rail and post locations of the bridge rail were approximately 28 mm (1.1 in.) and 41 mm (1.6 in.), respectively, as measured in the field. The maximum lateral dynamic deflections for midspan rail and post locations of the bridge rail were 127 mm (5.0 in.) and 188 mm (7.4 in.), respectively, as determined from high-speed analysis. The effective coefficient of friction was determined to be approximately 0.29.

10.4 Vehicle Damage

Exterior vehicle damage was moderate, as shown in Figures 80 through 82. Occupant compartment deformations to the right-front floorboard, as shown in Figure 83, were judged insufficient to cause serious injury to the vehicle occupants.

Vehicle damage occurred to several body locations, such as door and quarter panels, front bumper and grill, right-side wheels and rims, engine housing and hood, and rear bumper. Both right-side tires were cut and deflated in conjunction with a deformed right-front steel rim. The right corner of the front bumper and right-front quarter panel were crushed inward. The right corner of the rear bumper and tail light assembly were deformed inward. The right-side body panels were deformed due to vehicle-thrie beam interlock and contact between the vehicle's exterior sheet metal and the hex-head bolts located at the transition connection to the glulam rail. The engine housing was bent toward the left, away from the longitudinal centerline of the vehicle. Minor buckling of the engine hood occurred at the side supports. The lower edge of the right-side doors had a longitudinal cut or tear in the steel due to potential contact between the vehicle and a steel plate washer.

10.5 Occupant Risk Values

The longitudinal and lateral normalized occupant impact velocities were determined to be 6.49 m/s (21.3 ft/sec) and 6.28 m/s (20.6 ft/sec), respectively. The maximum 0.010-sec average occupant ridedown decelerations in the longitudinal and lateral directions were 6.8 g's and 11.0 g's, respectively. It is noted that the occupant impact velocities and occupant ridedown decelerations were within the suggested limits provided in NCHRP Report No. 230. The results of the occupant risk, determined from accelerometer data, are summarized in Figure 68. Results are shown graphically in Appendix G.

10.6 Discussion

The analysis of the test results for test FSCR-2 showed that the approach guardrail transition contained and smoothly redirected the test vehicle with controlled lateral deflections of the guardrail transition. There were no detached elements or fragments which showed potential for penetrating the occupant compartment nor presented undue hazard to other traffic. Deformations of, or intrusions into, the occupant compartment that could have caused serious injury did not occur. The test vehicle did not penetrate nor ride over the guardrail transition and remained upright during and after the collision. Vehicle roll, pitch, and yaw angular displacements were noted, but deemed acceptable because they did not adversely influence the occupant risk safety criteria nor cause rollover. After collision, the vehicle's trajectory revealed minimal intrusion into adjacent traffic lanes. In addition, the vehicle's exit angle was less than 60 percent of the impact angle. Therefore, test no. FSCR-2 was determined to be acceptable according to the safety performance criteria of test designation MSL-2 found in NCHRP Report No. 230.

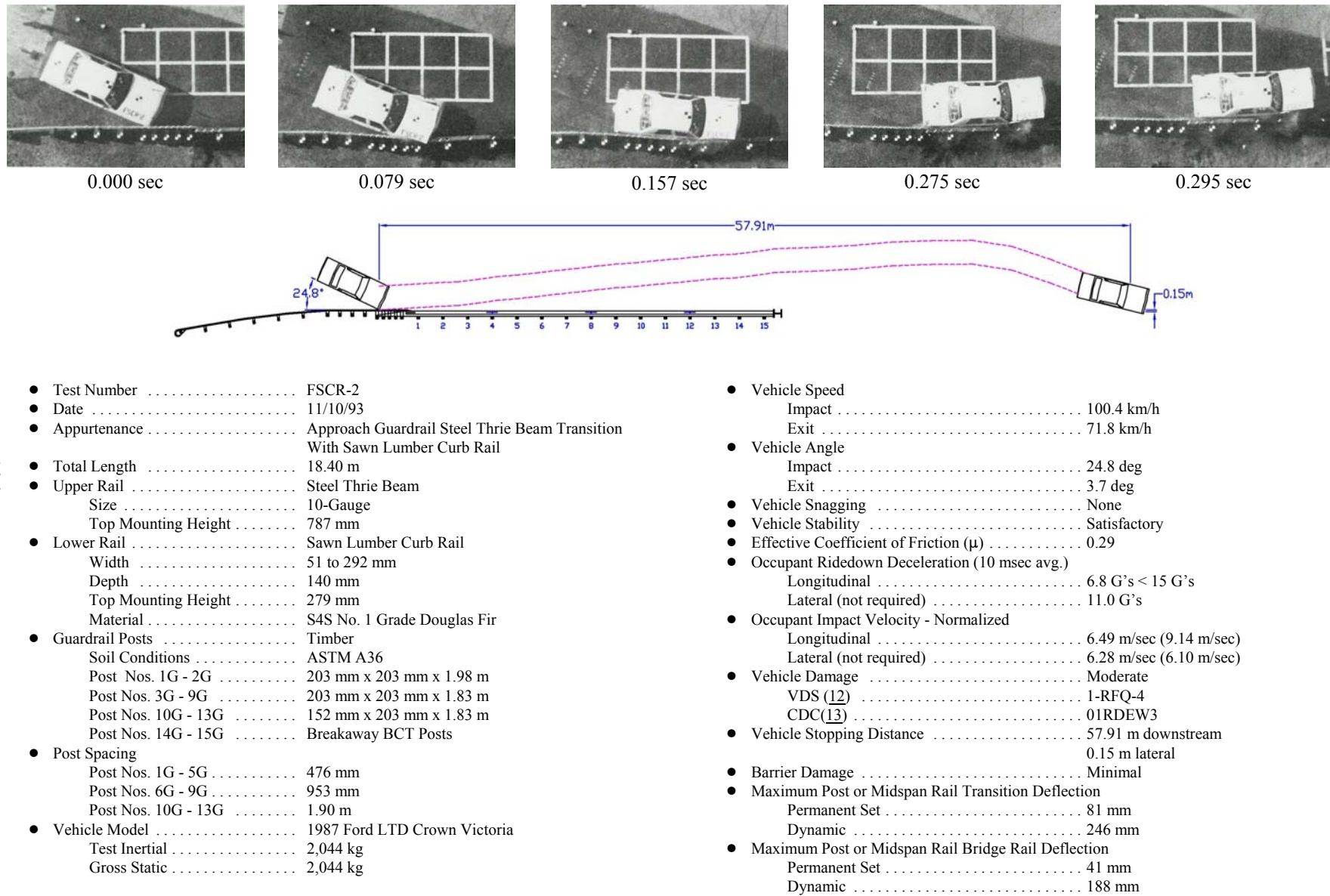


Figure 68. Summary of Test Results and Sequential Photographs, Test FSCR-2



0.000 sec



0.157 sec



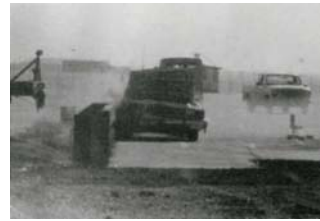
0.039 sec



0.275 sec



0.053 sec



0.295 sec



0.069 sec



0.079 sec

Figure 69. Sequential Photographs, Test FSCR-2



Figure 70. Documentary Photographs, Test FSCR-2



Figure 71. Documentary Photographs, Test FSCR-2



Figure 72. Documentary Photographs, Test FSCR-2



Figure 73. Impact Locations, Test FSCR-2



Figure 74. Final Vehicle Position and Trajectory Marks, Test FSCR-2



Figure 75. Thrie Beam Damage, Test FSCR-2



Figure 76. Curb Rail Damage, Test FSCR-2



Figure 77. Curb Rail Damage, Test FSCR-2



Figure 78. Deck Cracking, Test FSCR-2

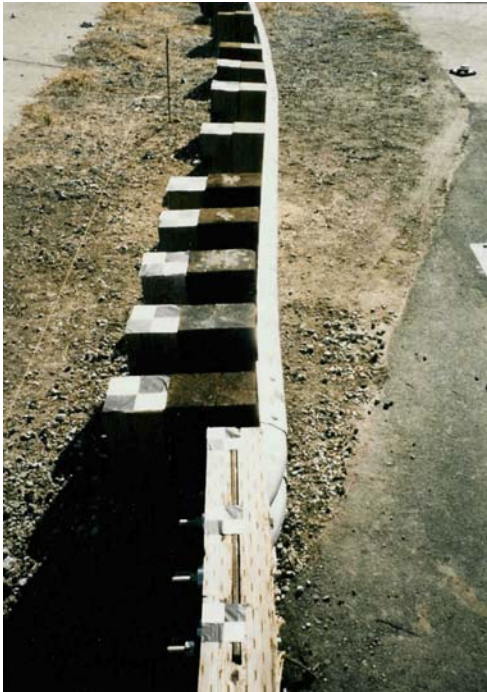


Figure 79. Permanent Set Deflection of Thrie Beam Rail and Glulam Rail, Test FSCR-2



Figure 80. Vehicle Damage, Test FSCR-2



Figure 81. Vehicle Damage, Test FSCR-2



Figure 82. Vehicle Damage, Test FSCR-2



Figure 83. Occupant Compartment Deformation, Test FSCR-2

11 CRASH TEST NO. 3 (BRIDGE RAILING)

11.1 Test FSCR-3

The 2,045-kg (4,509-lb) pickup truck impacted the bridge railing at a speed of 92.5 km/h (57.5 mph) and at an angle of 21.8 degrees. A summary of the test results and the sequential photographs are shown in Figure 84. Additional sequential photographs are shown in Figure 85. Documentary photographs of the crash test are shown in Figures 86 through 88.

11.2 Test Description

Initial vehicle impact was to occur between bridge post nos. 7 and 8, approximately 1,759 mm (5 ft - 9¼ in.) upstream from the centerline of post no. 8, as shown in Figure 89. However, due to technical difficulties with the vehicle guidance system, the pickup truck impacted the bridge rail at approximately 203 mm (8 in.) downstream from the centerline of post no. 9. After initial impact with the bridge rail, the right-front corner of the bumper and quarter panel crushed inward. In addition, the pickup truck impacted the bridge rail with the right-front tire airborne and a roll angle of 5.4 degrees counterclockwise away from the bridge rail. At 0.059 sec, the right-front corner of the pickup truck was positioned near post no. 10. At 0.098 sec, the maximum dynamic lateral deflections were measured at post no. 10. At 0.127 sec, the right-front corner of the pickup truck was near post no. 11. At 0.190 sec, the pickup truck was approximately parallel to the bridge rail with a velocity of 72.3 km/h (44.9 mph) and a roll angle of 9.0 degrees CW toward the bridge rail. At 0.350 sec, the pickup truck had a roll angle of approximately 19.0 degrees CW toward the bridge rail. At 0.386 sec, the vehicle exited the bridge railing at a speed of approximately 70.2 km/h (43.6 mph) and at an angle of approximately 10.4 degrees. At 0.509 sec, the right-front tire contacted the ground with a roll angle of approximately 27.8 degrees CW toward the bridge rail. At 0.599 sec, the

right-front tire was totally compressed into the ground, and the vehicle had a roll angle of approximately 29.8 degrees CW toward the bridge rail. At 1.078 sec, the left-front tire contacted the ground. At 1.178 sec, the pickup truck became horizontal with the ground. The vehicle's trajectory and final position are shown in Figures 84 and 90. The vehicle came to rest approximately 49.7 m (163 ft) downstream from the impact point.

11.3 Bridge Rail Damage

The minor bridge railing damage is shown in Figures 91 and 92. Scrapes and gouging approximately 3.96-m (13-ft) long occurred to the top-side and traffic-side faces of the glulam timber rail from the impact location to the downstream side of post no. 11. Minor scuff marks were also evident on the curb rail near post no. 10. No damage occurred to the timber bridge posts. One steel plate washer, located on the traffic-side face of the curb rail at post no. 10, was deformed due to wheel hub contact, as shown in Figure 92.

The maximum lateral permanent set deflections for midspan rail and post locations were approximately 10 mm (0.38 in.) and 11 mm (0.44 in.), respectively, as measured in the field. The maximum lateral dynamic deflections for midspan rail and post locations were 147 mm (5.8 in.) and 155 mm (6.1 in.), respectively, as determined from high-speed analysis. The effective coefficient of friction was determined to be approximately 0.40.

11.4 Vehicle Damage

Exterior vehicle damage was moderate, as shown in Figures 93 and 94. Due to the head-on impact with the steel shear post, front-end damage was more pronounced, as shown in Figure 94. Vehicle damage occurred to several body locations, such as door and quarter panels, front bumper and grill, right-side wheels and rims, and rear bumper. Both right-side tires were deflated.

Significant deformation occurred to the right-front steel rim and wheel-hub. The right corner of the front bumper and right-front quarter panel were crushed inward. In addition, the right corner of the rear bumper was bent inward during vehicle redirection. The right-side door and rear body panels were deformed and scraped due to contact between the vehicle's exterior sheet metal and the glulam timber rail. It should be noted that significant damage to the midpoint of the front bumper and undercarriage occurred due to the head-on impact with the shear post prior to impacting the bridge rail.

11.5 Occupant Risk Values

The longitudinal and lateral normalized occupant impact velocities were determined to be 7.07 m/s (23.2 ft/sec) and 9.63 m/s (31.6 ft/sec), respectively. The maximum 0.010-sec average occupant ridedown decelerations in the longitudinal and lateral directions were 7.2 g's and 8.6 g's, respectively. It is noted that the occupant impact velocities and occupant ridedown decelerations were within the suggested limits provided in NCHRP Report No. 350. The results of the occupant risk, determined from accelerometer data, are summarized in Figure 84. Results are shown graphically in Appendix H.

11.6 Discussion

The analysis of the test results for test FSCR-3 showed that the bridge rail adequately contained and redirected the test vehicle with controlled lateral displacements of the bridge rail. There were no detached elements or fragments which showed potential for penetrating the occupant compartment nor presented undue hazard to other traffic. Deformations of, or intrusions into, the occupant compartment that could have caused serious injury did not occur. The test vehicle did not penetrate nor ride over the bridge rail and remained upright during and after the collision. Vehicle

roll, pitch, and yaw angular displacements were noted, but they were deemed acceptable because they did not adversely influence the occupant risk safety criteria nor cause rollover. After collision, the vehicle's trajectory did not intrude into adjacent traffic lanes. In addition, the vehicle's exit angle of approximately 10.4 degrees was less than 60 percent of the original impact angle. The effective coefficient of friction, $\mu = 0.40$, was marginal ($\mu > 0.35$). Therefore, test no. FSCR-3 conducted on the bridge railing met all the TL-4 performance criteria provided in NCHRP Report No. 350. However, due to the technical difficulties with the vehicle guidance system, the truck did not impact within the tolerances of the speed and angle. Thus, this test would need to be repeated.

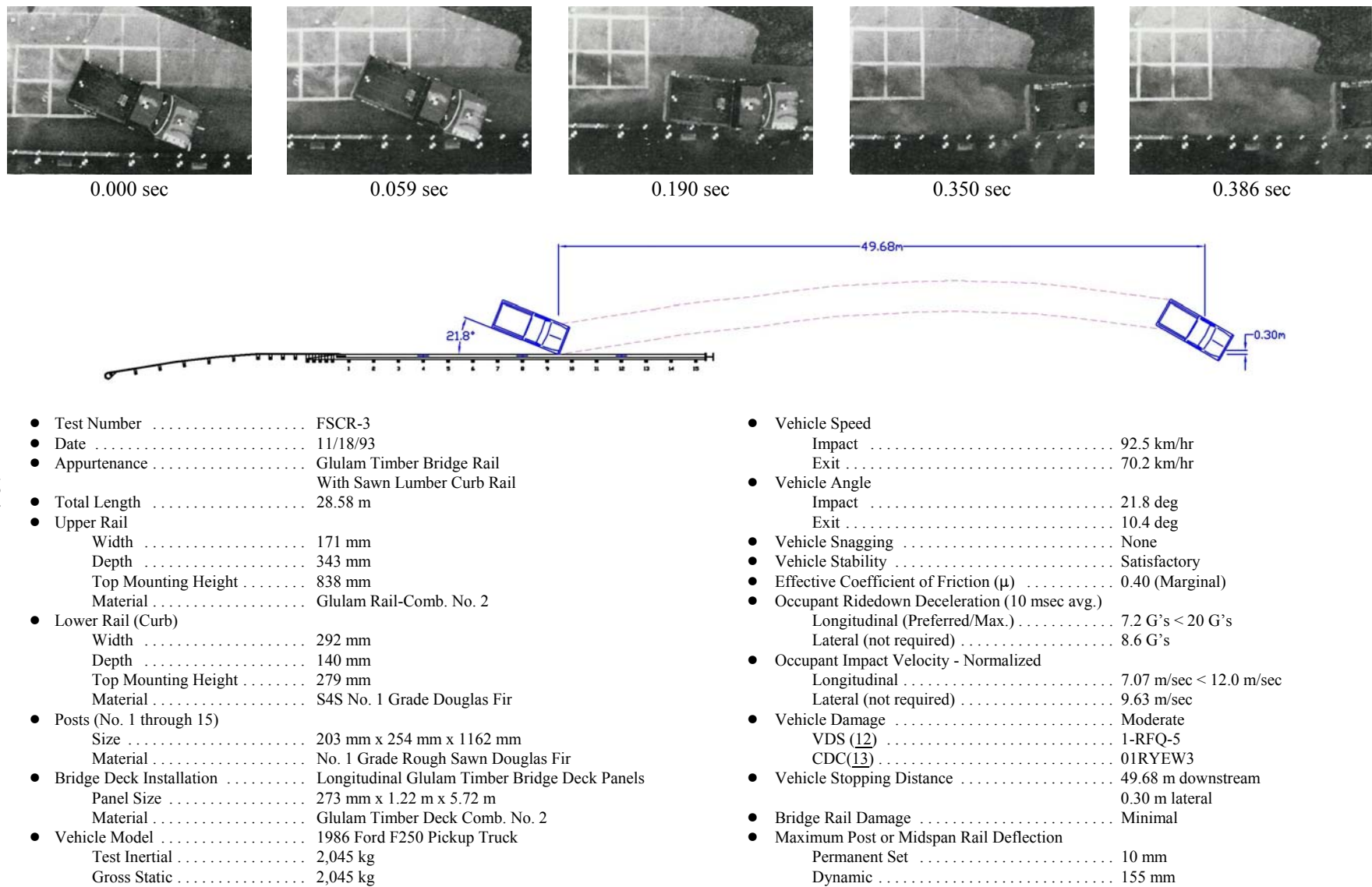


Figure 84. Summary of Test Results and Sequential Photographs, Test FSCR-3



0.000 sec



0.386 sec



0.059 sec



0.509 sec



0.190 sec



0.599 sec



0.350 sec

Figure 85. Additional Sequential Photographs, Test FSCR-3



Figure 86. Documentary Photographs, Test FSCR-3



Figure 87. Documentary Photographs, Test FSCR-3



Figure 88. Documentary Photographs, Test FSCR-3



Figure 89. Target Impact Location, Test FSCR-3



Figure 90. Final Vehicle Position and Trajectory Marks, Test FSCR-3



Figure 91. Bridge Rail Damage, Test FSCR-3



Figure 92. Bridge Rail Damage, Test FSCR-3



Figure 93. Vehicle Damage, Test FSCR-3



Figure 94. Front-End Vehicle Damage Due to Shear Post Impact, Test FSCR-3

12 CRASH TEST NO. 4 (BRIDGE RAILING)

12.1 Test FSCR-4

The 2,087-kg (4,600-lb) pickup truck impacted the bridge rail at a speed of 98.0 km/h (60.9 mph) and at an angle of 24.9 degrees. A summary of the test results and the sequential photographs are shown in Figure 95. Additional sequential photographs are shown in Figures 96 and 97.

12.2 Test Description

Initial impact occurred between bridge post nos. 7 and 8, approximately 1,759 mm (5 ft - 9 ¼ in.) upstream from post no. 8, as shown in Figure 98. After the initial impact with the bridge rail, the right-front corner of the bumper and quarter panel crushed inward. At 0.054 sec, the right-front tire deflated due to contact with the sawn lumber curb rail. At 0.068 sec, the right-front corner of the pickup truck was positioned near post no. 8. At 0.126 sec, the maximum dynamic lateral deflections were measured at post no. 8. At 0.146 sec, the right-front corner of the pickup truck was near post no. 9. The entire vehicle became airborne at approximately 0.217 sec. At 0.223 sec, the pickup truck was approximately parallel to the bridge rail with a velocity of 66.5 km/h (41.3 mph) and encountered a slight roll angle CW toward the bridge rail. At this same time, the right-front corner of the pickup truck was positioned near post no. 10. At 0.418 sec, the vehicle exited the bridge railing at a speed of approximately 62.9 km/h (39.1 mph) and at an angle of approximately 10.4 degrees. The vehicle's right-front tire contacted the ground at 0.512 sec. At 0.620 sec, the vehicle's left-front tire contacted the ground. At 0.748 sec, the maximum compression of the vehicle's front-end suspension occurred. The vehicle's trajectory and final position are shown in Figures 95 and 109. The vehicle came to rest approximately 38.6 m (126 ft - 7 in.) downstream from the impact point.

12.3 Bridge Rail Damage

The minor bridge railing damage is shown in Figures 99 and 100. Scrapes and gouging occurred to the upper glulam timber and sawn lumber curb rails. Significant tire and rim contact with the curb rail occurred from the downstream side of post no. 7 to the downstream side of post no. 8. Longitudinal cracking occurred toward the bottom traffic-side face of the glulam rail at post no. 8. The downstream edge of the glulam rail splice located at post no. 8 was fractured. Flexural failure occurred in the tension region of the glulam rail (or the back side of the vertical saw-cut section) and near the downstream end of the steel splice plate, as shown in Figures 101 and 102.

Permanent set in the curb rail was found at post nos. 7, 8, and 9. No physical damage occurred to the timber bridge posts or spacer blocks. However, rotation of post no. 8 occurred at the post to curb rail bolt attachment location, as shown in Figure 103. The high-strength bar, located transversely through the timber deck and on the upstream-side of post no. 8, pulled out of the high-strength nut and bearing plate located on the inside vertical deck surface, as shown in Figures 103 and 104. Note the residual of nut threads left on the end of the bar. One steel plate washer, located on the traffic-side face of the curb rail at post no. 8, was deformed due to wheel hub contact, as shown in Figure 105. Two steel plate washers, located on the back side of post nos. 8 and 9, were slightly deformed. Additional curb rail damage consisted of cracking along a vertical plane through the longitudinal centerline of the bolts, as shown in Figures 106 and 107. The glulam timber bridge deck received some surface cracks, as shown in Figures 107 and 108. The crack width ranged between 1.59 mm ($\frac{1}{16}$ in.) and 6.35 mm ($\frac{1}{4}$ in.).

The maximum lateral permanent set deflections for midspan rail and post locations were approximately 53 mm (2.1 in.) and 48 mm (1.9 in.), respectively, as measured in the field. The

maximum lateral dynamic deflections for midspan rail and post locations were 292 mm (11.5 in.) and 361 mm (14.2 in.), respectively, as determined from high-speed analysis. The effective coefficient of friction was determined to be approximately 0.54.

12.4 Vehicle Damage

Exterior vehicle damage was moderate, as shown in Figures 110 and 111. Deformations to the right-side floorboard and on the center hump located below the seat and behind the gear shift, as shown in Figure 112, were judged to be insufficient to cause serious injury to the vehicle occupants. In addition, no deformation occurred to the interior front dashboard.

Vehicle damage occurred to several body locations, such as door and quarter panels, front bumper, right-side tires and rims, rear bumper, engine mount, and interior floorboard. The right-front tire was deflated and slightly removed from the rim. The right-front steel rim was deformed. In addition, the right-front tire, rim, and attached steering mechanism were pushed backward into the engine compartment. Small dents were found in the right-rear steel rim. The right-side engine mount was deformed inward toward the engine. The right-front section of steel frame located within the engine housing received minor deformation. The right corner of the front bumper and right-front quarter panel were crushed inward. Small glulam timber fibers were embedded in various locations (i.e., cracks, joints, etc.) in the vehicle's sheet metal due to contact with the timber rail. The front bumper encountered a buckling point at its midpoint. The right corner of the rear bumper and right-rear quarter panel were also deformed. The right-side door was deformed and scraped. Small hairline cracks were found in the lower right-side corner of the front windshield.

12.5 Occupant Risk Values

The longitudinal and lateral normalized occupant impact velocities were determined to be 8.20 m/s (26.9 ft/sec) and 7.38 m/s (24.2 ft/sec), respectively. The maximum 0.010-sec average occupant ridedown decelerations in the longitudinal and lateral directions were 10.0 g's and 12.5 g's, respectively. It is noted that the occupant impact velocities and occupant ridedown decelerations were within the suggested limits provided in NCHRP Report No. 350. The results of the occupant risk, determined from accelerometer data, are summarized in Figure 95. Results are shown graphically in Appendix I.

12.6 Discussion

Analysis of the test results for test FSCR-4 showed that the bridge rail adequately contained and redirected the test vehicle with controlled lateral displacements of the bridge rail. There were no detached elements or fragments which showed potential for penetrating the occupant compartment nor presented undue hazard to other traffic. Deformations of, or intrusions into, the occupant compartment that could have caused serious injury did not occur. The test vehicle did not penetrate nor ride over the bridge rail and remained upright during and after the collision. Vehicle roll, pitch, and yaw angular displacements were noted, but they were deemed acceptable because they did not adversely influence the occupant risk safety criteria nor cause rollover. After collision, the vehicle's trajectory revealed minimal intrusion into adjacent traffic lanes. In addition, the vehicle's exit angle was less than 60 percent of the impact angle. The effective coefficient of friction, $\mu=0.54$, was marginal ($\mu>0.35$). Therefore, test no. FSCR-4 conducted on the bridge railing was determined to be acceptable according to the TL-4 safety performance criteria provided in NCHRP Report No. 350.

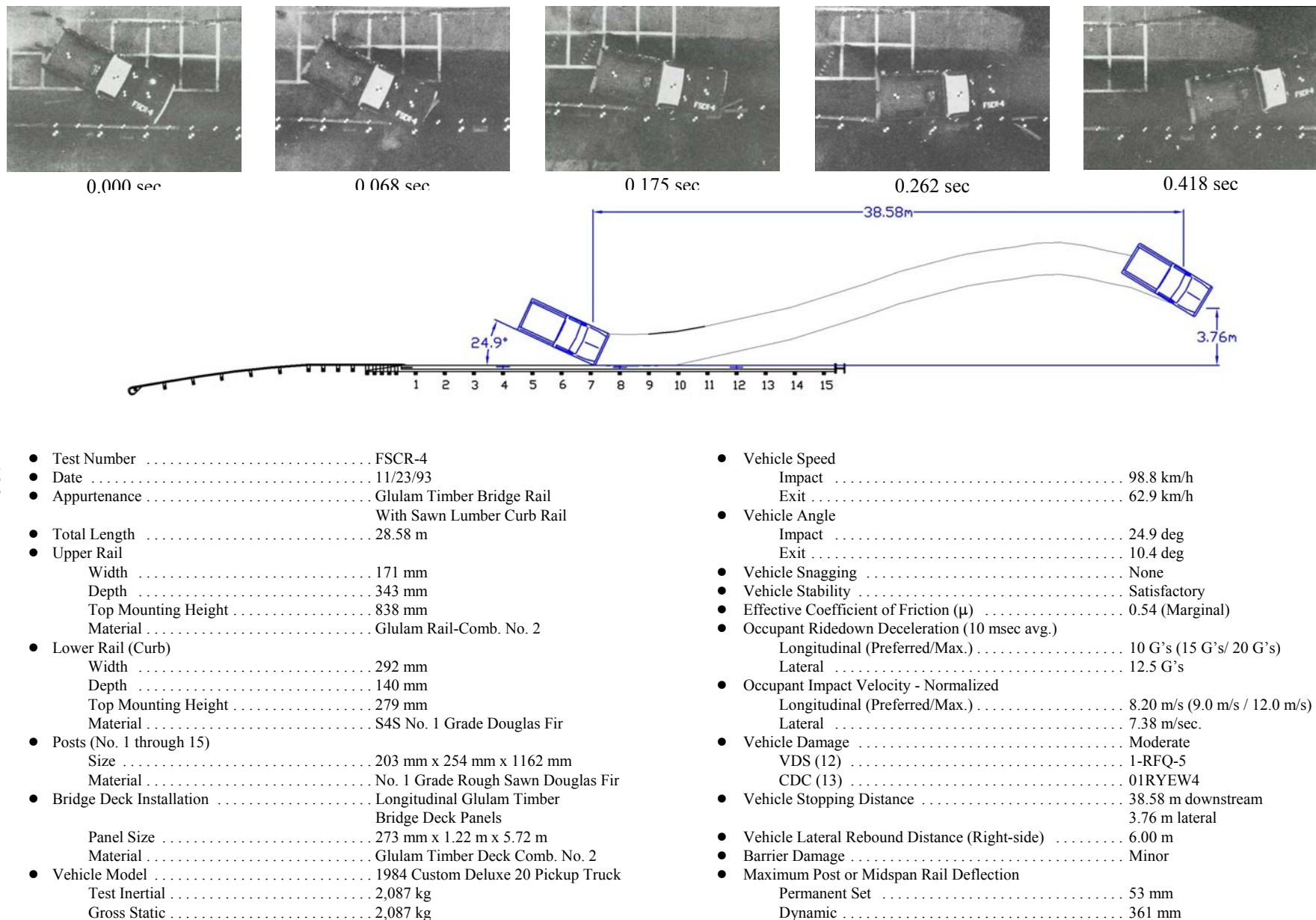


Figure 95. Summary of Test Results and Sequential Photographs, Test FSCR-4



0.000 sec



0.175 sec



0.054 sec



0.223 sec



0.068 sec



0.262 sec



0.146 sec



0.418 sec

Figure 96. Sequential Photographs, Test FSCR-4



0.000 sec



0.223 sec



0.054 sec



0.262 sec



0.068 sec



0.418 sec



0.146 sec



0.175sec

Figure 97. Additional Sequential Photographs, Test FSCR-4



Figure 98. Impact Locations, Test FSCR-4



Figure 99. Bridge Rail Damage, Test FSCR-4



Figure 100. Bridge Rail Damage, Test FSCR-4

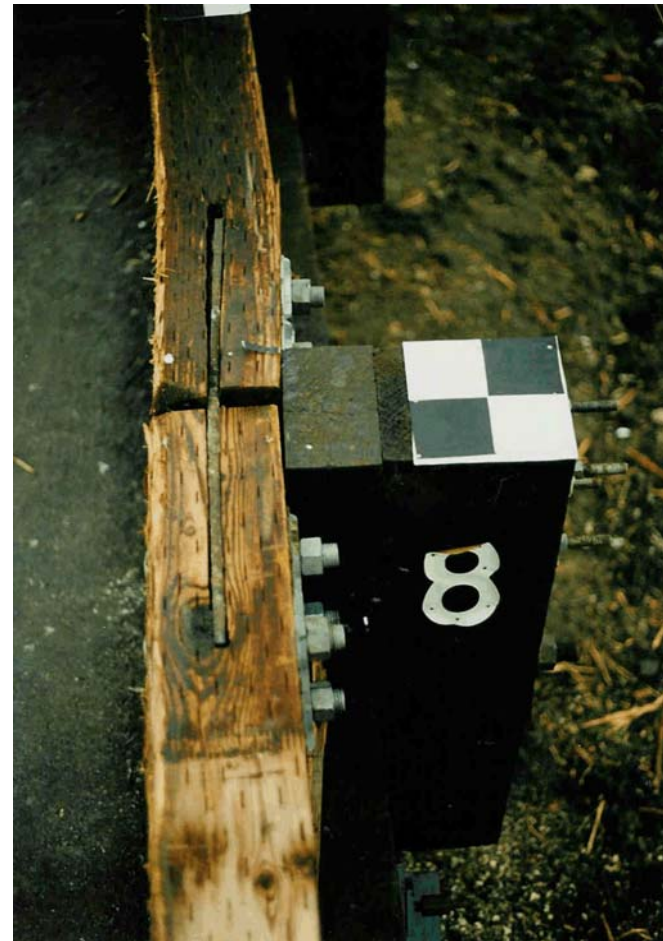


Figure 101. Glulam Rail Deformation at Post No. 8, Test FSCR-4

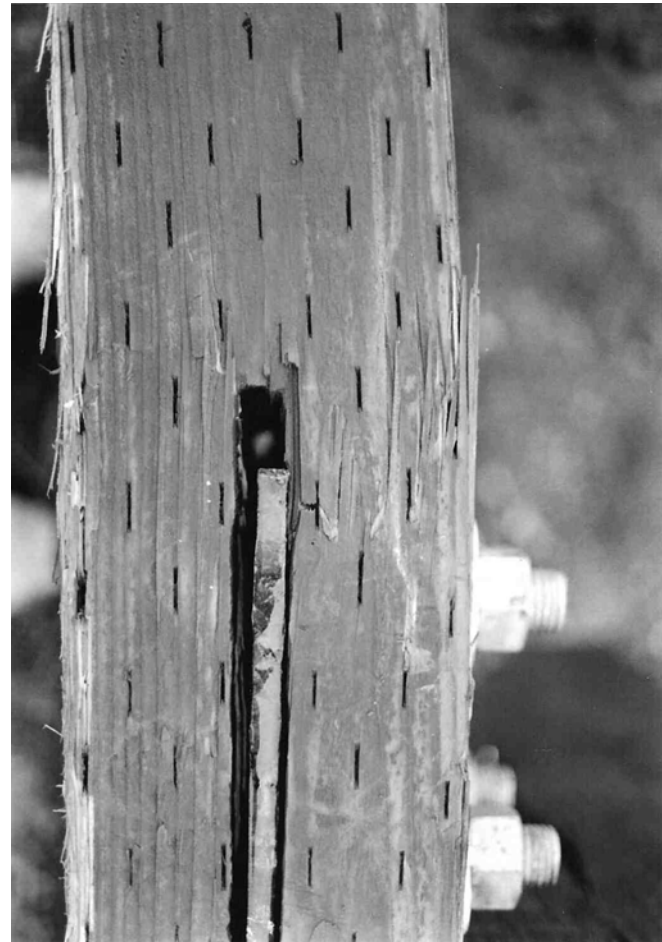


Figure 102. Glulam Rail Fracture at Post No. 8, Test FSCR-4



Figure 103. Damage at Post No. 8, Test FSCR-4

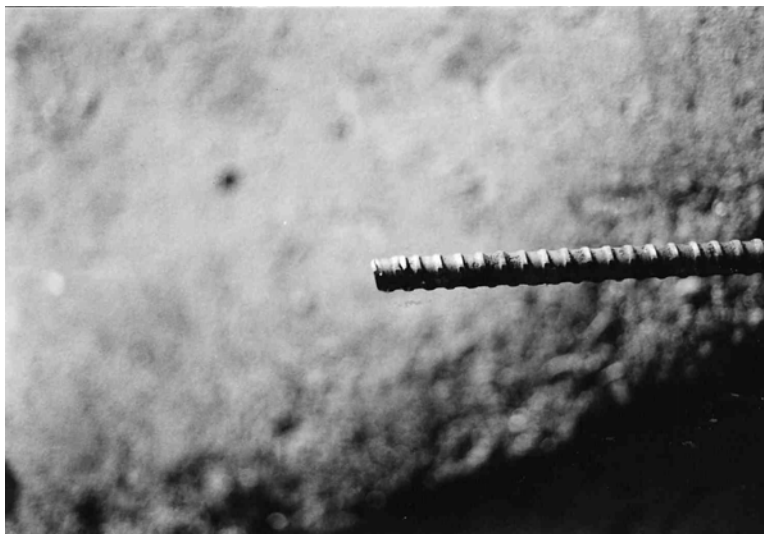


Figure 104. Internal Deck-Side end of High-Strength Bar Located at Post No. 8 (Note residual nut threads left on the end of the bar), Test FSCR-4



Figure 105. Plate washer deformation at Post No. 8, Test FSCR-4

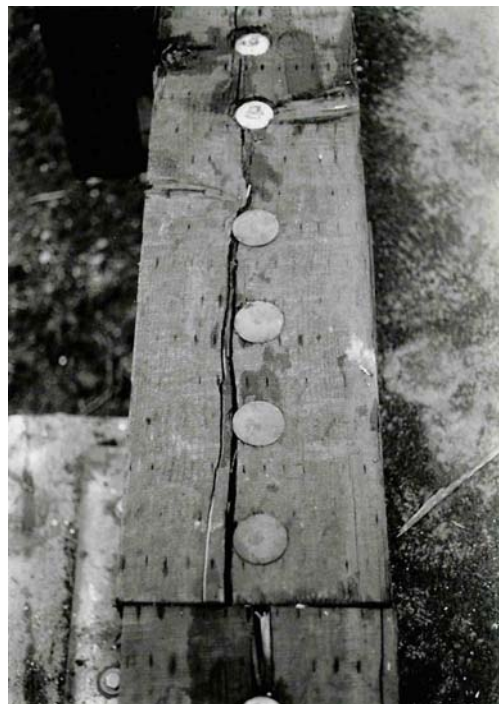
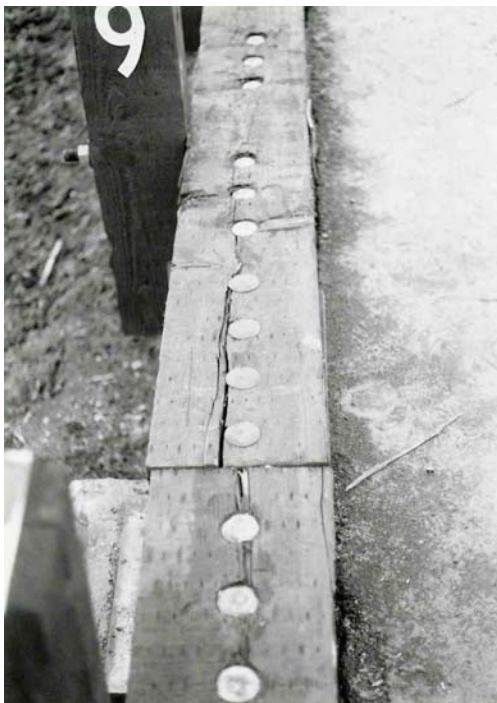


Figure 106. Curb Rail Damage Between Post Nos. 8 through 10, Test FSCR-4



Figure 107. Deck Cracking Between Post Nos. 6 and 7, 8 and 9, Test FSCR-4

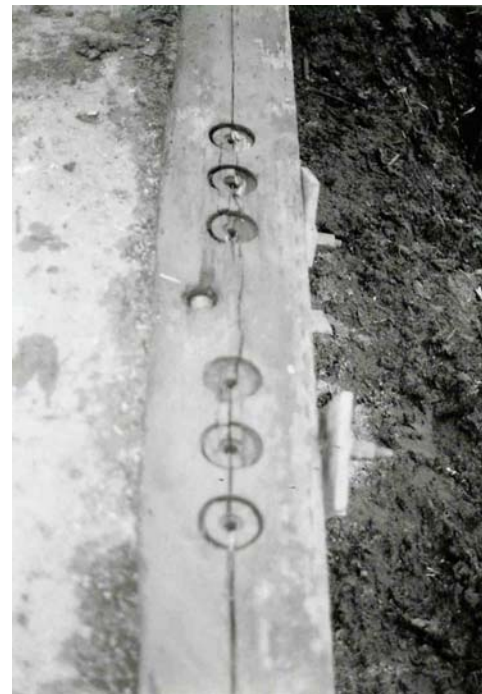
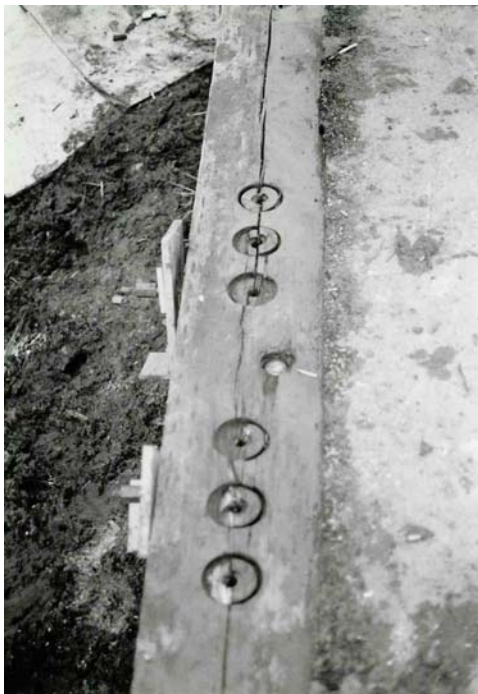
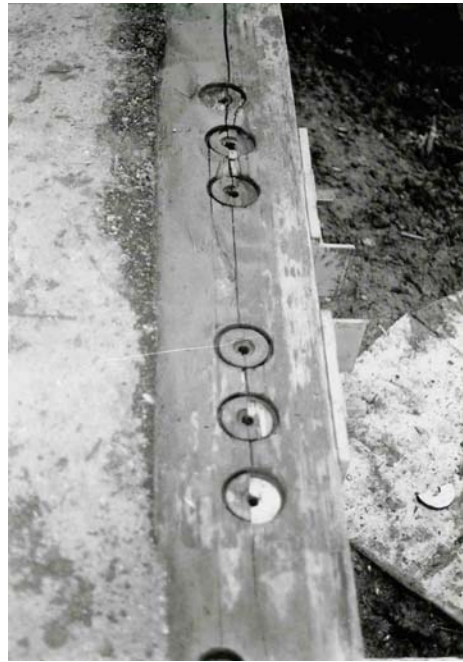
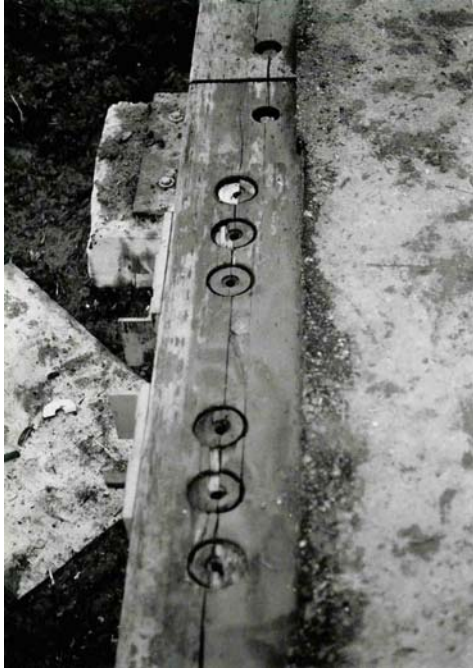


Figure 108. Deck Cracking at Post Nos. 7 and 8, Test FSCR-4



Figure 109. Final Position, Test FSCR-4



Figure 110. Vehicle Damage, Test FSCR-4



Figure 111. Vehicle Damage, Test FSCR-4



Figure 112. Occupant Compartment Deformation, Test FSCR-4

13 SUMMARY AND CONCLUSIONS

A glulam bridge railing with curb system and an attached approach guardrail transition system were successfully developed and full-scale crash tested for use on longitudinal glulam timber deck bridges. Four full-scale vehicle crash tests were performed on the bridge railing and approach guardrail transition. Three tests were conducted on the bridge railing according to the TL-4 safety performance criteria presented in NCHRP Report No. 350. The one test on the approach guardrail transition was conducted according to the MSL-2 safety performance criteria presented in NCHRP Report No. 230. A summary of the safety performance evaluations for the crash tests are provided in Tables 5 and 6.

As mentioned previously, prior to the development of this wood bridge railing system, no other TL-4 railing systems had been developed for use on longitudinal glulam timber deck bridges. However, this research program clearly demonstrates that crashworthy wood railing systems are feasible for use on these types of bridges. The development of the wood bridge railing and transition system addressed the concerns for aesthetics, economy, material availability, ease of construction, and reasonable margin of structural adequacy. In addition, the wood bridge railing and transition systems were relatively easy to install and should have reasonable construction labor costs.

The first crash test, test no. FSCR-1, was performed on the glulam bridge rail with a single-unit truck. The truck was safely contained and redirected with minimal barrier deflections and moderate barrier damage. Three posts fractured away from the bridge rail due to the truck box extending over the rail. Minor surface cracks were found on the glulam bridge deck. Therefore, test no. FSCR-1 was determined to be acceptable according to the PL-2 safety performance criteria

presented in AASHTO. Later, it was determined to be acceptable according to the TL-4 criteria of NCHRP Report No. 350.

The second crash test, test no. FSCR-2, was performed on the approach guardrail transition for the glulam bridge rail with a sedan. The sedan was safely contained and redirected with minimal barrier deflections and moderate barrier damage. The curb rail was fractured within the impacted region. Minor surface cracks were found on the glulam bridge deck. Therefore, test no. FSCR-2 was determined to be acceptable according to the MSL-2 safety performance criteria presented in NCHRP Report No. 230.

The GC-8000 bridge railing was originally designed and was to be evaluated according to the AASHTO PL-2 guidelines. However, following the successful 8,165-kg (18,000-lb) single-unit truck test, it was determined that the bridge railing could potentially meet the NCHRP Report No. 350 pickup truck strength test. Therefore, the 2,000-kg (4,409-lb) pickup test at 100 km/h (62.1 mph) and 25 degrees was conducted instead of the 2,449-kg (5,400-lb) pickup test at 96.6 km/h (60 mph) and 20 degrees.

Thus, the third crash test, test no. FSCR-3, was performed on the glulam bridge rail with a pickup truck. However, due to technical difficulties with the vehicle guidance system, the pickup impacted the bridge railing but at a slower speed and lower angle. Although the truck did not impact within the tolerances, the truck was safely contained and redirected. However, due to the fact that the impact conditions were not within the allowable tolerances, this pickup test would need to be repeated.

The fourth crash test, test no. FSCR-4, was the repeat test of test no. FSCR-3. This test was performed on the glulam bridge rail with a pickup truck. The pickup was safely contained and

redirected with minimum barrier deflections and damage. Minor surface cracks were found on the glulam bridge deck. Therefore, test no. FSCR-4 was determined to be acceptable according to the test designation 4-11 safety performance criteria presented in NCHRP Report No. 350.

Table 5. NCHRP Report No. 350 TL-4 Evaluation Results - Wood System (Bridge Railing)

Evaluation Factors	Evaluation Criteria	Test No.		
		FSCR-1	FSCR-3	FSCR-4
Structural Adequacy	A. Test article should contain and redirect the vehicle; the vehicle should not penetrate, underide, or override the installation although controlled lateral deflection of the test article is acceptable.	S	S	S
Occupant Risk	D. Detached elements, fragments or other debris from the test article should not penetrate or show potential for penetrating the occupant compartment, or present an undue hazard to other traffic, pedestrians, or personnel in a work zone. Deformations of, or intrusions into, the occupant compartment that could cause serious injuries should not be permitted.	S	S	S
	F. The vehicle should remain upright during and after collision although moderate roll, pitching, and yawing are acceptable.	NR	S	S
	G. It is preferable, although not essential, that the vehicle remain upright during and after collision.	S	NR	NR
Vehicle Trajectory	K. After collision it is preferable that the vehicle's trajectory not intrude into adjacent traffic lanes.	S	S	S
	L. The occupant impact velocity in the longitudinal direction should not exceed 12 m/s and the occupant ridedown acceleration in the longitudinal direction should not exceed 20 g's.	NR	S	S
	M. The exit angle from the test article preferably should be less than 60 percent of test impact angle, measured at time of vehicle loss of contact with test device.	S	S	S

S - Satisfactory
M - Marginal
U - Unsatisfactory
NR - Not Required

Table 6. NCHRP Report No. 230 Evaluation Results - Wood System (Transition)

Evaluation Factors	Evaluation Criteria	Test No.
		FSCR-2
Structural Adequacy	A. Test article shall smoothly redirect the vehicle; the vehicle shall not penetrate or go over the installation although controlled lateral deflection of the test article is acceptable.	S
	D. Detached elements, fragments or other debris from the test article shall not penetrate or show potential for penetrating the passenger compartment or present undue hazard to other traffic.	S
Occupant Risk	E. The vehicle shall remain upright during and after collision although moderate roll, pitching and yawing are acceptable. Integrity of the passenger compartment must be maintained with essentially no deformation or intrusion.	S
Vehicle Trajectory	H. After collision, the vehicle trajectory and final stopping position shall intrude a minimum distance, if at all, into adjacent traffic lanes.	S
	I. In test where the vehicle is judged to be redirected into or stopped while in adjacent lanes, vehicle speed change during test article collision should be less than 24.1 km/h (15 mph) and the exit angle from the test article should be less than 60 percent of test impact angle, both measured at time of vehicle loss of contact with test device.	S

S - Satisfactory
 M - Marginal
 U - Unsatisfactory
 NR - Not Required

14 RECOMMENDATIONS

A glulam rail with curb bridge railing system, as described in this report, was successfully crash tested according to the criteria found in NCHRP Report No. 350. Along with the glulam bridge rail, an approach guardrail transition was successfully crash tested according to the criteria found in NCHRP Report No. 230. The results of these tests indicate that this design is a suitable design for use on higher performance roadways. It is suggested that the research described herein could be further developed using the data collected from testing to modify future designs. However, any design modifications made to the bridge railing system and approach transition may require verification through the use of full-scale vehicle crash testing.

It should be noted that further testing should be conducted if it is deemed necessary that the transition meet the NCHRP Report No. 350 TL-4 criteria. Further testing will be required because an 8,000-kg (17,637-lb) single-unit truck test or a 2,000-kg (4,409-lb) pickup truck test was not conducted on the approach guardrail transition.

Following this research study, FPL and MwRSF engineers prepared a set of standard bridge railing plans for use on some timber deck bridges (14). As a result, design details for the GC-8000 bridge railing system are provided in the set of plans for both English and SI units (15).

15 REFERENCES

1. Ross, H.E., Sicking, D.L., Zimmer, R.A., and Michie, J.D., *Recommended Procedures for the Safety Performance Evaluation of Highway Features*. National Cooperative Highway Research Program (NCHRP) Report No. 350, Transportation Research Board, Washington, D.C., 1993.
2. Hancock, K.L., Hansen, A.G., and Mayer, J.B., *Aesthetic Bridge Rails, Transitions, and Terminals for Park Roads and Parkways*. Report FHWA-RD-90-052, FHWA, U.S. Department of Transportation, May 1990.
3. *Guide Specifications for Bridge Railings*, American Association of State Highway and Transportation Officials (AASHTO), Washington, D.C., 1989.
4. Faller, R.K., Ritter, M.A., Holloway, J.C., Pfeifer, B.G., and Rosson, B.T., *Performance Level 1 Bridge Railings for Timber Decks*, Transportation Research Record 1419, TRB, National Research Council, Washington D.C., October 1993, pp. 21-34.
5. Ritter, M.A., Faller, R.K., Holloway, J.C., Pfeifer, B.G., and Rosson, B.T., *Development and Testing of Bridge Railings for Longitudinal Timber Decks by Full-Scale Crash Testing*, Draft Report to the U.S. Department of Agriculture, Forest Service, Forest Products Laboratory, Transportation Research Report No. TRP-03-29-94, Civil Engineering Department, University of Nebraska-Lincoln, August 1992.
6. Michie, J.D., *Recommended Procedures for the Safety Performance Evaluation of Highway Appurtenances*, National Cooperative Highway Research Program (NCHRP) Report No. 230, Transportation Research Board, Washington, D.C., March 1981.
7. American Wood-Preservers' Association Book of Standards, American Wood-Preservers' Association, Woodstock, Maryland, 1991.
8. Hinch, J, Yang T-L and Owings, R., *Guidance Systems for Vehicle Testing*, ENSCO, Inc., Springfield, VA, 1986.
9. *Center of Gravity Test Code - SAE J874 March 1981*, SAE Handbook Vol. 4, Society of Automotive Engineers, Inc., Warrendale, Pennsylvania, 1986.
10. Taborck, J.J., "Mechanics of Vehicles - 7", Machine Design Journal, May 30, 1957.
11. Powell, G.H., *Barrier VII: A Computer Program for Evaluation of Automobile Barrier Systems*. Report FHWA RD-73-51, FHWA, U.S. Department of Transportation, April 1973.
12. *Vehicle Damage Scale for Traffic Accident Investigators*, Traffic Accident Data Project Technical Bulletin No. 1, National Safety council, Chicago, IL, 1971.

13. *Collision Deformation Classification, Recommended Practice J224 March '80*, SAE Handbook Vol. 4, Society of Automotive Engineers, Warrendale, Pennsylvania, 1985.
14. Ritter, M.A., Faller, R.K., Lee, P.D.H., Rosson, B.T., and Duwaldi, S.R., *Plans for Crash Tested Bridge Railings for Longitudinal Wood Decks*, General Technical Report No. FPL-GTR-87, United States Department of Agriculture, Forest Service, Forest Products Laboratory, Madison, Wisconsin, September 1995.
15. Ritter, M.A., Faller, R.K., Lee, P.D.H., Rosson, B.T., and Duwaldi, S.R., *Plans for Crash-Tested Wood Bridge Railings for Concrete Decks*, General Technical Report No. FPL-GTR-108, United States Department of Agriculture, Forest Service, Forest Products Laboratory, U.S. DOT Federal Highway Administration, Madison, Wisconsin, August 1998.

16 APPENDICES

APPENDIX A

BARRIER VII Computer Models

Figure A-1. Model of the AASHTO PL-2 Curb Rail Bridge Rail System (FSCR-1,3,4)

Figure A-2. Model of the Approach Guardrail Transition for the AASHTO PL-2 Curb System (FSCR-2)

Figure A-3. Idealized Finite Element, 2 Dimensional Vehicle Model for the 8,000-kg (17,637-lb) Single-Unit Truck

Figure A-4. Idealized Finite Element, 2 Dimensional Vehicle Model for the 2,000-kg (4,409-lb) Pickup Truck

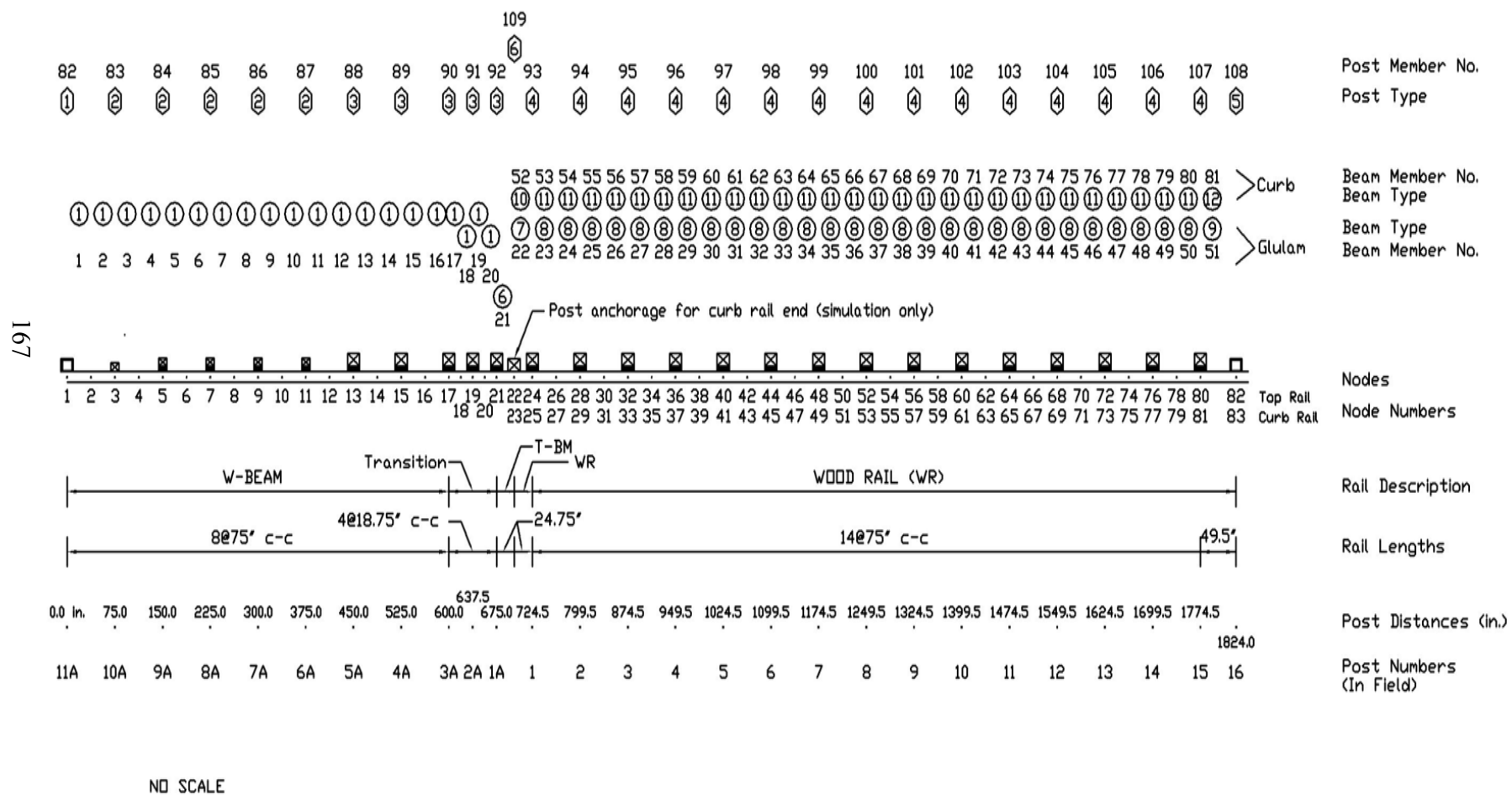


Figure A-1. Model of the AASHTO PL-2 Curb Rail Bridge Rail System (FSCR-1,3,4).

Approach Transition for PL-2 Curb System

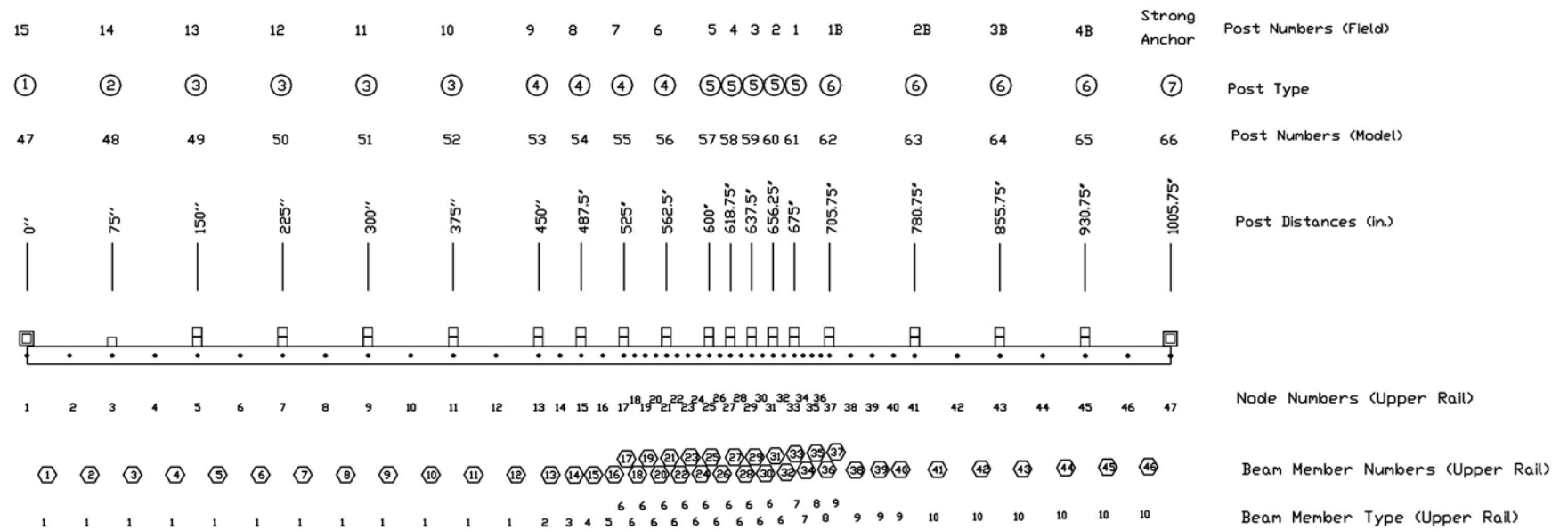


Figure A-2. Model of the Approach Guardrail Transition for the AASHTO PL-2 Curb System (FSCR-2).

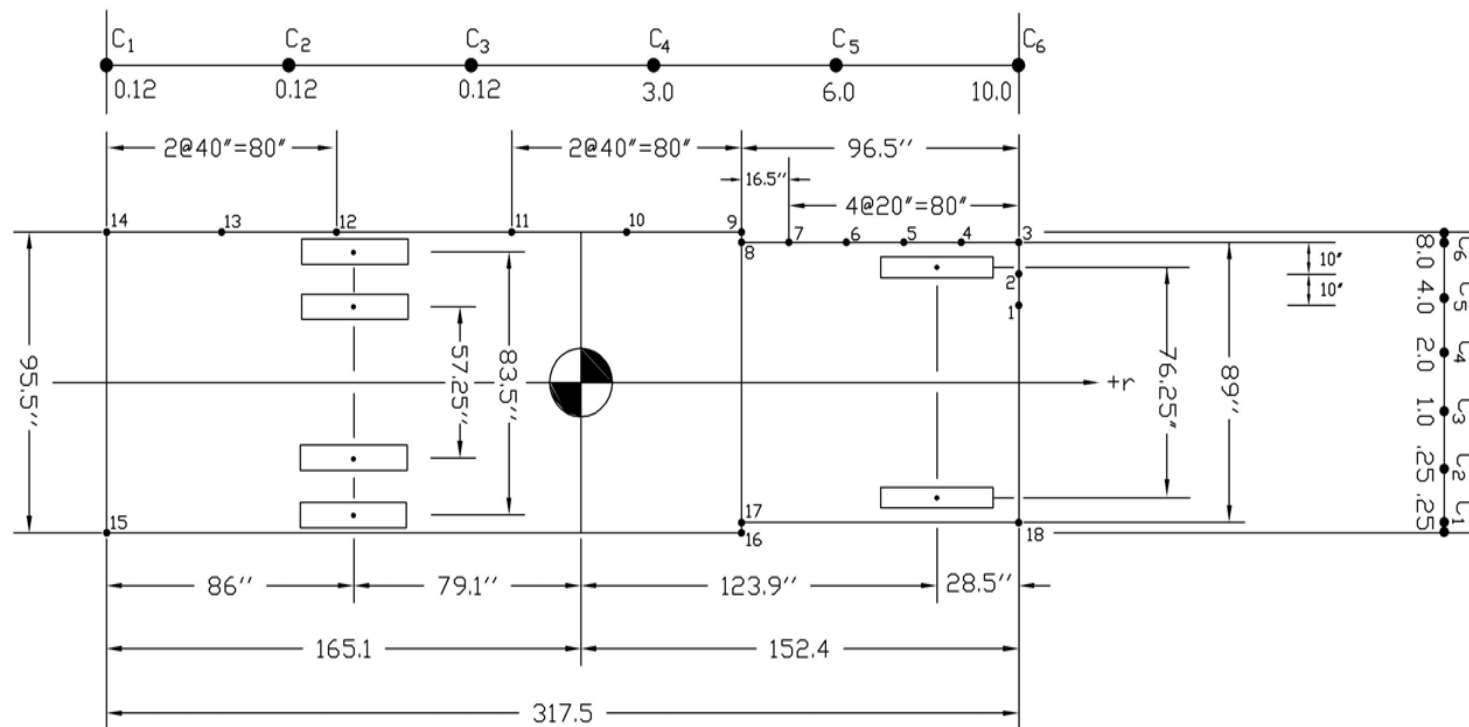


Figure A-3. Idealized Finite Element, 2 Dimensional Vehicle Model for the 8,000-kg (17,637-lb) Single-Unit Truck

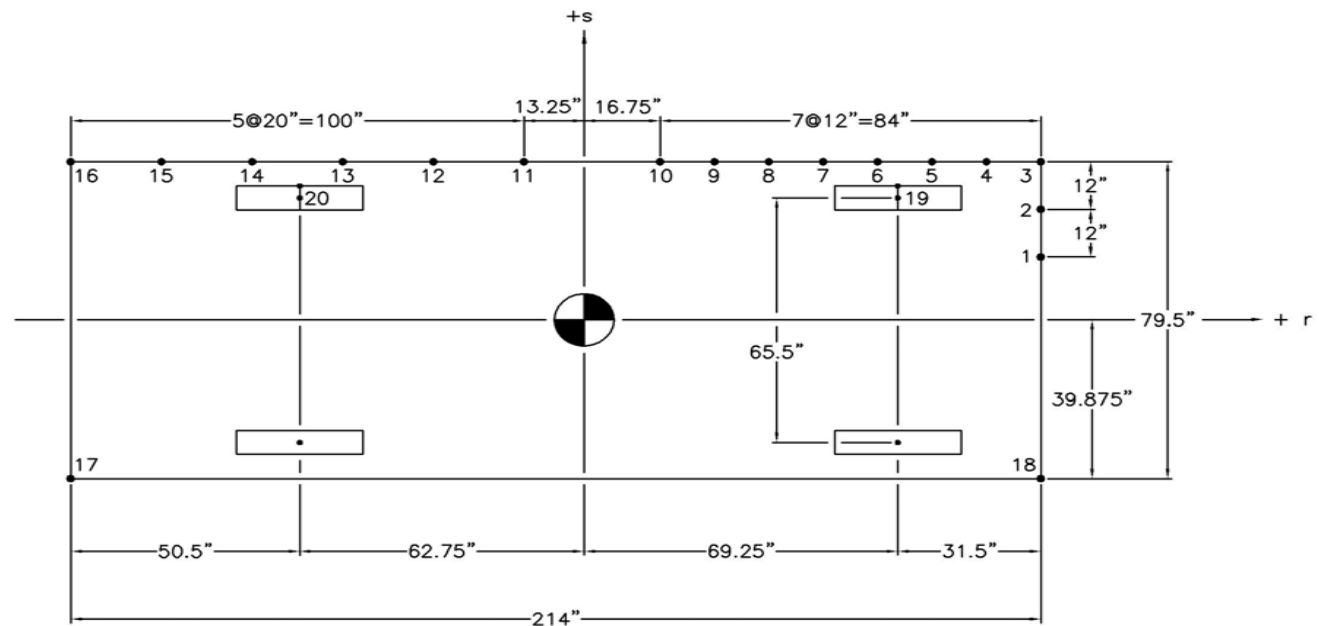


Figure A-4. Idealized Finite Element, 2 Dimensional Vehicle Model for the 2,000-kg (4,409-lb) Pickup Truck

APPENDIX B

Structural Properties of Rail and Post Elements

Table B-1. Structural Quantities for Railing Elements of GC-8000 Bridge Railing.

FSCR-1,3,4:

Member Type (Size)	Area (in ²)	Moment of Inertia About (in. ⁴)	Modulus of Elasticity ¹ (ksi)	Weight (lbs/ft)	Nominal Yield Force (kips)	Section Modulus (in. ³)	Nominal Yield Moment (kip-in.)	Plastic Modulus (in. ³)	Nominal Plastic Moment (kip-in.)
W-beam (12-gauge)	1.99	C-axis: 2.31	30,000.0	6.92	99.5	1.37	68.5	1.93	96.5
Glulam Rail 6.75"x13.5"	91.1	C-axis: 346.0	1,417.0	31.6	150.3	NA	522.8	NA	NA
Curb Rail 5.5"x11.5"	63.25	C-axis: 697.1	1,333.0	15.45	68.9	NA	192.0	NA	NA

FSCR-2:

Member Type (Size)	Area (in ²)	Moment of Inertia About (in. ⁴)	Modulus of Elasticity ¹ (ksi)	Weight (lbs/ft)	Nominal Yield Force (kips)	Section Modulus (in. ³)	Nominal Yield Moment (kip-in.)	Plastic Modulus (in. ³)	Nominal Plastic Moment (kip-in.)
W-beam (12-gauge)	1.99	C-axis: 2.31	30,000.0	6.92	99.5	1.37	68.5	1.93	96.5
W-beam-to-Thrie-Beam (12-gauge)	2.13	2.48	30,000.0	7.4	106.2	NA	73.8	NA	NA
	2.4	2.84	30,000.0	8.38	120.0	NA	84.0	NA	NA
	2.68	3.2	30,000.0	9.35	134.0	NA	94.0	NA	NA
	2.96	3.58	30,000.0	10.32	148.0	NA	104.2	NA	NA
Thrie-Beam (10-gauge)	4.0	4.82	30,000.0	13.95	200.0	2.8	140.0	3.92	196.0
Glulam Rail 6.75"x13.5"	91.1	C-axis: 346.0	1,417.0	31.6	150.3	NA	522.8	NA	NA

NA - Not available

Table B-2. Structural Quantities for Post Elements of GC-8000 Bridge Railing.

FSCR-1,3,4:

Member Type	Member Size	Top Node Height (in.)	Bottom Node Height (in.)	Stiffness Along (kips/in.)	Effective Weight (lbs)	Nominal Yield Moment About (kip-in.)	Failure Shear Force Along (kips)	Failure Deflection Along (in.)
W-beam Post	6" x 8"	21.0	0.0	A-axis: 15.0	50.0	A-axis: 231.0	A-axis: 18.8	A-axis: 20.0
				B-axis: 11.0		B-axis: 315.0	B-axis: 13.8	B-axis: 20.0
Transition Post	8" x 8"	21.0	0.0	A-axis: 15.0	77.0	A-axis: 315.0	A-axis: 18.8	A-axis: 20.0
				B-axis: 15.0		B-axis: 315.0	B-axis: 18.8	B-axis: 20.0
Wood Rail Post	8" x 10"	18.0	0.25	A-axis: 4.89	69.67	A-axis: 764.3	A-axis: 38	A-axis: 7.6
				B-axis: 7.63		B-axis: 611.41	B-axis: 45.0	B-axis: 6.1

FSCR-2:

Member Type	Member Size	Top Node Height (in.)	Bottom Node Height (in.)	Stiffness Along (kips/in.)	Effective Weight (lbs)	Nominal Yield Moment About (kip-in.)	Failure Shear Force Along (kips)	Failure Deflection Along (in.)
W-beam Post	6" x 8"	21.0	0.0	A-axis: 1.95	70.4	A-axis: 191.1	A-axis: 18.8	A-axis: 20.0
				B-axis: 1.56		B-axis: 214.2	B-axis: 13.8	B-axis: 20.0
Transition Post	8" x 8"	21.0	0.0	A-axis: 1.95	93.9	A-axis: 307.4	A-axis: 18.8	A-axis: 20.0
				B-axis: 1.95		B-axis: 307.4	B-axis: 18.8	B-axis: 20.0
Thrie-beam Post	8" x 8"	21.0	0.0	A-axis: 1.95	93.9	A-axis: 307.4	A-axis: 25.0	A-axis: 20.0
				B-axis: 1.95		B-axis: 307.4	B-axis: 18.8	B-axis: 20.0
Wood Rail Post	8" x 10"	18.0	0.0	A-axis: 4.89	69.67	A-axis: 764.3	A-axis: 38.0	A-axis: 7.6
				B-axis: 7.63		B-axis: 611.41	B-axis: 45.0	B-axis: 6.1

APPENDIX C

Typical BARRIER VII Input Data Files (CIP)

Note that the example BARRIER VII input data file included in Appendix C corresponds with the critical impact point for a sedan (test FSCR-2).

[illegible]

14	0.037	0.273	0.833	18.0				
15	0.018	0.222	0.833	37.0				
16	0.037	0.273	0.833	18.0				
17	0.044	0.533	1.110	17.0				
18	5.0	15.0	40.0	5.0				
19	5.0	15.0	40.0	5.0				
1	96.0	15.5	1	12.0	1	0		
2	96.0	25.5	2	12.0	1	0		
3	96.0	37.5	3	12.0	1	0		
4	84.0	37.5	4	12.0	1	0		
5	72.0	37.5	5	12.0	1	0		
6	60.0	37.5	6	12.0	1	0		
7	48.0	37.5	7	12.0	1	0		
8	36.0	37.5	8	12.0	1	0		
9	-55.0	37.5	9	12.0	1	0		
10	-67.0	37.5	10	12.0	1	0		
11	-79.0	37.5	11	12.0	1	0		
12	-91.0	37.5	12	12.0	1	0		
13	-103.0	37.5	13	12.0	1	0		
14	-115.0	37.5	14	12.0	1	0		
15	-115.0	25.5	15	12.0	1	0		
16	-115.0	-37.5	16	1.0	0	0		
17	96.0	-37.5	17	1.0	0	0		
18	56.0	33.0	18	1.0	0	0		
19	-62.0	33.0	19	1.0	0	0		
1	56.0	31.0	0.0	1410.0				
2	56.0	-31.0	0.0	565.0				
3	-62.0	31.0	0.0	610.0				
4	-62.0	-31.0	0.0	150.0				
1	0.0	0.0						
3	609.375	0.0	25.0	60.0	0.0	0.0	15.0	

APPENDIX D

Typical BARRIER VII Input Data Files (SUT, typical)

Note that the example BARRIER VII input data file included in Appendix D corresponds with the typical impact point for a single unit truck (test FSCR-1).

83	11	4	2	109	18	2	0			
0.0010	0.0010			0.80	100	0	1.0	1		
1	5	5	5		5	1				
1	0.0		0.0							
17	600.0		0.0							
21	675.0		0.0							
22	699.75		0.0							
23	699.75		0.0							
24	724.5		0.0							
25	724.5		0.0							
80	1774.5		0.0							
81	1774.5		0.0							
82	1824.0		0.0							
83	1824.0		0.0							
1	17	15	1	0.0						
17	21	3	1	0.0						
24	80	27	2	0.0						
25	81	27	2	0.0						
1	52		0.3							
82	80	78	76	74	72	70	68	66	64	
62	60	58	56	54	52	50	48	46	44	
42	40	38	36	34	32	30	28	26	24	
22	21	20	19	18	17	16	15	14	13	
12	11	10	9	8	7	6	5	4	3	
2	1									
2	31		0.3							
83	81	79	77	75	73	71	69	67	65	
63	61	59	57	55	53	51	49	47	45	
43	41	39	37	35	33	31	29	27	25	
23										
100	12									
1	2.31		1.99		37.50		30000.0	6.92	99.5	68.5 0.10
2	2.48		2.13		18.75		30000.0	7.41	106.5	73.5 0.10
3	2.83		2.41		18.75		30000.0	8.38	120.5	83.5 0.10
4	3.17		2.68		18.75		30000.0	9.35	134.0	93.5 0.10
5	3.52		2.96		18.75		30000.0	10.32	148.0	103.5 0.10
6	3.76		3.10		24.75		30000.0	10.81	155.0	110.0 0.10
7	346.0		91.1		24.75		1417.0	31.6	150.3	522.8 0.10
8	346.0		91.1		37.50		1417.0	31.6	150.3	522.8 0.10
9	346.0		91.1		49.50		1417.0	31.6	150.3	522.8 0.10
10	697.1		63.25		24.75		1333.0	15.45	68.9	192.0 0.10
11	697.1		63.25		37.50		1333.0	15.45	68.9	192.0 0.10
12	697.1		63.25		49.50		1333.0	15.45	68.9	192.0 0.10
300	6									
1	21.0		0.0		6338.0		13943.0	94.7	6820.0	1540.0 0.10
2	310.0		70.0		1.0		1.0			
3	18.8		13.8		20.0		20.0	11.0	50.0	315.0 231.0 0.10
4	18.8		18.8		20.0		20.0	15.0	77.0	315.0 315.0 0.10
5	38.0		45.0		7.6		6.1	7.63	69.67	611.41 764.30 0.10
6	310.0		70.0		1.0		1.0			
7	8.25		0.0		6338.0		13943.0	94.7	6820.0	1540.0 0.10
8	310.0		70.0		1.0		1.0			
9	1	2	16	1	101		0.0	0.0	0.0	
17	17	18	0	0	102		0.0	0.0	0.0	
18	18	19	0	0	103		0.0	0.0	0.0	
19	19	20	0	0	104		0.0	0.0	0.0	
20	20	21	0	0	105		0.0	0.0	0.0	
21	21	22	0	0	106		0.0	0.0	0.0	
22	22	24	0	0	107		0.0			

2	152.4	34.5	1	10.0	1	0	0	0
3	152.4	44.5	1	15.0	1	0	0	0
4	132.4	44.5	1	20.0	1	0	0	0
5	112.4	44.5	2	20.0	1	0	0	0
6	92.4	44.5	2	20.0	1	0	0	0
7	72.4	44.5	2	18.25	1	0	0	0
8	55.9	44.5	2	11.5	1	0	0	0
9	55.9	47.75	3	23.25	0	0	0	0
10	15.9	47.75	4	40.0	0	0	0	0
11	-24.1	47.75	5	40.0	0	0	0	0
12	-85.1	47.75	5	40.0	0	0	0	0
13	-125.1	47.75	5	40.0	0	0	0	0
14	-165.1	47.75	5	20.0	0	0	0	0
15	-165.1	-47.75	5	1.0	0	0	0	0
16	55.9	-47.75	3	1.0	0	0	0	0
17	55.9	-44.5	2	1.0	0	0	0	0
18	152.4	-44.5	1	1.0	0	0	0	0
19	-79.1	45.75	7	1.0	1	0	0	0
20	123.9	42.12	6	1.0	1	0	0	0
1	123.9	38.12	0.0	2214.				
2	123.9	-38.12	0.0	2214.				
3	-79.1	41.75	0.0	1157.				
4	-79.1	-41.75	0.0	1157.				
5	-79.1	28.62	0.0	1157.				
6	-79.1	-28.62	0.0	1157.				
1	0.0	0.0						
3	949.5	0.0	15.0	50.0		0.0	0.0	10.0

APPENDIX E

Typical BARRIER VII Input Data Files (PU, typical)

Note that the example BARRIER VII input data file included in Appendix E corresponds with the typical impact point for a pickup truck (tests FSCR-3,4).

[illegible]

3	100.75	39.875	2	12.0	1	0	0	0
4	88.75	39.875	2	12.0	1	0	0	0
5	76.75	39.875	2	12.0	1	0	0	0
6	64.75	39.875	2	12.0	1	0	0	0
7	52.75	39.875	2	12.0	1	0	0	0
8	40.75	39.875	2	12.0	1	0	0	0
9	28.75	39.875	2	12.0	1	0	0	0
10	16.75	39.875	2	12.0	1	0	0	0
11	-13.25	39.875	3	12.0	1	0	0	0
12	-33.25	39.875	3	12.0	1	0	0	0
13	-53.25	39.875	3	12.0	1	0	0	0
14	-73.25	39.875	3	12.0	1	0	0	0
15	-93.25	39.875	3	12.0	1	0	0	0
16	-113.25	39.875	4	12.0	1	0	0	0
17	-113.25	-39.875	4	12.0	0	0	0	0
18	100.75	-39.875	1	12.0	0	0	0	0
19	69.25	37.75	5	1.0	1	0	0	0
20	-62.75	37.75	6	1.0	1	0	0	0
1	69.25	37.75		0.0	608.			
2	69.25	-37.75		0.0	608.			
3	-62.75	37.75		0.0	492.			
4	-62.75	-37.75		0.0	492.			
1	0.0	0.0						
3	1174.5	0.0	25.0	62.14		0.0	0.0	5.0

APPENDIX F

Accelerometer Data Analysis - Test FSCR-1

Figure F-1. Graph of Longitudinal Deceleration, Test FSCR-1

Figure F-2. Graph of Longitudinal Occupant Impact Velocity, Test FSCR-1

Figure F-3. Graph of Longitudinal Occupant Displacement, Test FSCR-1

Figure F-4. Graph of Lateral Deceleration, Test FSCR-1

Figure F-5. Graph of Lateral Occupant Impact Velocity, Test FSCR-1

Figure F-6. Graph of Lateral Occupant Displacement, Test FSCR-1

Figure F-7. Graph of Roll, Pitch and Yaw Angular Displacements, Test FSCR-1

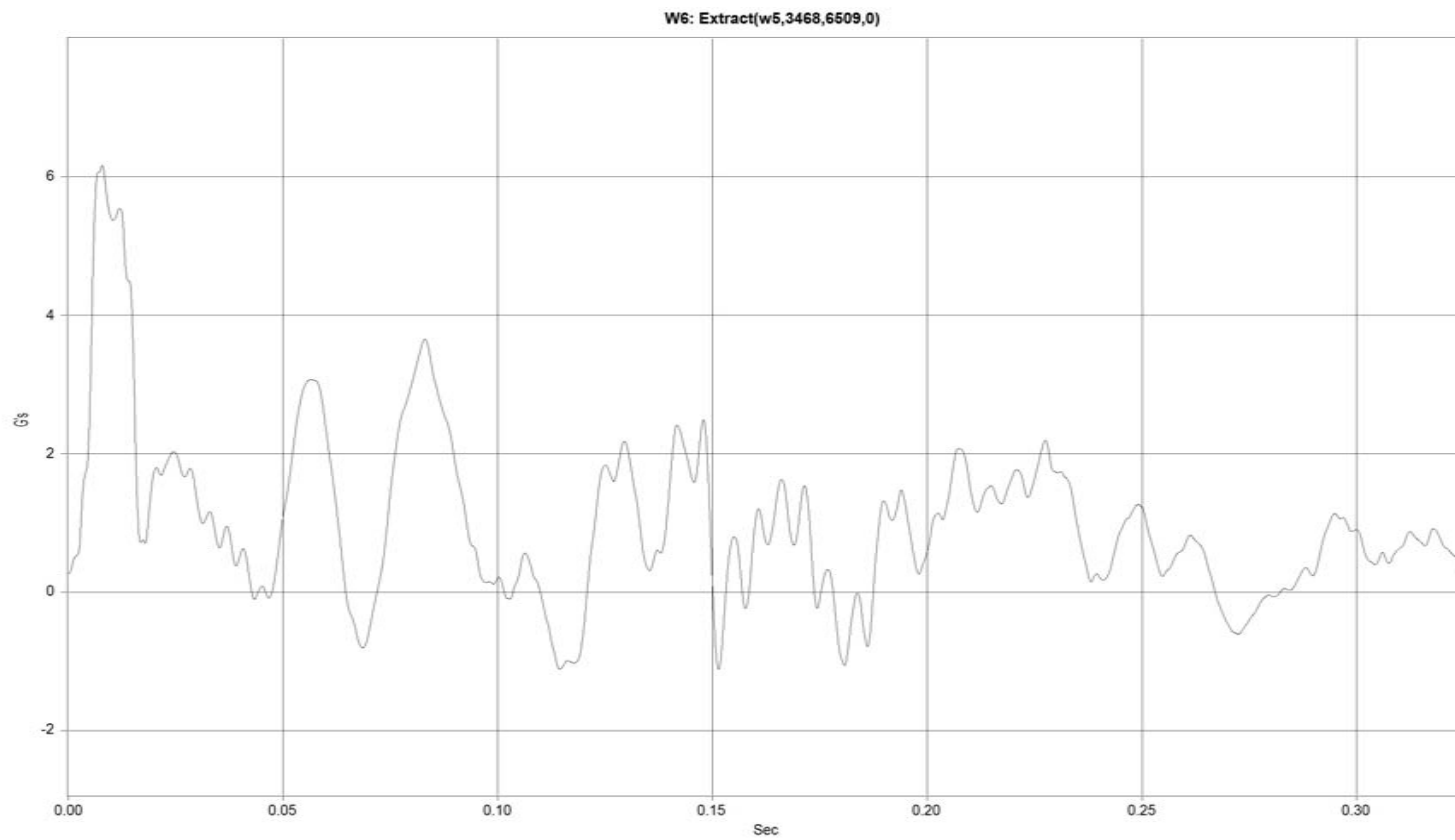


Figure F-1. Graph of Longitudinal Deceleration, Test FSCR-1

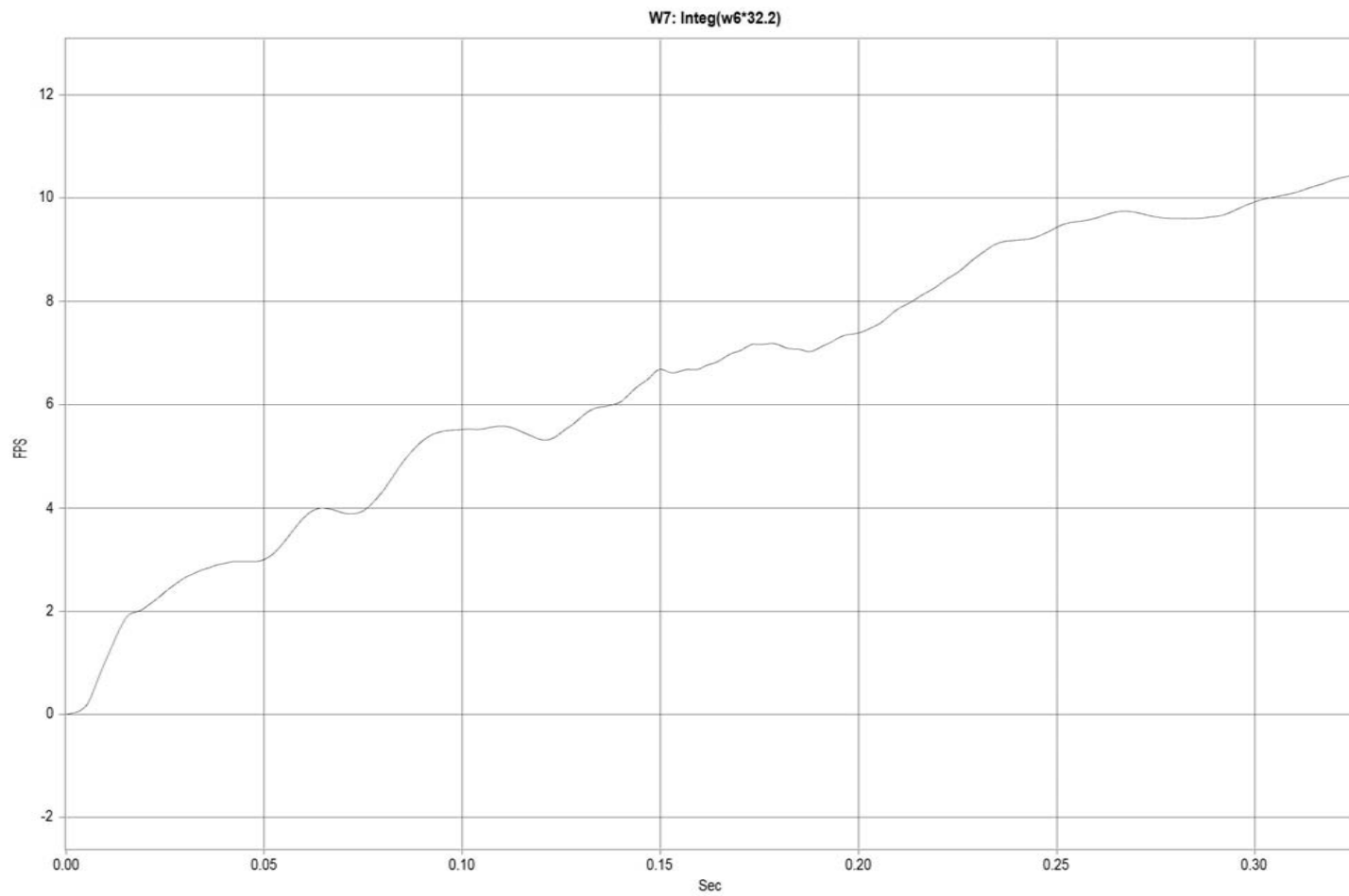


Figure F-2. Graph of Longitudinal Occupant Impact Velocity, Test FSCR-1

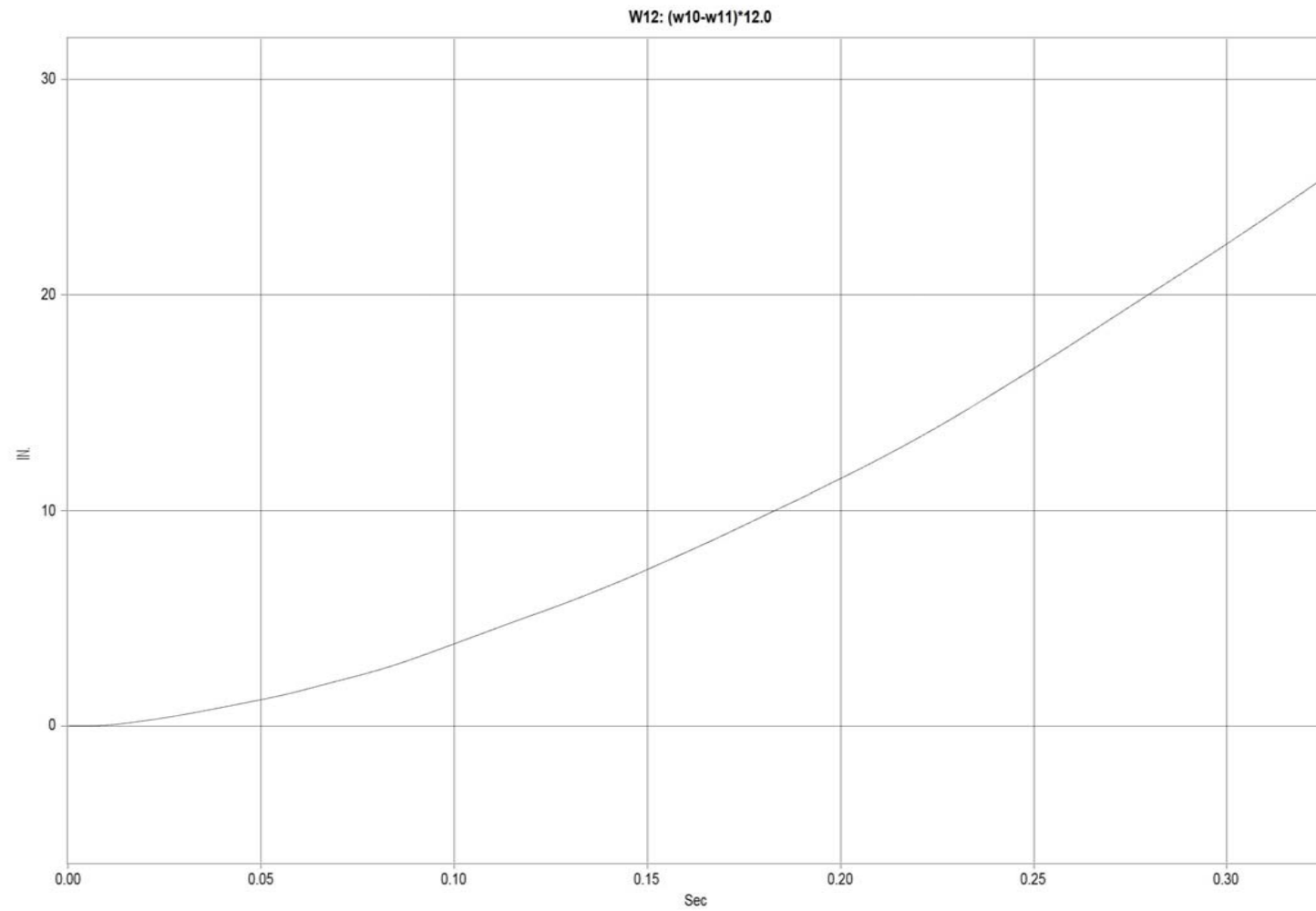


Figure F-3. Graph of Longitudinal Occupant Displacement, Test FSCR-1

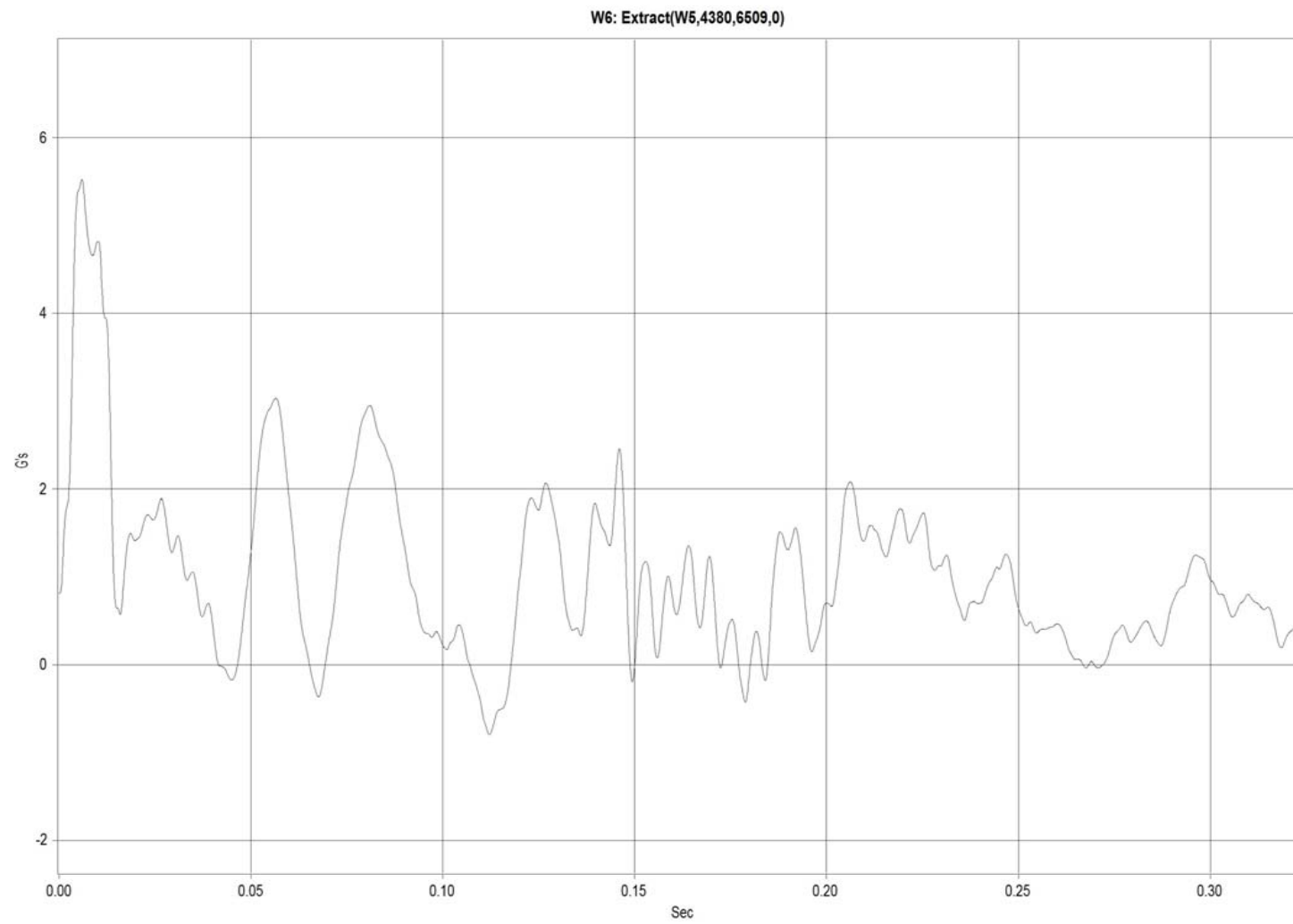


Figure F-4. Graph of Lateral Deceleration, Test FSCR-1

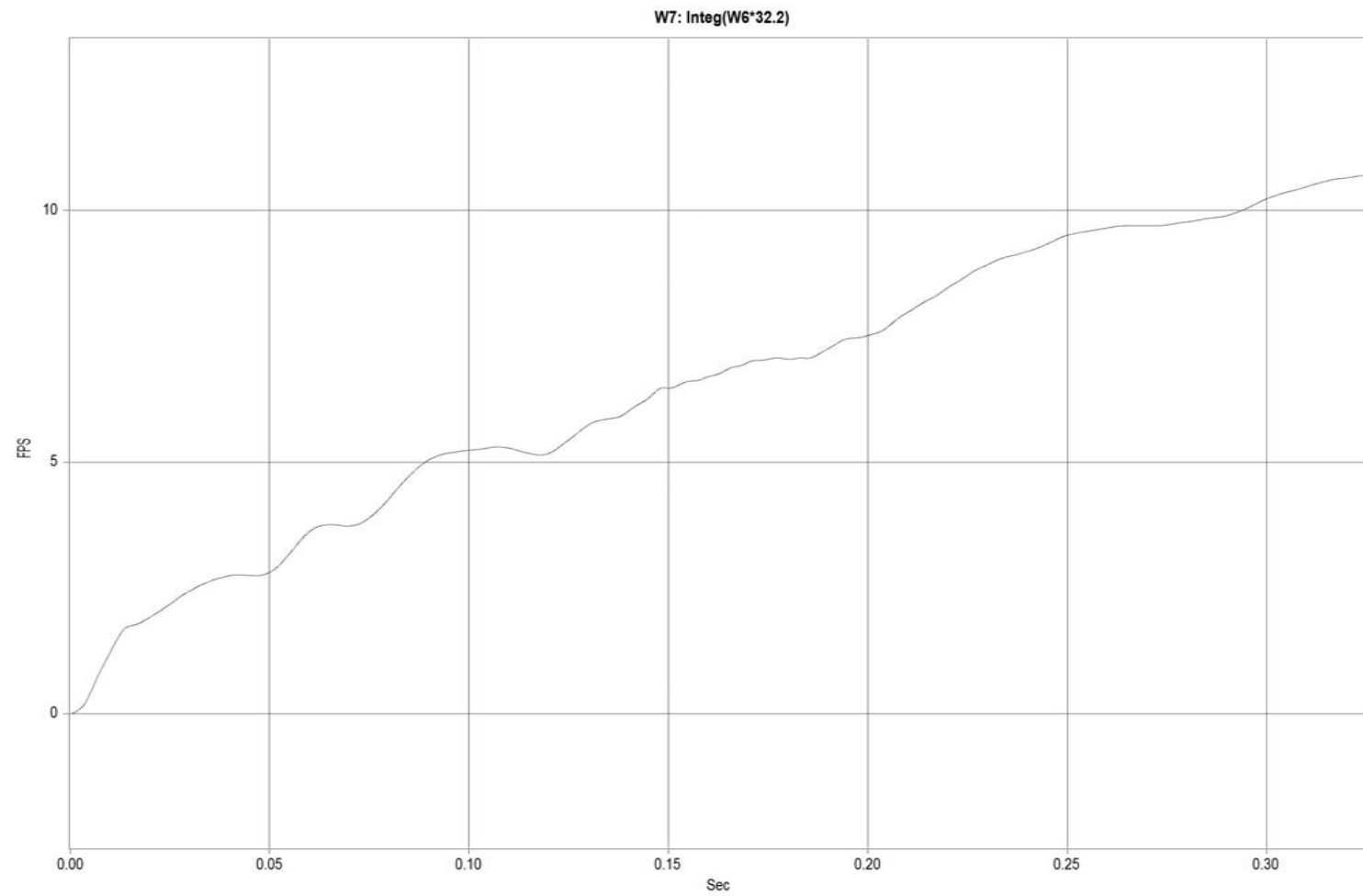


Figure F-5. Graph of Lateral Occupant Impact Velocity, Test FSCR-1

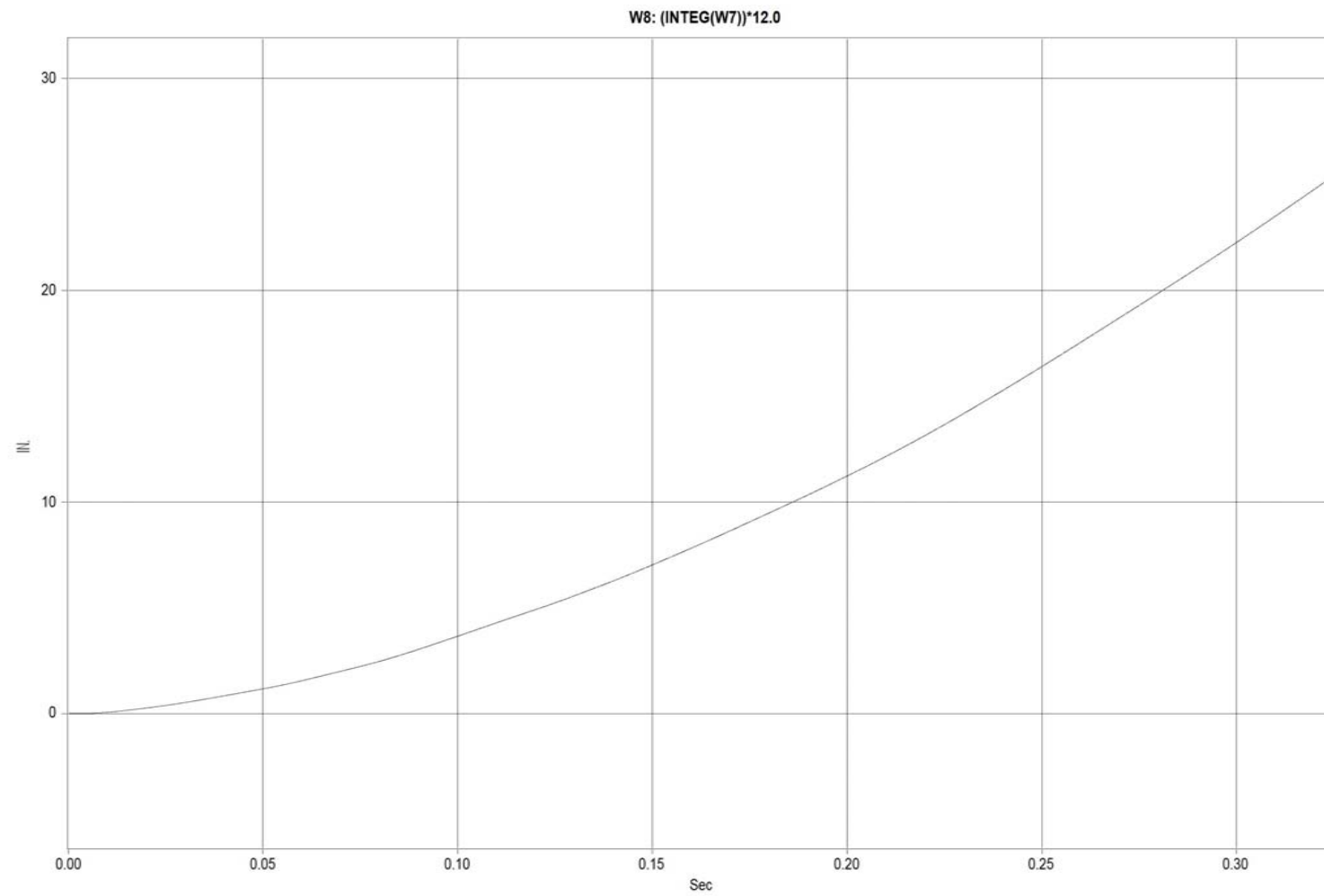


Figure F-6. Graph of Lateral Occupant Displacement, Test FSCR-1

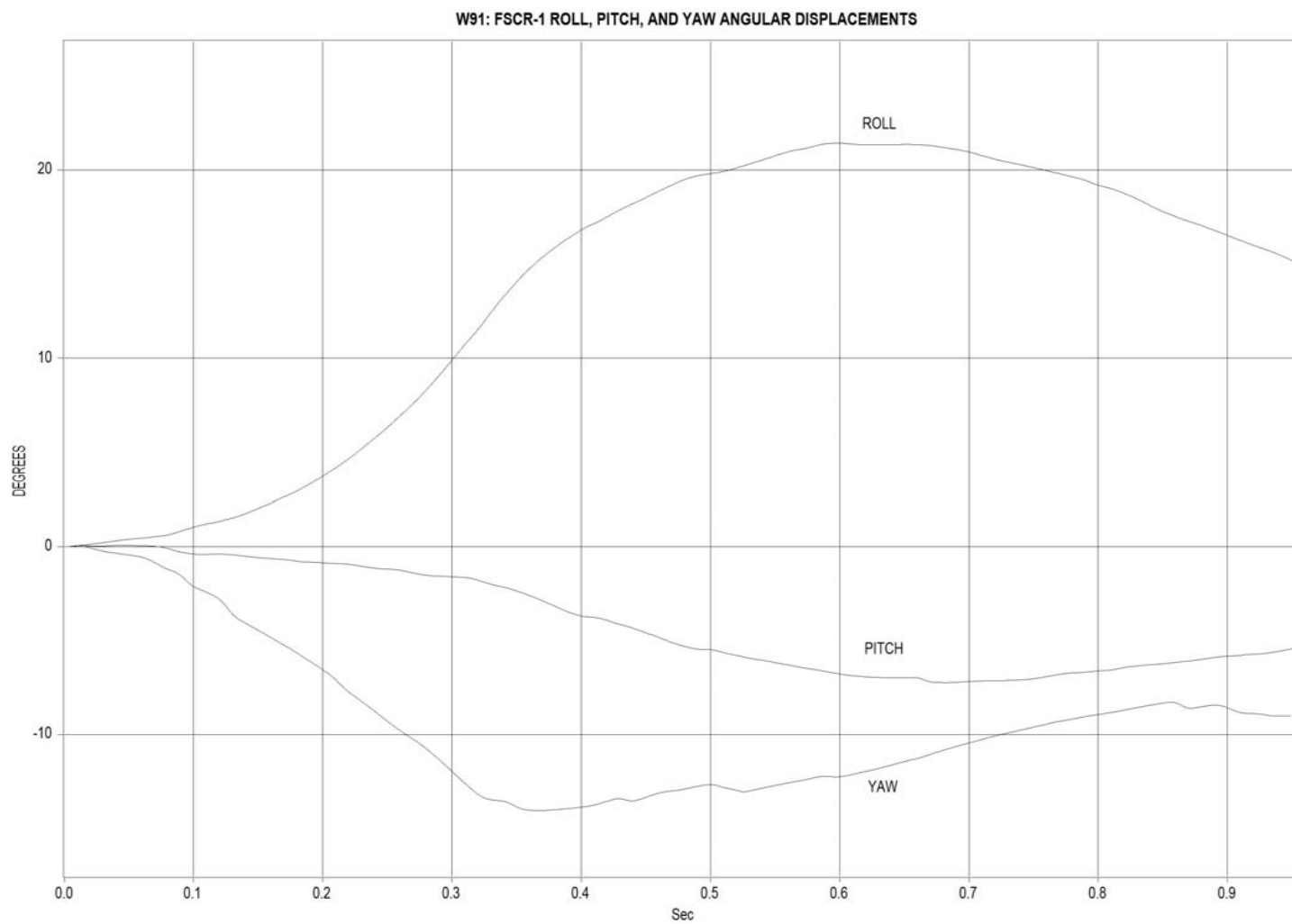


Figure F-7. Graph of Roll, Pitch and Yaw Angular Displacements, Test FSCR-1

APPENDIX G

Accelerometer Data Analysis - Test FSCR-2

Figure G-1. Graph of Longitudinal Deceleration, Test FSCR-2

Figure G-2. Graph of Longitudinal Occupant Impact Velocity, Test FSCR-2

Figure G-3. Graph of Longitudinal Occupant Displacement, Test FSCR-2

Figure G-4. Graph of Lateral Deceleration, Test FSCR-2

Figure G-5. Graph of Lateral Occupant Impact Velocity, Test FSCR-2

Figure G-6. Graph of Lateral Occupant Displacement, Test FSCR-2

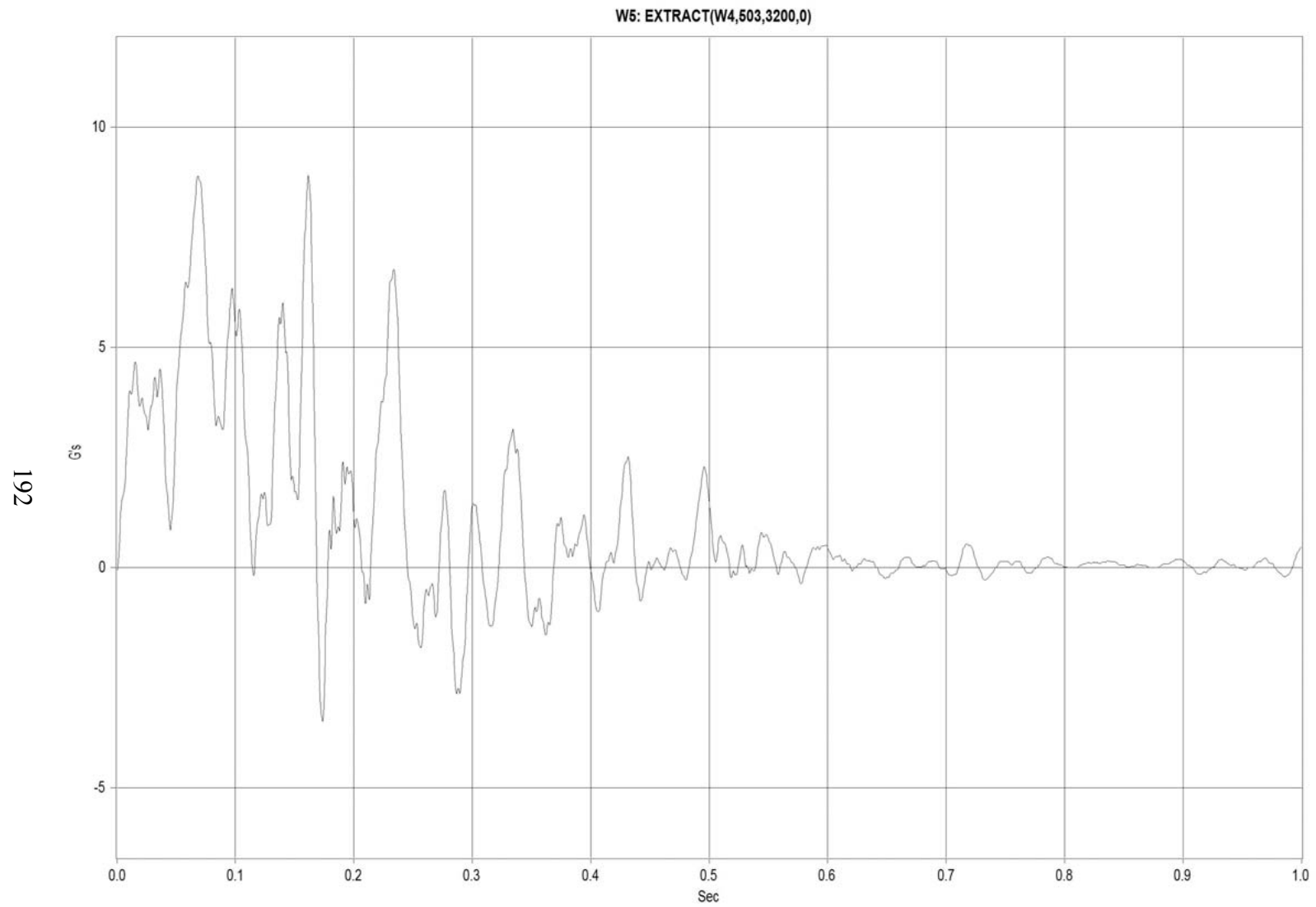


Figure G-1. Graph of Longitudinal Deceleration, Test FSCR-2

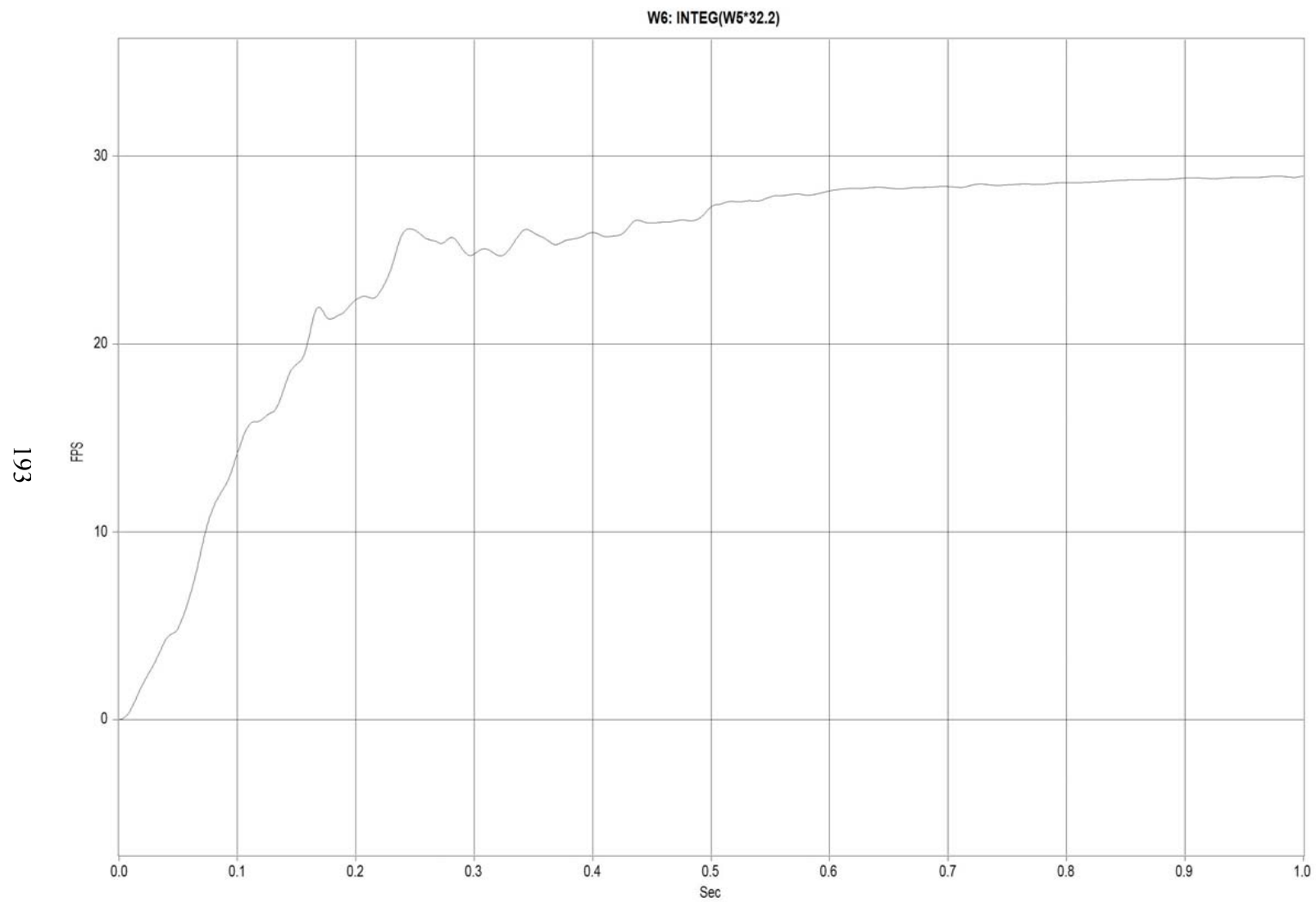


Figure G-2. Graph of Longitudinal Occupant Impact Velocity, Test FSCR-2

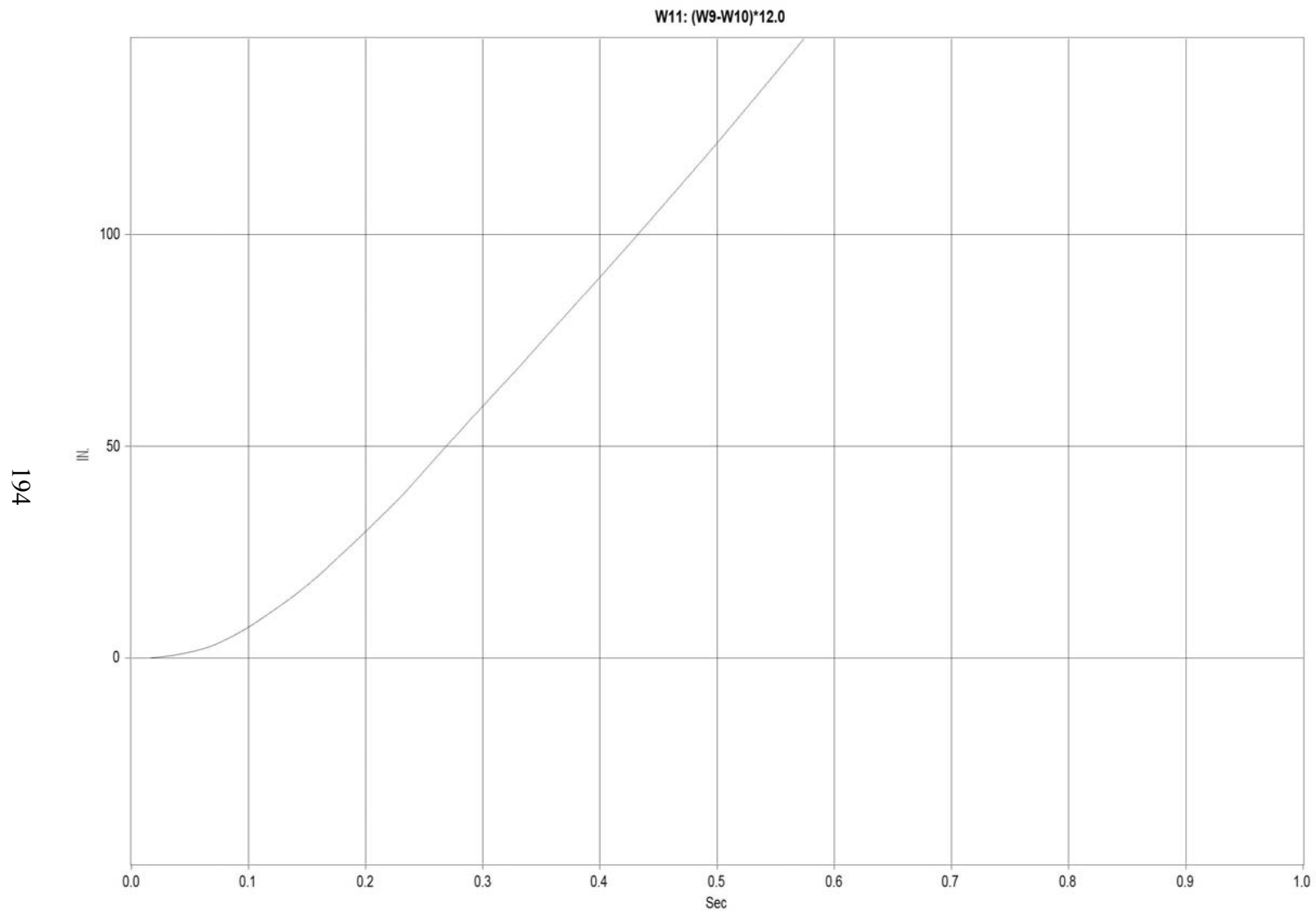


Figure G-3. Graph of Longitudinal Occupant Displacement, Test FSCR-2

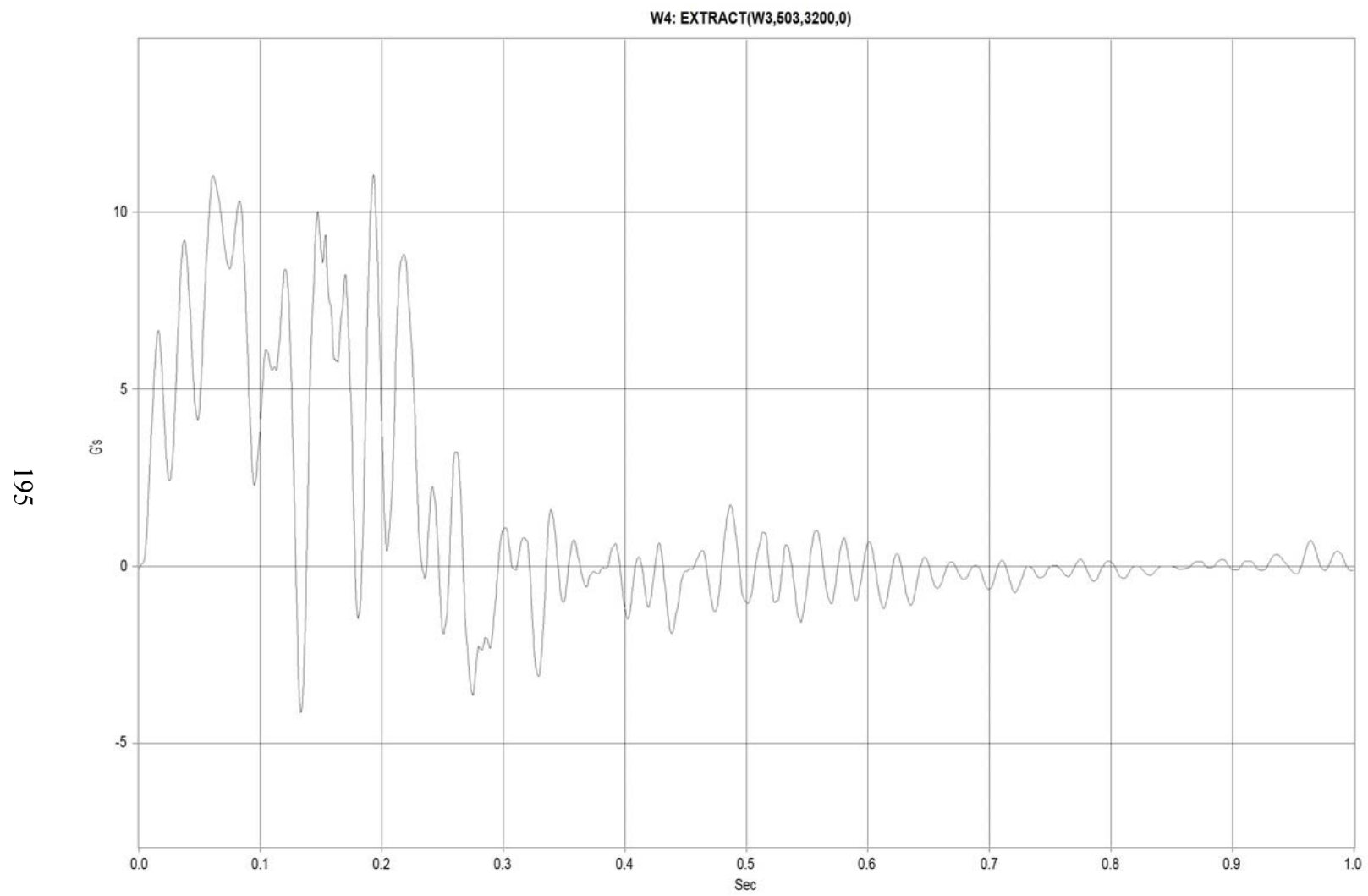


Figure G-4. Graph of Lateral Deceleration, Test FSCR-2

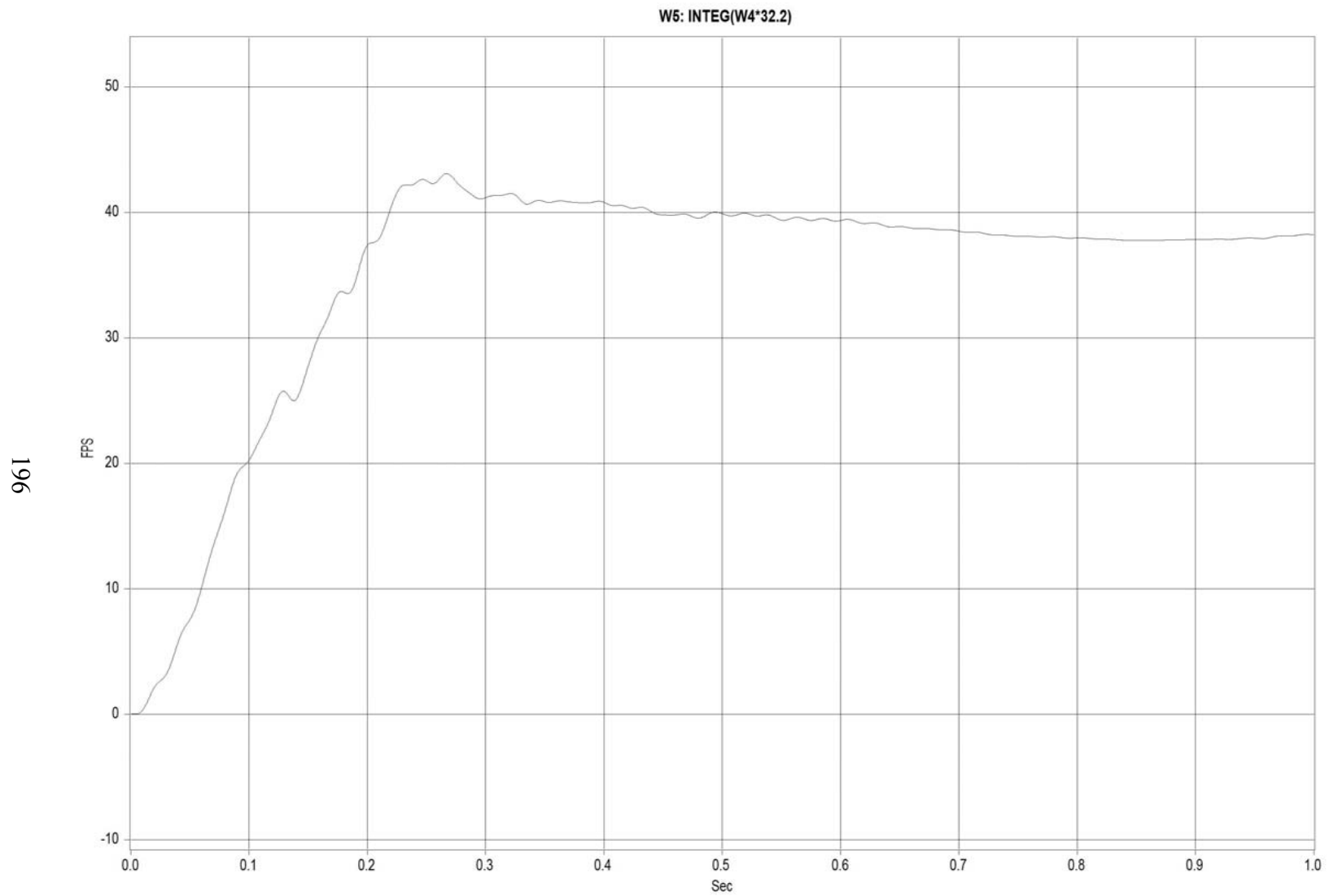


Figure G-5. Graph of Lateral Occupant Impact Velocity, Test FSCR-2

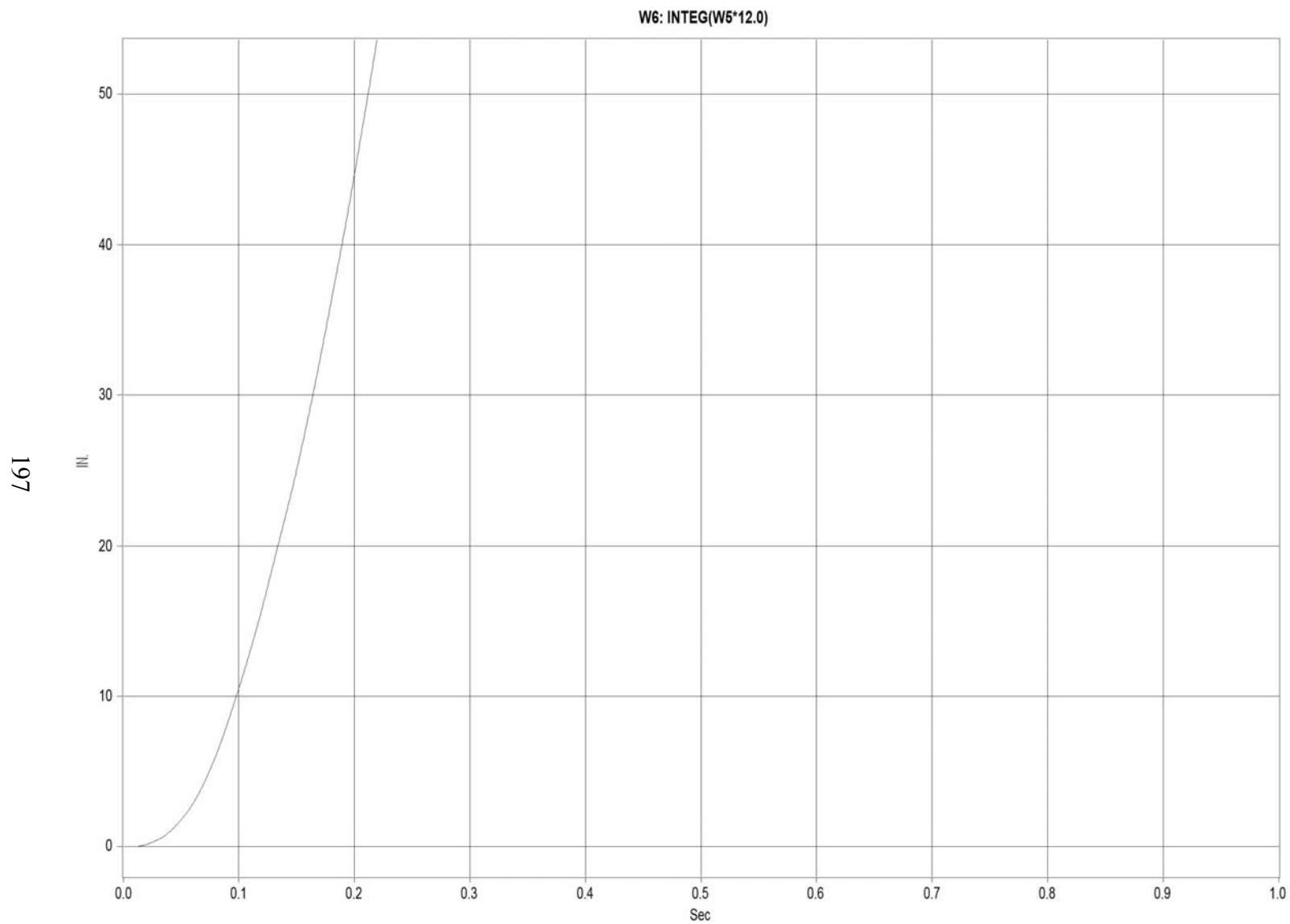


Figure G-6. Graph of Lateral Occupant Displacement, Test FSCR-2

APPENDIX H

Accelerometer Data Analysis - Test FSCR-3

Figure H-1. Graph of Longitudinal Deceleration, Test FSCR-3

Figure H-2. Graph of Longitudinal Occupant Impact Velocity, Test FSCR-3

Figure H-3. Graph of Longitudinal Occupant Displacement, Test FSCR-3

Figure H-4. Graph of Lateral Deceleration, Test FSCR-3

Figure H-5. Graph of Lateral Occupant Impact Velocity, Test FSCR-3

Figure H-6. Graph of Lateral Occupant Displacement, Test FSCR-3

Figure H-7. Graph of Roll, Pitch and Yaw Angular Displacements, Test FSCR-3

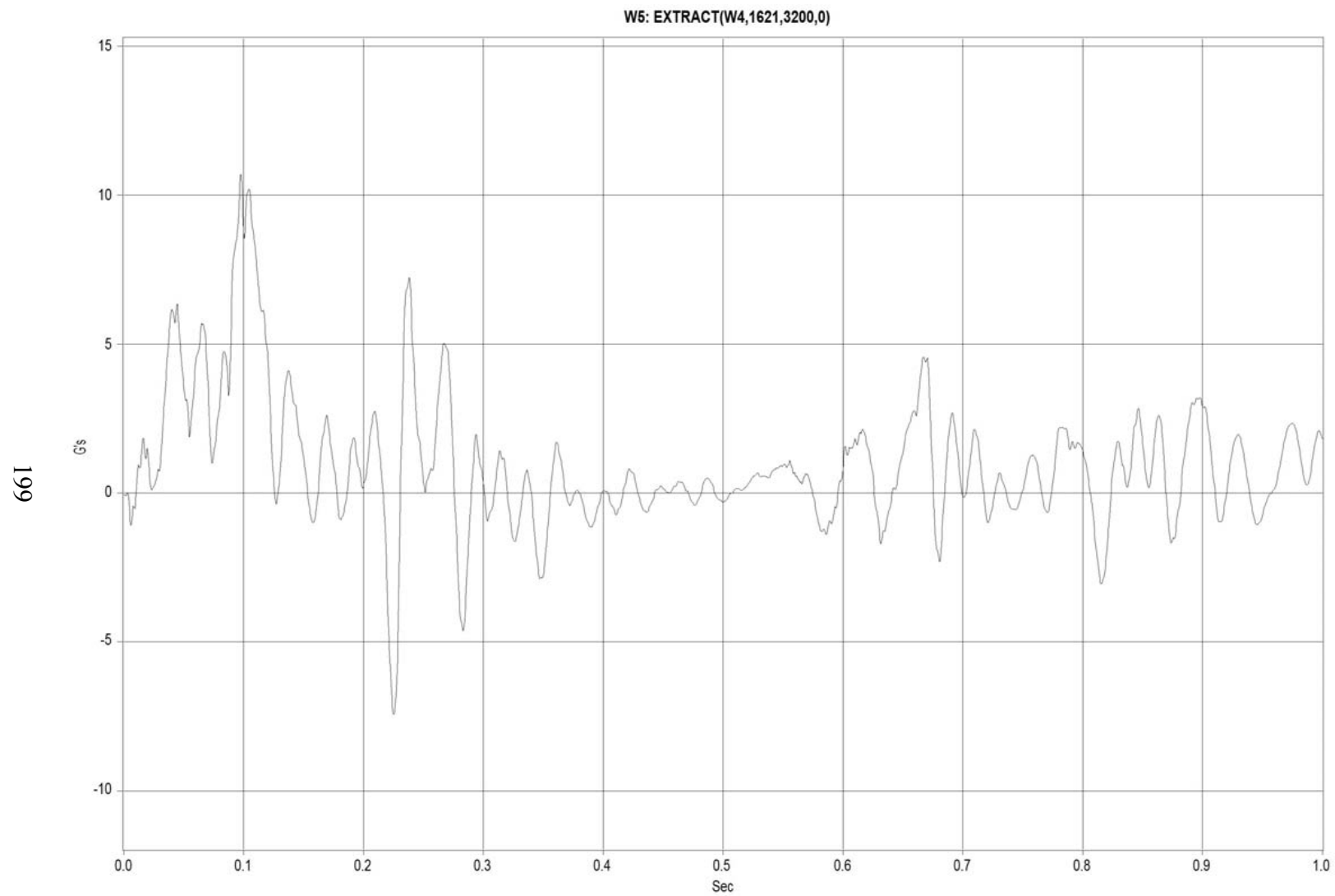


Figure H-1. Graph of Longitudinal Deceleration, Test FSCR-3

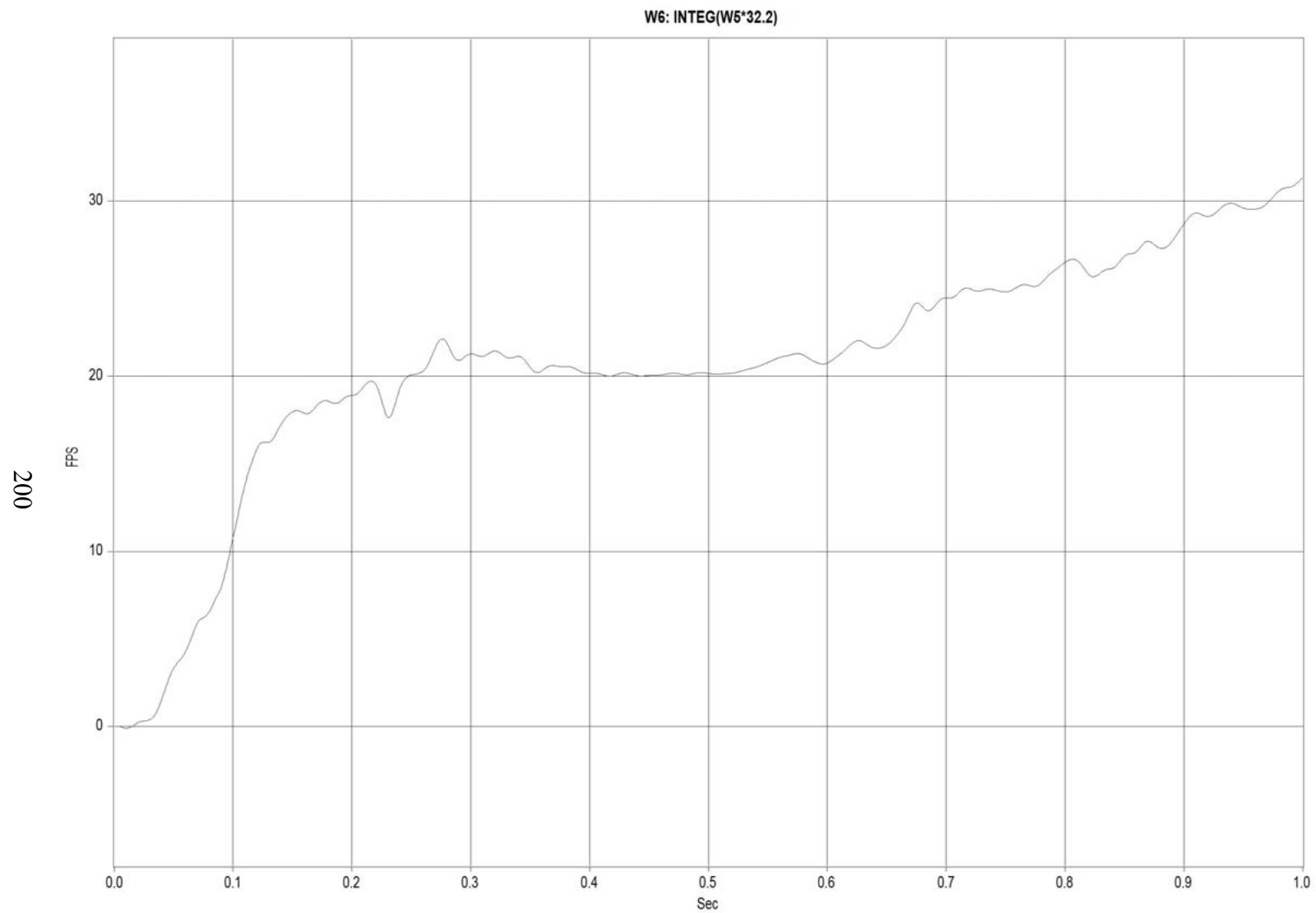


Figure H-2. Graph of Longitudinal Occupant Impact Velocity, Test FSCR-3

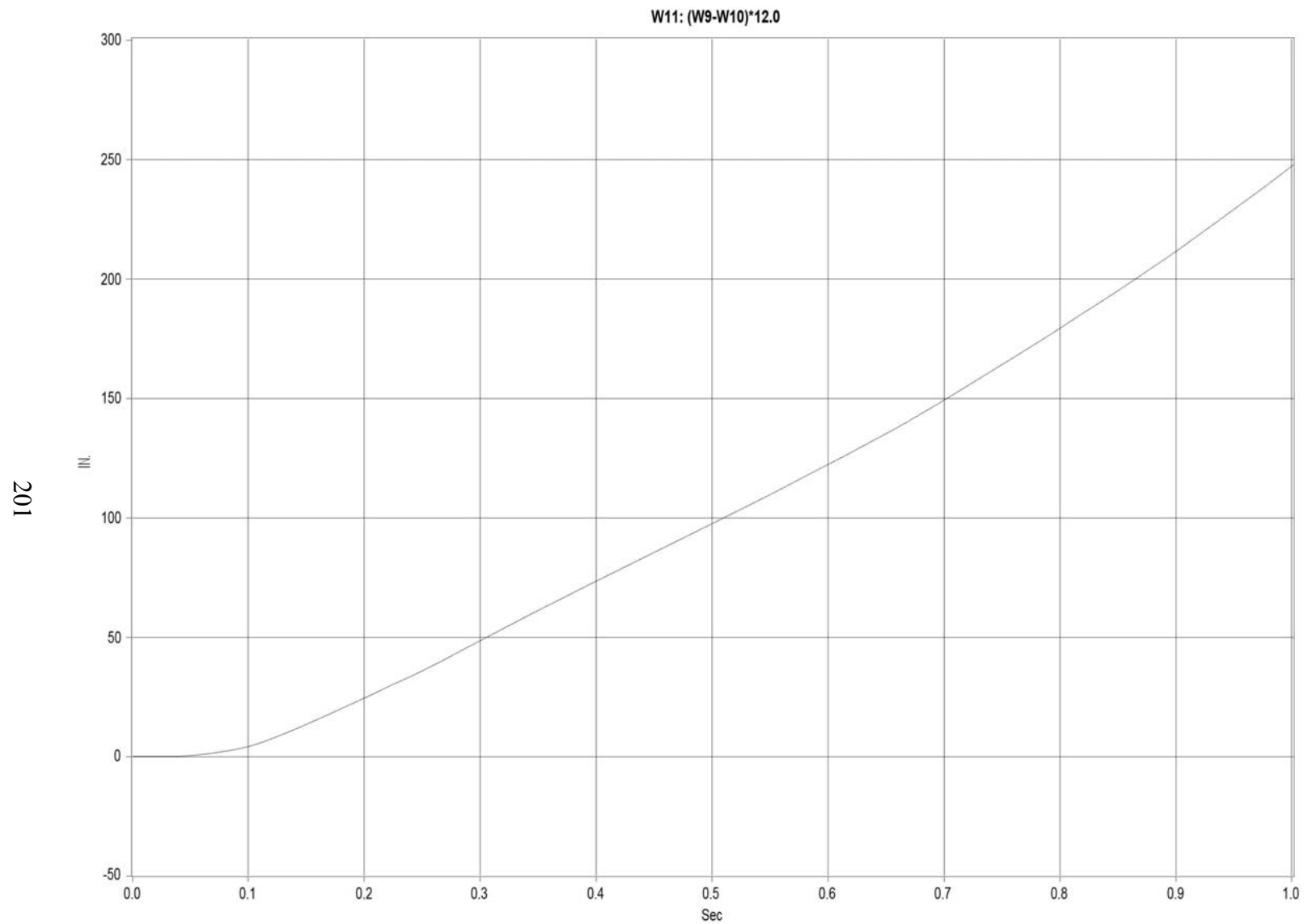


Figure H-3. Graph of Longitudinal Occupant Displacement, Test FSCR-3

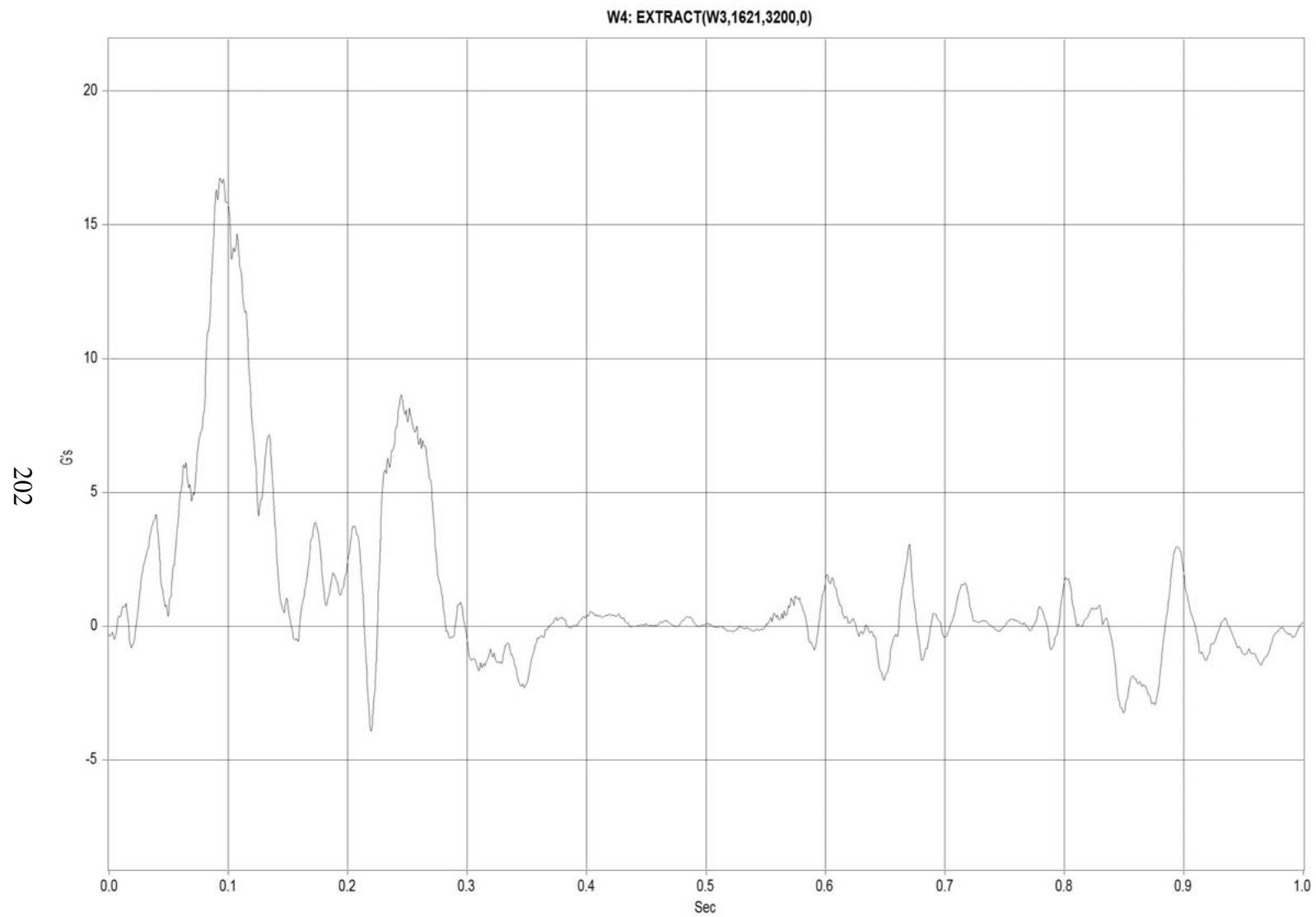


Figure H-4. Graph of Lateral Deceleration, Test FSCR-3

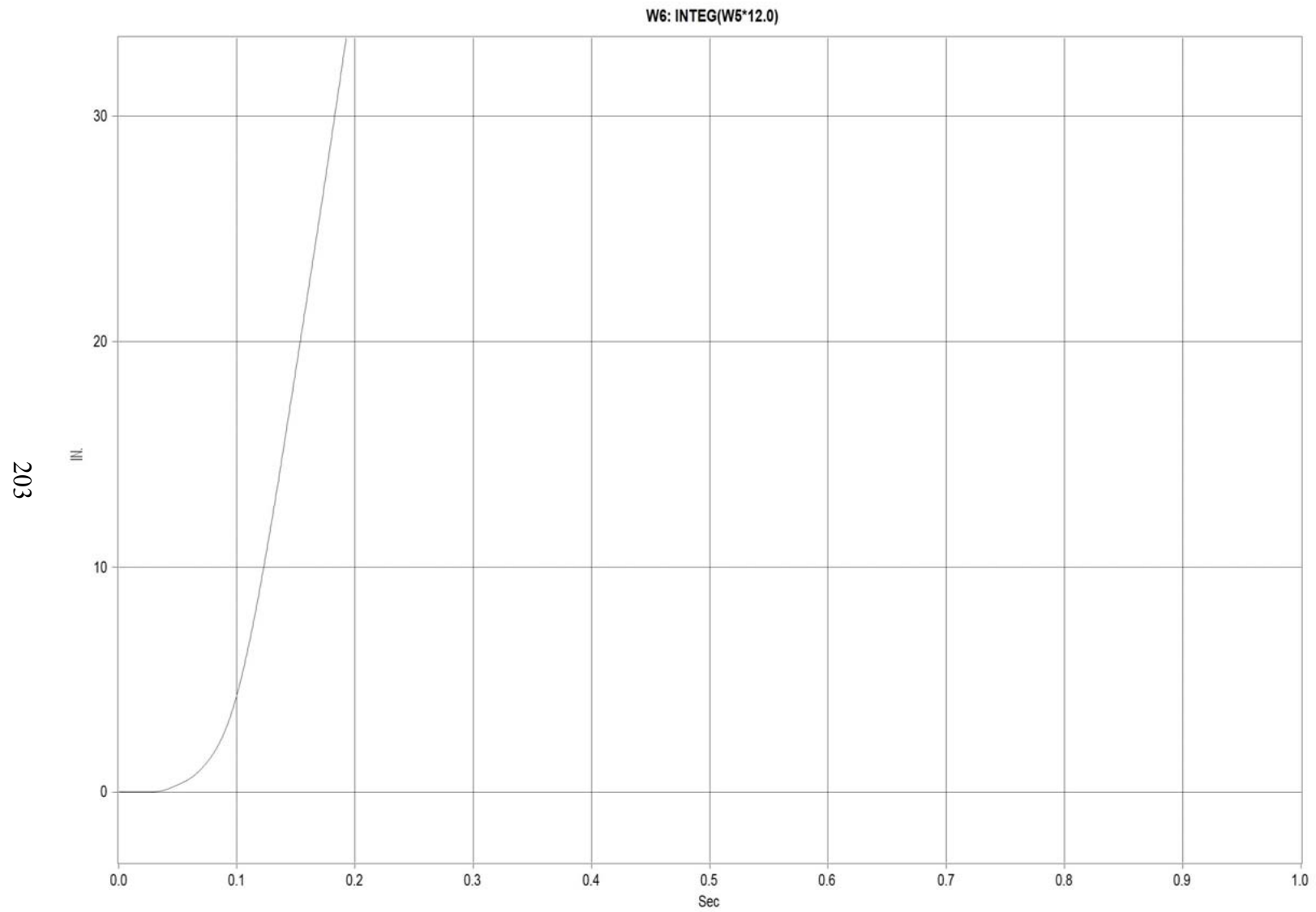


Figure H-5. Graph of Lateral Occupant Impact Velocity, Test FSCR-3

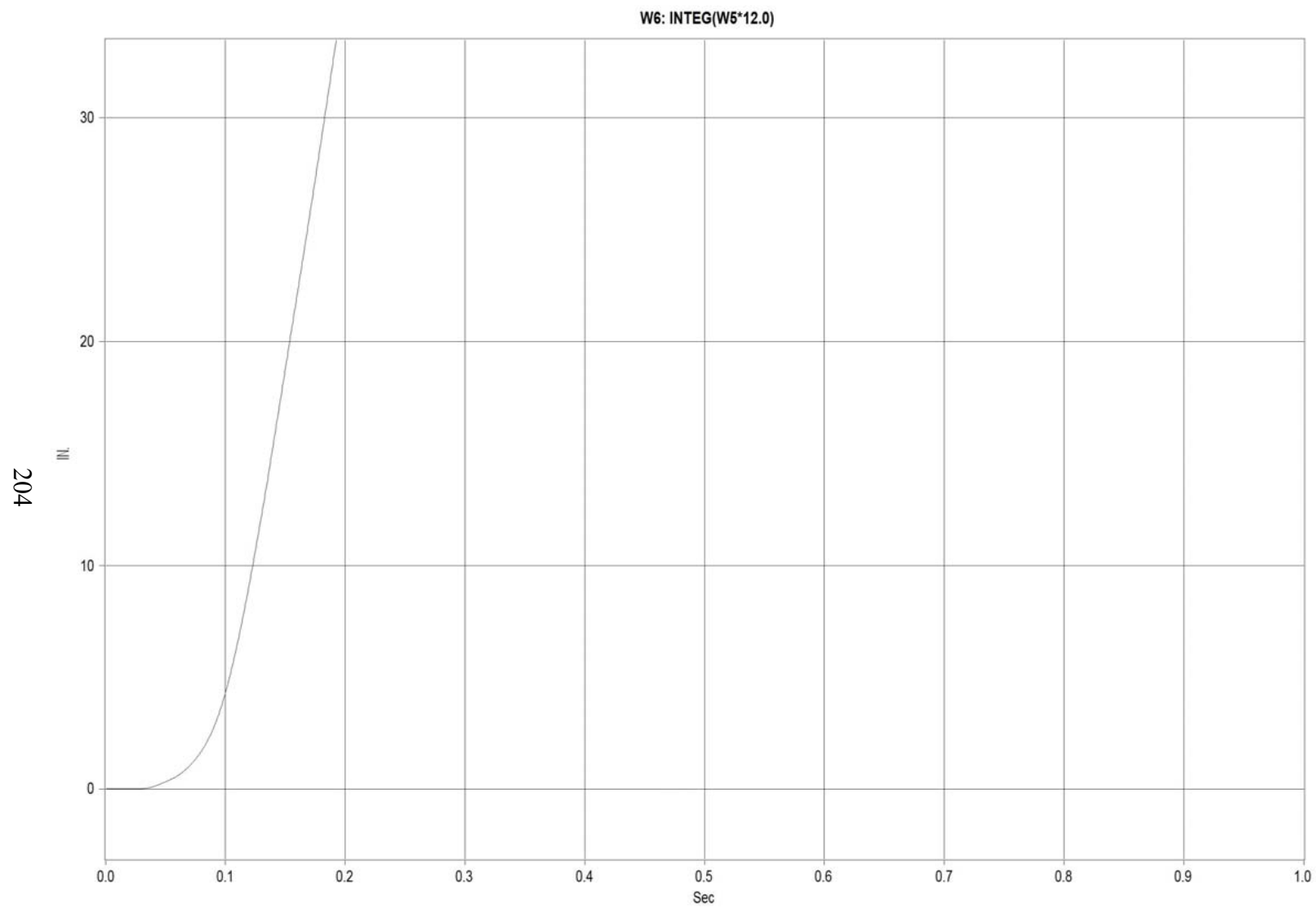


Figure H-6. Graph of Lateral Occupant Displacement, Test FSCR-3

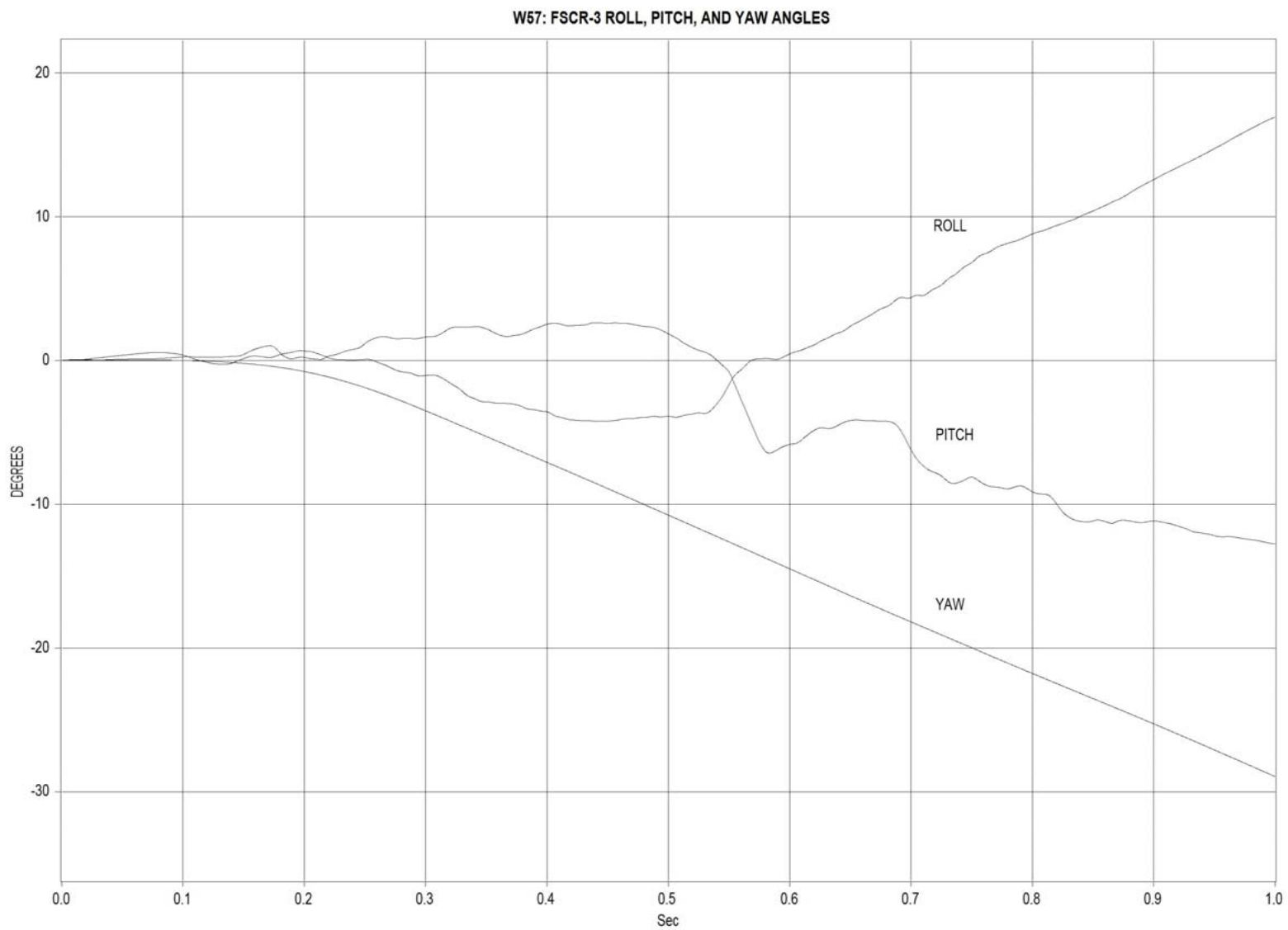


Figure H-7. Graph of Roll, Pitch and Yaw Angular Displacements, Test FSCR-3

APPENDIX I

Accelerometer Data Analysis - Test FSCR-4

Figure I-1. Graph of Longitudinal Deceleration, Test FSCR-4

Figure I-2. Graph of Longitudinal Occupant Impact Velocity, Test FSCR-4

Figure I-3. Graph of Longitudinal Occupant Displacement, Test FSCR-4

Figure I-4. Graph of Lateral Deceleration, Test FSCR-4

Figure I-5. Graph of Lateral Occupant Impact Velocity, Test FSCR-4

Figure I-6. Graph of Lateral Occupant Displacement, Test FSCR-4

Figure I-7. Graph of Roll, Pitch and Yaw Angular Displacements, Test FSCR-4

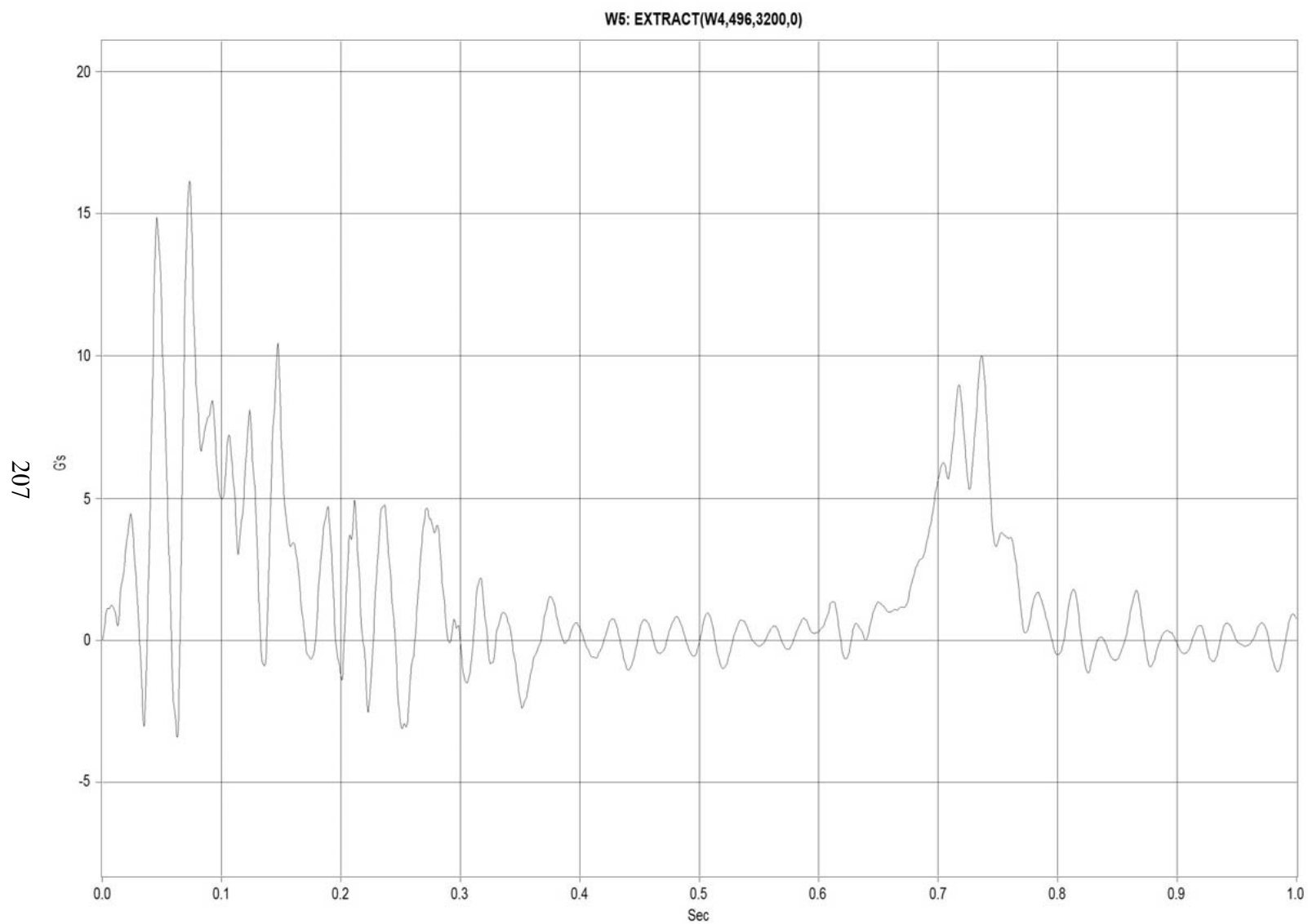


Figure I-1. Graph of Longitudinal Deceleration, Test FSCR-4

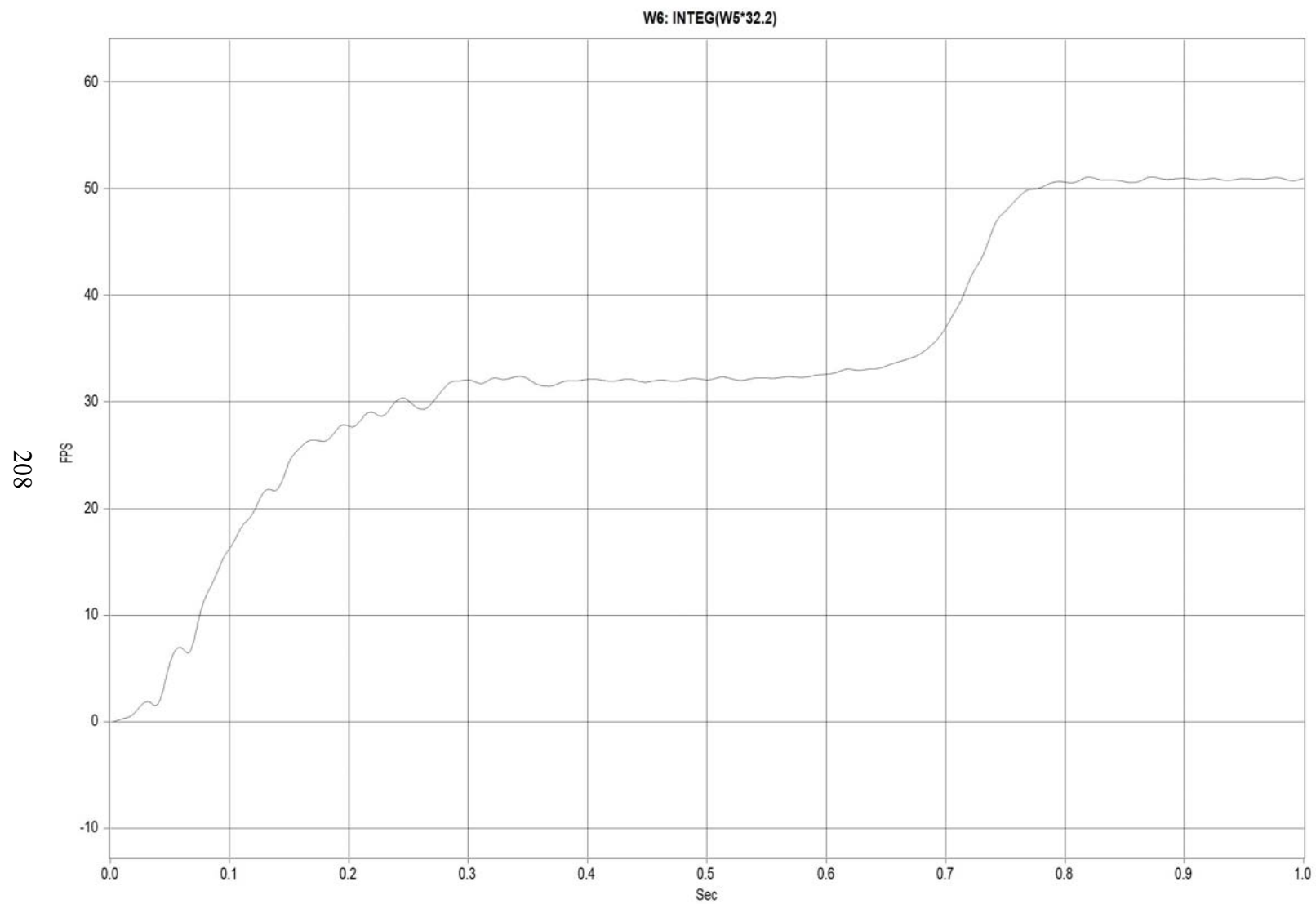


Figure I-2. Graph of Longitudinal Occupant Impact Velocity, Test FSCR-4

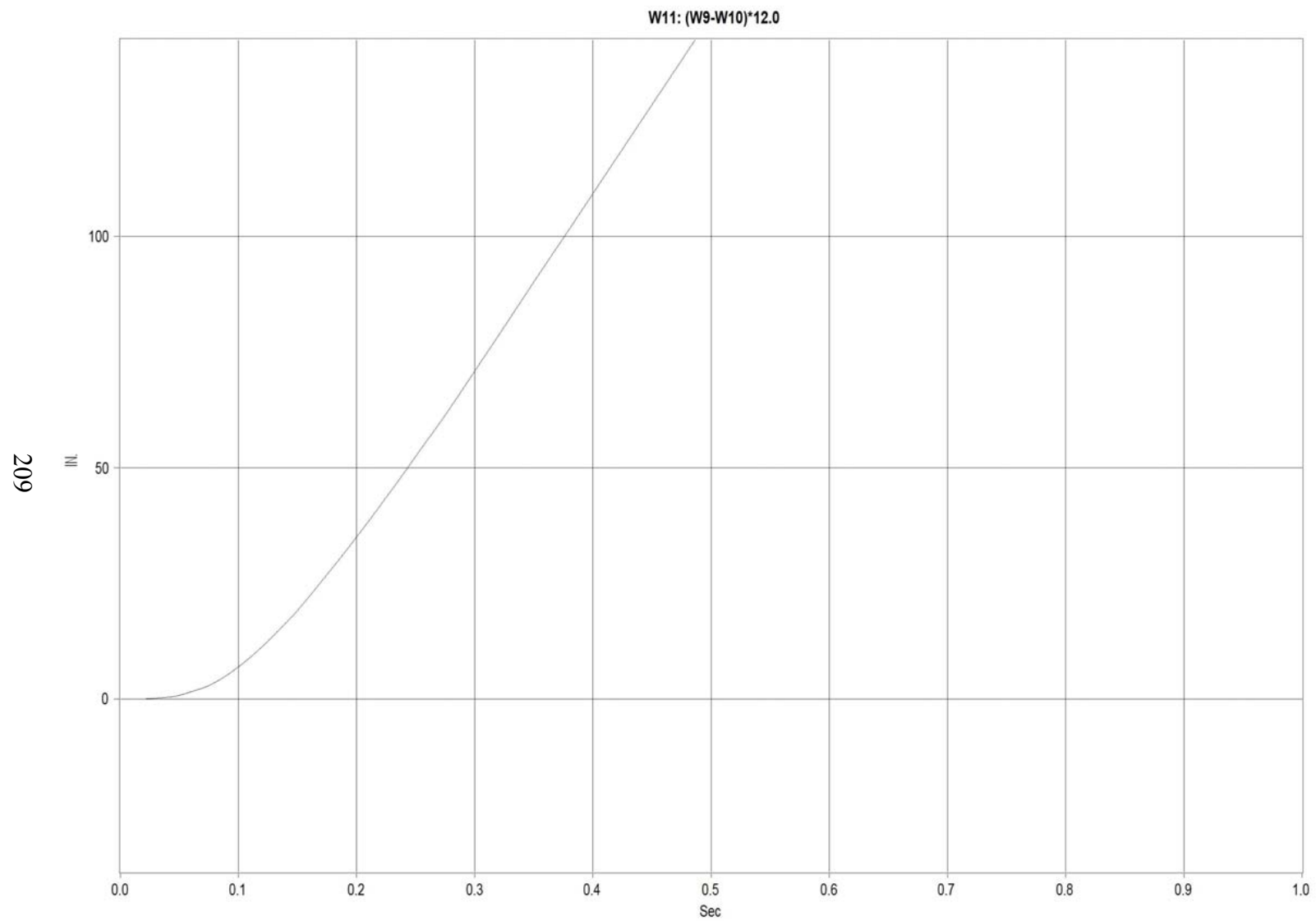


Figure I-3. Graph of Longitudinal Occupant Displacement, Test FSCR-4

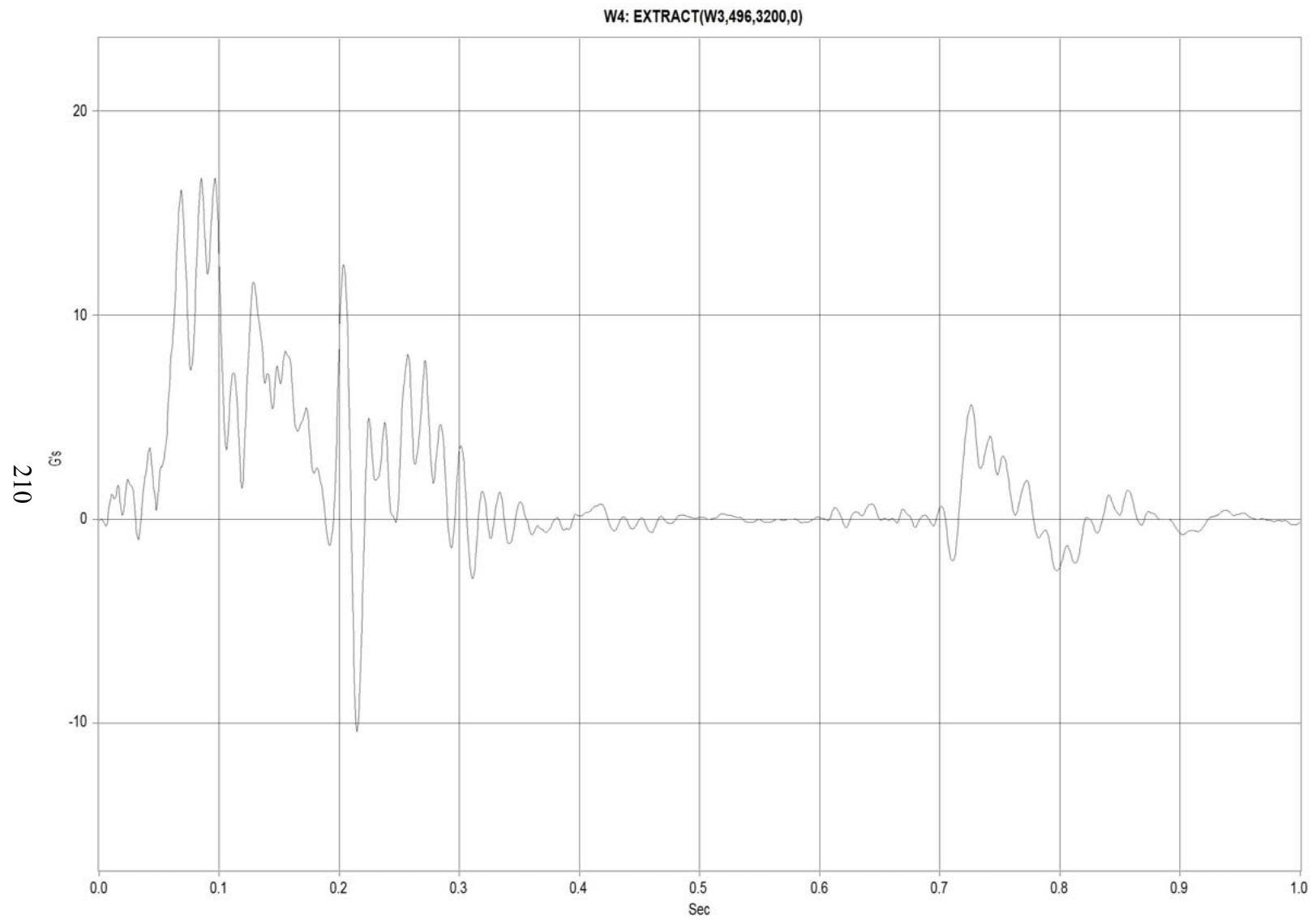


Figure I-4. Graph of Lateral Deceleration, Test FSCR-4

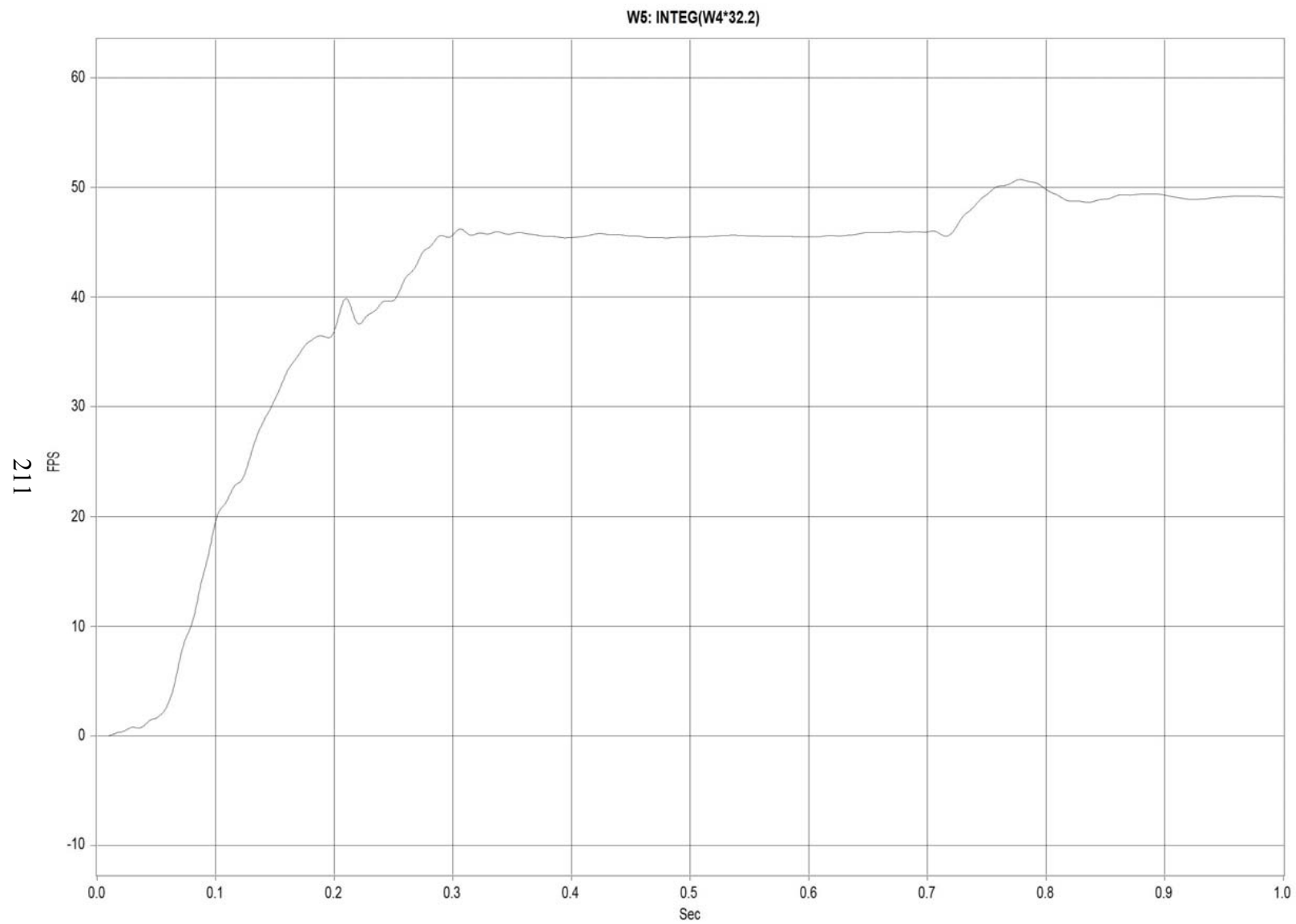


Figure I-5. Graph of Lateral Occupant Impact Velocity, Test FSCR-4

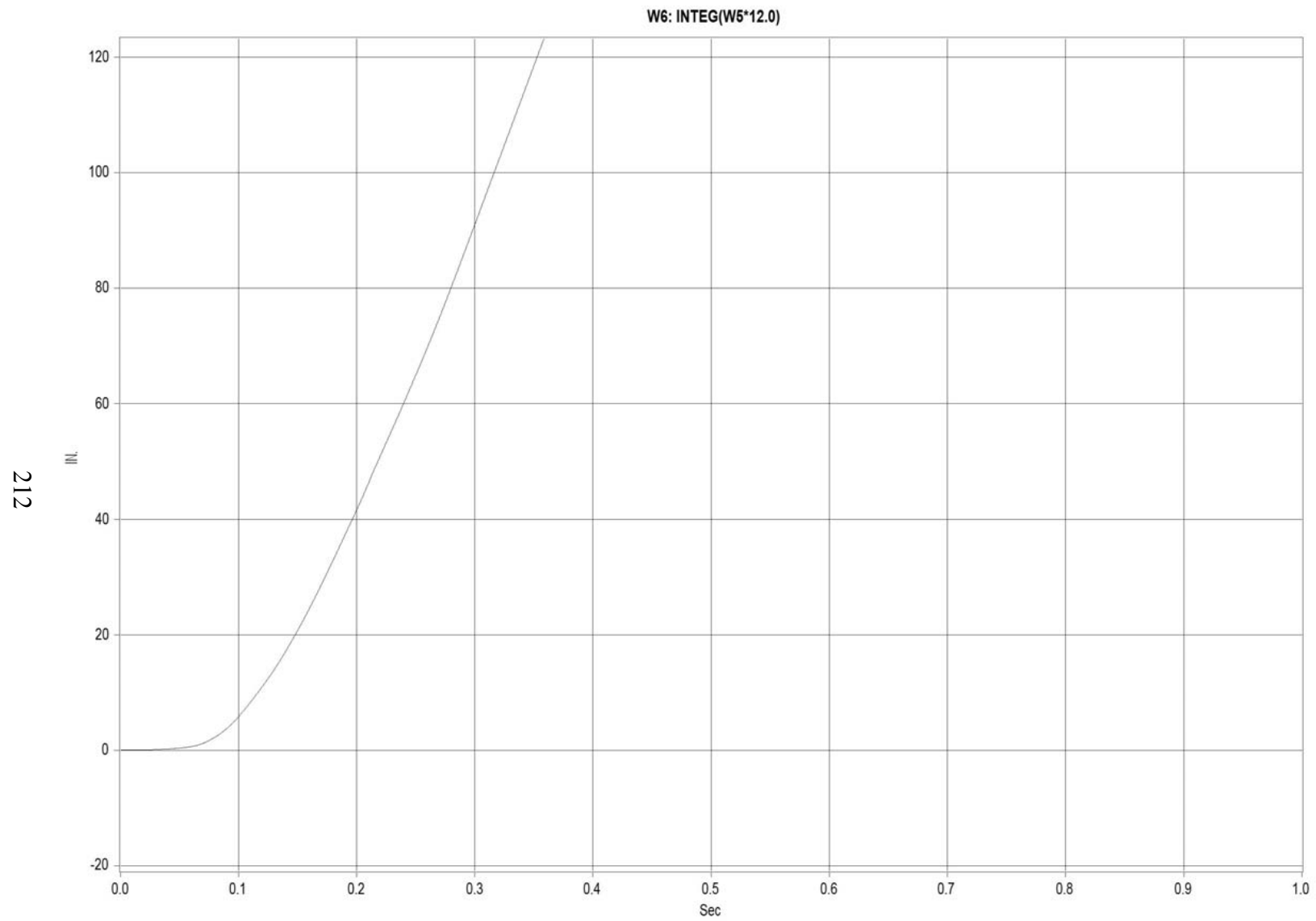


Figure I-6. Graph of Lateral Occupant Displacement, Test FSCR-4

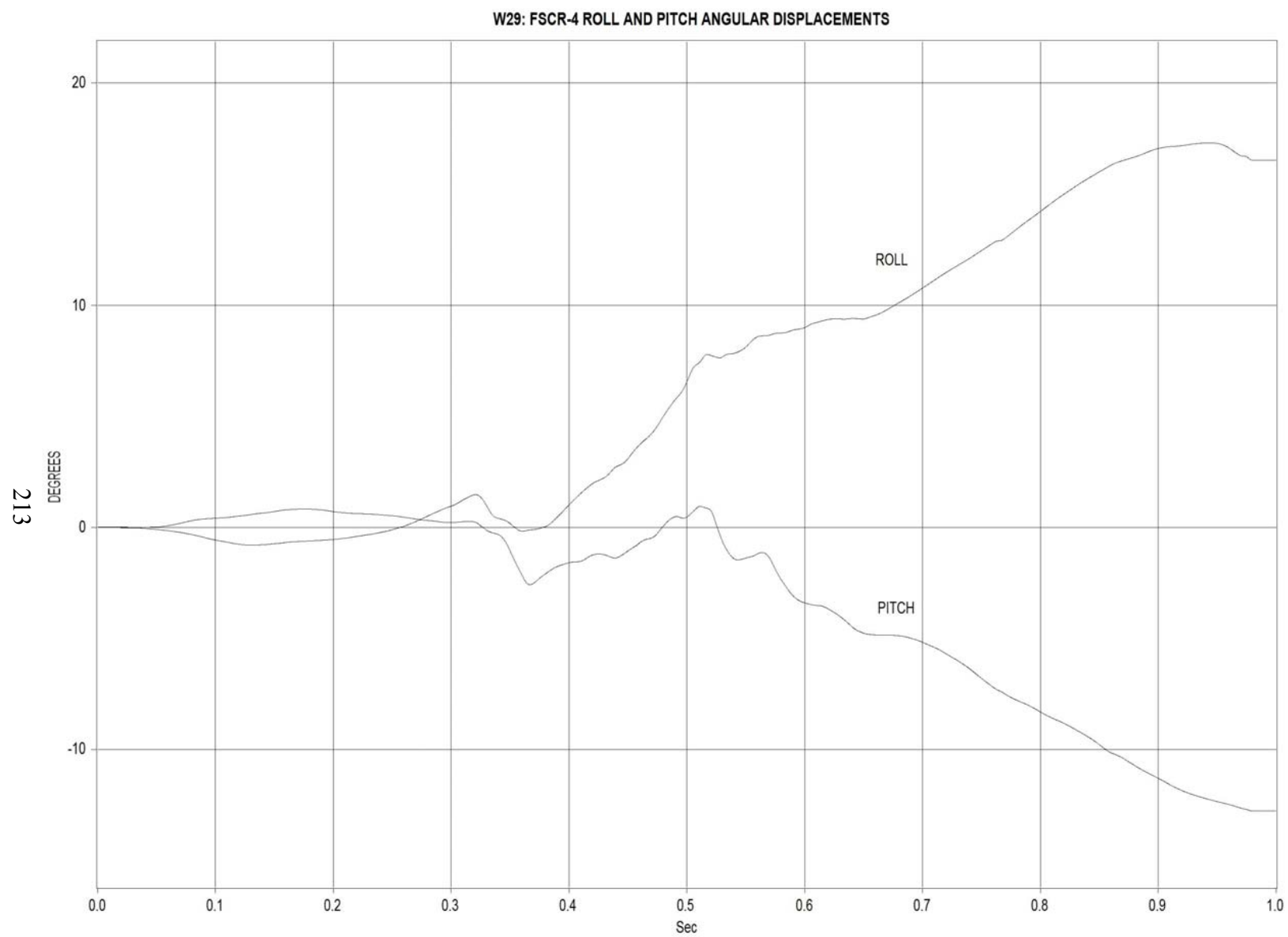


Figure I-7. Graph of Roll and Pitch Angular Displacements, Test FSCR-4